AUT Journal of Mathematics and Computing

AUT J. Math. Comput., 7(2) (2026) 213-269
https://doi.org/10.22060/AJMC.2026.24592.1441

Review Article

Numerical methods for the time-fractional diffusion equation: A review

Amin Ghoreyshi, Mostafa Abbaszadeh*, Mehdi Dehghan

Department of Applied Mathematics, Faculty of Mathematics and Computer Sciences, Amirkabir University of Technology (Tehran Polytechnic), No. 424, Hafez Ave., 15914 Tehran, Iran

ABSTRACT: This review paper focuses on the numerical solution of the time-fractional diffusion equation using various discretization techniques. For the time-fractional derivative, we consider methods such as L–type approximations and Grünwald–Letnikov-based formulas, while for the spatial diffusion term, we utilize the compact finite difference method, finite element method, spectral element method, meshless method, Chebyshev spectral method, and finite block method. In addition, stability and convergence theorems are presented, accompanied by numerical examples that confirm the theoretical results.

Review History:

Received:18 August 2025
Revised:02 February 2026
Accepted:15 February 2026
Available Online:01 May 2026

Keywords:

Time-fractional diffusion equation
L–type approximations
Weighted and shifted Grünwald–Letnikov formulas
Finite difference methods
Finite element method

MSC (2020):

26A33; 35K05; 35R11; 65M06

1. Introduction

The origins of fractional calculus can be traced back to 1695, when Leibniz first posed the question of the meaning of a derivative of non-integer order. Since then, numerous prominent mathematicians and scientists, including Euler, Liouville, Riemann, and many others, have contributed to its theoretical development. Fractional calculus has emerged as a powerful tool for modeling a wide range of complex phenomena, particularly those characterized by nonlocal behavior and long-term memory effects. Unlike classical integer-order calculus, which often falls short in capturing the hereditary and memory-dependent properties of certain processes, fractional calculus naturally incorporates these effects through its nonlocal operators [20, 95, 119, 123, 134, 138, 148, 166].

* *Corresponding author.*

E-mail addresses: aminghoreyshi@aut.ac.ir, amin.ghoreyshi7@gmail.com (A. Ghoreyshi), m.abbaszadeh@aut.ac.ir (M. Abbaszadeh), mdehghan@aut.ac.ir, mdehghan.aut@gmail.com (M. Dehghan)

Fractional differential equations (FDEs) have therefore found applications in diverse fields involving anomalous or memory-driven dynamics, such as wave propagation in complex media, viscoelasticity, heat conduction with memory, anomalous diffusion, temperature control, signal processing, and solid mechanics [26, 89, 106, 122, 149]. In addition, fractional operators have been successfully employed in the analysis of chaotic dynamical systems, providing a more accurate description of their intrinsic irregularities [21].

Due to the inherent complexity of fractional models, closed-form exact solutions are typically unattainable; as a result, significant effort has been dedicated to developing efficient and reliable numerical methods for FDEs. While a wide range of well-established numerical techniques exists for classical integer-order differential equations, the design of accurate and computationally efficient methods for FDEs remains relatively limited, owing to the intrinsic nonlocality and memory effects associated with fractional operators. This challenge has motivated scholars and researchers to devise robust and stable numerical schemes, leading to the development of various approaches such as spectral methods [22, 23, 24, 25, 72, 86, 187, 188], finite element method (FEM) [28, 50, 66, 91, 94, 115], finite difference methods (FDMs) [52, 53, 55, 56, 74, 93, 102, 124, 146, 185, 195, 201], spectral element method (SEM) [8, 186], physics-informed neural networks [14, 135], spline methods [88, 145, 157], meshless methods [2, 11, 114, 125, 132, 133] and polynomial-based methods [49, 70, 128, 129, 150, 151, 152, 153, 154].

1.1. Time–fractional diffusion equation

Time-fractional diffusion equations (TFDEs) are fundamental in modeling subdiffusive motion, which is particularly relevant in complex systems such as glassy and disordered materials, where particle pathways are constrained by geometric or energetic limitations. These equations are obtained from the classical diffusion equation by replacing the first-order time derivative with a fractional derivative of order $\alpha \in (0,1)$ in the Riemann–Liouville or Caputo sense, effectively capturing anomalous diffusion. Unlike classical models, fractional differential equations require fewer restrictive assumptions, preserving the essential physical characteristics of the problem. Metzler and Klafter [122] demonstrated that fractional diffusion equations describe non-Markovian diffusion processes with memory, while Giona et al. [69] proposed such equations for modeling relaxation phenomena in complex viscoelastic materials.

Fractional derivatives are widely employed to model anomalous diffusion, where particle spreading follows a power-law rather than the Gaussian scaling of classical Brownian motion [122, 139]. This behavior is well characterized by fractional partial differential equations (FPDEs), which effectively describe a broad class of non-Markovian random walks [111].

The TFDE is a linear fractional partial differential equation whose analytic solutions are often unavailable, making numerical methods essential.In contrast to the classical case, its numerical approximation requires information from all previous time layers at each time step, leading to high computational costs even in one-dimensional problems. The complexity increases substantially for two- and three-dimensional cases, highlighting the importance of developing stable, high-order numerical schemes [16].

The study of problems involving fractional temporal derivatives of order $\alpha \in (0,1)$ has received considerable attention in recent years due to their broad applicability in modeling diverse physical processes; see, for example, [79, 105, 122].

In this review, we concentrate on the TFDE which is expressed in the following form

$$\begin{cases} {}_0^C\mathcal{D}_t^{\alpha} u(x,y,t) - \varepsilon \Delta u(x,y,t) = f(x,y,t), & (x,y,t) \in \Omega \times (0,T], \\ u(x,y,t) = g(x,y,t), & (x,y,t) \in \partial\Omega \times (0,T], \\ u(x,y,0) = v(x,y), & (x,y,t) \in \Omega, \end{cases} \tag{1}$$

where ${}_0^C\mathcal{D}_t^{\alpha}$ denotes the Caputo fractional derivative of order $\alpha \in (0,1)$, $\varepsilon > 0$ is the diffusion coefficient, Δ represents the Laplace operator, and f is the source function. The set $\Omega \subset \mathbb{R}^2$ denotes the spatial domain, with $\partial\Omega$ representing its boundary, g specifying the boundary condition, and v denoting the initial condition.

1.2. A brief literature review

Eq. (1) arises in a wide range of engineering, biological, and physical processes where anomalous diffusion is observed [18, 118, 131, 156, 179]. It is well established that classical integer-order differential equation models often fail to adequately capture anomalous behaviors [122, 138], such as those occurring in subdiffusive and superdiffusive phenomena.

As previously mentioned, the analytic solution of the TFDE is generally attainable only for simple initial and boundary conditions [37, 39, 147], which makes the development of numerical methods indispensable for practical applications. The numerical computation of fractional differential equations, however, is particularly challenging due to the nonlocal nature of the fractional derivative, by definition, the solution at a given time depends on its entire history. Consequently, considerable research has been devoted to the numerical solution of Eq. (1); for example,

Li and Chen [91] provided a comprehensive review of numerical techniques for FPDEs. Shen et al. [160] solved the TFDE using FDM and presented a detailed analysis of their methodology. Zhuang and Liu [204, 205] studied implicit FDM for the TFDE in one and two dimensions. Lin and Xu [110] solved the TFDE utilizing the Legendre spectral method in space and FDM for time variable. They also analyzed their proposed methodology and achieved the accuracy of $\mathcal{O}(\tau^{2-\alpha} + M^{-p})$, where p is the degree of polynomial. Zhao and Sun [199] proposed a box-type method combined with L1 discretization for fractional derivative for the TFDE. Mohebbi et al. [124] proposed a fully discrete implicit scheme in which the spatial derivative is approximated using a fourth-order compact scheme, while the fractional derivative is discretized via the standard Grünwald–Letnikov formula. The authors in [190] derived an unconditionally stable method by combining FDM and FEM for the TFDE. Yang et al. [183] established a numerical scheme based on orthogonal spline collocation method and finite difference approach for Eq. (1). In [61], the authors proposed a numerical scheme that integrates a recently developed non-polynomial collocation method for solving FDEs with the method of lines. In [197], the authors noted that since fractional derivatives are integrals with weakly singular kernels, discretization on a uniform mesh may result in poor accuracy. Consequently, they investigated a compact finite difference approach of the Caputo derivative on non-uniform meshes. The authors in [75] investigated a high-order approximation for the TFDE, employing a Grünwald–Letnikov-type formula for the time discretization in combination with a compact finite difference scheme for the spatial discretization. Zeng et al. [191] investigated a second-order and unconditional stable numerical algorithm combining FDM and FEM for the TFDE. In [54], the compact FDMs of sixth- and eighth-order is investigated for TFDE. The authors in [117] examined a spectral method based on Legendre polynomials for the numerical solution of Eq. (1). In [189], the combination of FEM and Crank-Nicolson scheme is studied for solving Eq. (1). The authors in [30] proposed a mixed numerical method that employs the FDM in the spatial domain and the spectral method in the temporal domain. Li et al. [106] discussed an application of TFDE in signal smoothing and also applied explicit and implicit FDM for solving it. Yeganeh et al. [184] constructed a numerical methodology based on local discontinuous Galerkin (LDG) and FDM for the TFDE. Furthermore, Liu et al. [116] developed a numerical method for the TFDE based on LDG and weighted and shifted Grünwald difference operator. In [195], the authors presented a high-order numerical method for a class of TFDE. They reformulate the original equation to eliminate the need for a discrete approximation of the convection term. They then apply a fourth-order compact scheme for the spatial derivative and a second-order midpoint formula for the time Riemann–Liouville fractional derivative. Alikhanov and Huang [17] developed and analyzed an L–type difference scheme for the Caputo fractional derivative, achieving high-order accuracy in both space and time for the TFDE with variable coefficients. Ramezani and Mokhtari [143] developed a scheme for the TFDE combining B-splines with FDM. Chen et al. [36] proposed an image denoising algorithm based on the TFDE to obtain high-quality images, employing a finite difference approach for its numerical solution. In [203], the time-fractional derivative in the TFDE is discretized using the L2 formula combined with the sum-of-exponentials approximation. The spatial discretization is carried out using the standard Legendre spectral method. In [12], a precise numerical estimation of the TFDE is presented using the spectral tau method based on seventh-kind Chebyshev polynomials. Li and Ding [102] utilized a new non-uniform temporal mesh to accurately handle the weak singularity of the solution near the initial time. To this end, they first transformed the original problem into an equivalent integral formulation to facilitate numerical treatment. They proposed two new numerical integration formulas developed by combining the fractional rectangle and fractional trapezoidal methods. Based on central difference discretization in space, efficient numerical schemes were proposed. In [103], the authors addressed challenges in TFDEs caused by initial-time solution singularities by introducing a novel splitting technique that relaxes step-size ratio restrictions, allowing greater flexibility in nonuniform temporal meshes. They combine a refined L2-type temporal approximation with a fourth-order compact spatial discretization to develop an efficient and rigorously analyzed numerical scheme. Zhang et al. [193] presented a compact finite difference approach for the TFDE and also analyze their proposed methodology using the Fourier method. Furthermore, numerous other studies have been conducted in this field; interested readers may refer to [16, 84, 95, 165, 166, 168, 196] for further details.

1.3. Description of present work

The present work reviews various numerical methods for solving Eq. (1). First, we introduce several approximation techniques for the fractional time derivative, including Grünwald–Letnikov-based schemes such as the standard Grünwald–Letnikov method and the weighted and shifted Grünwald–Letnikov formulas of second-, third- and fourth-order accuracy. We then examine the widely used L–type approximations, including the L1, L1-2, L2-1$_\sigma$, and L1-2-3 schemes. For the spatial derivatives, different discretization techniques are considered, including the compact FDM, the meshless multiquadric radial basis function (MQ–RBF) approach, the FEM, the SEM, spectral methods, and the finite block method (FBM), the latter of which enables the solution of problems on irregular domains through a mapping strategy. Furthermore, we present convergence and stability analyses for the proposed schemes, accompanied by numerical examples that validate the theoretical results.

1.4. The outline of paper

The paper is organized as follows. In §2, we introduce the basic notations and definitions, along with the function spaces that provide the necessary mathematical framework. §3 presents the Grünwald–Letnikov-based formulas and the L–type approximation schemes. In §4, we propose numerical schemes for solving the TFDE using the compact FDM. §5 discusses meshless schemes based on the MQ–RBF approach. In §6, we develop FEM schemes, while §7 addresses SEM formulations. §8 focuses on spectral methods, and §9 introduces FBM and the mapping strategy for complex geometries. Finally, §10 provides concluding remarks and a summary of the main findings.

2. Preliminaries

In this section, we introduce key notations and definitions that will be used in the subsequent discussions.

2.1. Basic definitions and notations

This subsection includes some definitions and notations that are useful for our theoretical claims.

Definition 2.1. *The symbol Δ denotes the Laplace operator and is introduced by*

$$\Delta := \frac{\partial^2}{\partial x^2} + \frac{\partial^2}{\partial y^2}.$$

Definition 2.2 ([20, 138, 166]). *The gamma function is defined as follows*

$$\Gamma(\alpha) := \int_0^\infty t^{\alpha-1} e^{-t}\, dt,$$

where $\alpha \in \mathbb{R}^+$.

Definition 2.3 ([20, 95, 134, 138, 166]). *The left Riemann–Liouville fractional derivative operator for u is given by*

$${}_0^{RL}\mathcal{D}_t^\alpha u\,(x,y,t) := \frac{\partial^m}{\partial^m \varsigma} \int_0^t \mathcal{K}_{m-\alpha}\,(t-\varsigma)\, u\,(x,y,\varsigma)\, d\varsigma, \qquad \mathcal{K}_\alpha\,(t) := \frac{t^{\alpha-1}}{\Gamma\,(\alpha)},$$

in which $m \in \mathbb{N}$ and $m-1 \le \alpha < m$, with $t \in (0,T]$.

Definition 2.4 ([20, 95, 134, 138, 166]). *The left Grünwald–Letnikov fractional derivative operator for the function u is introduced by*

$${}_0^{GL}\mathcal{D}_t^\alpha f(t) := \lim_{\tau\to 0} \tau^{-\alpha} \sum_{k=0}^{N} (-1)^k \binom{\alpha}{k} u(x,y,t-k\tau),$$

for a given $\alpha > 0$, and $t \in (0,T]$.

Definition 2.5 ([20, 95, 134, 138, 166]). *The left Caputo fractional derivative operator for the function u is defined as*

$${}_0^{C}\mathcal{D}_t^\alpha u\,(x,y,t) := \int_0^t \mathcal{K}_{m-\alpha}\,(t-\varsigma)\, \partial_\varsigma^m u\,(x,y,\varsigma)\, d\varsigma,$$

where $m \in \mathbb{N}$ with $m-1 < \alpha \le m$, $\alpha > 0$ and $t \in (0,T]$.

Definition 2.6 ([20, 138]). *The one–parameter Mittag–Leffler function is denoted by E_α and presented as follows*

$$E_\alpha(t) := \sum_{k=0}^{\infty} \frac{t^k}{\Gamma(\alpha k+1)}, \quad \alpha \in \mathbb{R}^+.$$

For TFDEs, the left-sided Caputo derivative is preferred because it incorporates only the past history of the process from the initial time to the current time, preserving causality and naturally representing memory effects in anomalous diffusion models [34, 122].

Throughout this manuscript, two types of nodes are employed for discretization. For spatial discretization, both uniform and Chebyshev nodes are utilized, depending on the method under consideration. In the temporal direction, only uniform nodes are applied. The definition of Chebyshev nodes is presented as follows.

Definition 2.7 ([29, 65, 174]). *The zeros of Chebyshev polynomial of degree $M \geq 1$ can be computed over any arbitrary interval (a, b) using the formula*

$$x_k = \frac{a+b}{2} + \frac{b-a}{2} \cos\left(\frac{2k+1}{2M}\pi\right), \tag{2}$$

for $k = 0, 1, \ldots, M-1$.

For time discretization, we assume that the temporal domain $(0, T]$ is uniformly partitioned as $\{t_n\}_{n=0}^{N}$, where $t_n = n\tau$ and $\tau = \dfrac{T}{N}$ denotes the time step size. The grid functions are denoted by

$$u(x, y, t_n) = u^n, \qquad f(x, y, t_n) = f^n.$$

Also, we introduce the following notation, which will be useful for further sections

$$u(x, y, t_n) = u^n, \qquad u^{n+\sigma} = \sigma u^{n+1} + (1-\sigma) u^n.$$

2.2. Function spaces

Let u be a complex measurable function on Ω. The norm of space $\mathcal{L}^p(\Omega)$ is presented as follows [27, 31, 51, 137, 141, 159]

$$\begin{cases} \|u\|_p^p := \displaystyle\int_\Omega |u(x, y)|^p d\mu, & 1 \leq p < \infty, \\ \|u\|_\infty := \operatorname*{esssup}_{(x,y)\in\Omega} |u(x, y)|. \end{cases}$$

Also, the norm of Sobolev space $\mathcal{H}^s(\Omega)$ is defined as [27, 31, 51, 137, 141, 159]

$$\|u\|_{\mathcal{H}^s(\Omega)}^2 := \sum_{0\leq\alpha+\beta\leq s} \left\| \frac{\partial^{\alpha+\beta}}{\partial x^\alpha \partial y^\beta} u(x, y) \right\|^2, \qquad s > 0,$$

for two dimensions. It is also necessary to know the following notation

$$\mathcal{H}_0^1(\Omega) := \left\{ u \in \mathcal{H}^1(\Omega) \middle| \; u|_{\partial\Omega} = 0 \right\}.$$

Now, assume that $\omega_x := \{x_i\}_{i=0}^{M_x}$ and $\omega_y := \{y_j\}_{j=0}^{M_y}$ are two one–dimensional partitions of the domain Ω in the x- and y-directions, respectively. We introduce the mesh as $\omega := \omega_x \times \omega_y$. Moreover, the space of piecewise polynomials over the partition ω is given as follows

$$\mathcal{P}(\omega) := \left\{ u \in \mathcal{C}^1(\Omega) \,|\, u \in \mathcal{P}([x_{i-1}, x_i]), i = 1, 2, \ldots, M_x \right\} \otimes \left\{ u \in \mathcal{C}^1(\Omega) \,|\, u \in \mathcal{P}([y_{j-1}, y_j]), j = 1, 2, \ldots, M_y \right\}, \tag{3}$$

where the resulting space consists of all functions that can be presented as finite linear combinations of tensor-product basis functions of the form $u_x u_y$.

Definition 2.8 ([120, 166, 172]). *The function space defined below is employed associated with the family of Grünwald–Letnikov based formulas*

$$\mathcal{S}^{n+\alpha}(\mathbb{R}) := \left\{ v \in \mathcal{L}^1(\mathbb{R}) \left| \int_{-\infty}^{+\infty} (1 + |\mu|)^{n+\alpha} |\mathcal{F}[v]| \, d\mu < \infty \right. \right\}, \qquad n \geq 1,$$

where $\mathcal{F}$ presents the Fourier transform.

3. Numerical approximations for fractional Caputo derivative

In general, Definitions 2.3, 2.4, and 2.5 are not equivalent, as discussed in [91, 95]. However, when the function u has sufficient regularity, that is, $u \in \mathcal{C}^m(\Omega)$, then the Riemann–Liouville and Grünwald–Letnikov definitions are equivalent. In such cases, one has

$${}_0^{RL}\mathcal{D}_t^\alpha u(x, y, t) = {}_0^{GL}\mathcal{D}_t^\alpha u(x, y, t).$$

Moreover, the relationship between the Riemann–Liouville and Caputo derivatives is given by

$${}_0^{RL}\mathcal{D}_t^\alpha u(x, y, t) = {}_0^{C}\mathcal{D}_t^\alpha u(x, y, t) + \sum_{k=0}^{m-1} \frac{\partial_t^k u(x, y, 0) \left(t^{k-\alpha}\right)}{\Gamma(k+1-\alpha)}.$$

On the other side, if $\partial_t^k u(x,y,0) = 0$ for all $0 \le k < m$, then the Riemann–Liouville and Caputo derivatives coincide

$$ {}_0^{RL}\mathcal{D}_t^\alpha u(x,y,t) = {}_0^{C}\mathcal{D}_t^\alpha u(x,y,t). $$

The Caputo derivative is often favored in modeling physical phenomena due to its compatibility with classical initial and boundary conditions. Unlike the Riemann–Liouville derivative, which requires fractional-order initial terms that are difficult to interpret and measure, the Caputo derivative enables the direct incorporation of standard initial conditions. Furthermore, the Caputo derivative of a constant is zero, consistent with classical calculus, whereas the Riemann–Liouville derivative of a constant is singular at $t = 0$. These advantages make the Caputo definition more practical for both physical modeling and numerical implementation [119, 123, 138].

While this review paper predominantly focuses on the Caputo derivative due to its compatibility with traditional initial and boundary conditions in physical modeling, it is worth noting that other definitions—such as the Riemann–Liouville and Riesz fractional derivatives—are widely used in the study of space-fractional and space–time fractional partial differential equations, particularly for modeling strong non-local interactions and anomalous diffusion. These derivatives are essential in a variety of applications, including anomalous diffusion in heterogeneous or porous media with long-range interactions; Lévy processes and jump-diffusion models in finance and statistical physics; viscoelastic and complex materials exhibiting power-law memory effects; turbulence modeling and geophysical flow simulations; image and signal processing via fractional-order filters, regularization, and edge detection; wave propagation in complex media; and transport processes in biological systems with sub- or super-diffusive behavior. High-order numerical schemes for these operators have been developed and successfully applied in several works (see, e.g., [87, 119, 122, 138, 172]).

Based on these considerations, the current section focuses on the numerical approximation of the Caputo fractional derivative.

3.1. Grünwald–Letnikov based approximations

In this section, the definitions given in §2.1 and the remarks at the beginning of §3 are employed to give approximations of Caputo derivative. We know that if the function u has sufficient regularity, then the Riemann–Liouville and Grünwald–Letnikov derivatives are coincide. Moreover, if the initial integer-order derivatives vanish, then the Riemann–Liouville and Caputo derivatives are equivalent. Hence, using Definitions 2.4 and 2.5 implies [120]

$$ {}_0^{C}\mathcal{D}_t^\alpha u^n \approx \tau^{-\alpha} \sum_{k=0}^{n} g_k^{(\alpha)} u^{n-k}, \qquad g_k^{(\alpha)} = (-1)^k \binom{\alpha}{k}. \tag{4} $$

The coefficients $g_k^{(\alpha)}$ can alternatively be computed using the following recursive relation

$$ \begin{cases} g_0^{(\alpha)} = 1, \\ g_k^{(\alpha)} = \left(1 - \dfrac{\alpha+1}{k}\right) g_{k-1}^{(\alpha)}, \end{cases} \qquad k = 1, 2, \ldots. \tag{5} $$

The formula given in Eq. (4) is known as the *standard Grünwald–Letnikov formula*, which provides a first-order accurate estimation for any $\alpha > 0$. However, it has been observed that this formulation may lead to instability in numerical schemes when applied to FDEs with $1 < \alpha < 2$ [95, 120, 138]. To mitigate this issue, the *shifted Grünwald–Letnikov formula* is introduced as follows

$$ {}_0^{C}\mathcal{D}_t^\alpha u^n \approx \tau^{-\alpha} \sum_{k=0}^{n+p} g_k^{(\alpha)} u^{n-k+p}, \qquad p \in \mathbb{N}, \tag{6} $$

to enhance numerical stability. Tadjeran et al. [170] showed that this shifted approach, i.e. Eq. (6), is more suitable for constructing stable numerical schemes and achieves the first-order accuracy. The best performance of the shifted Grünwald–Letnikov approximation is achieved by minimizing the value $\left|p - \frac{\alpha}{2}\right|$ [91, 95, 120, 130, 134]. Furthermore, for $1 < \alpha \le 2$, the optimal choice is $p = 1$. Tian et al. [172] introduced high-order accurate approximations, weighted and shifted Grünwald–Letnikov (WSGL) formulas, for approximating the fractional Riemann–Liouville derivative. Wang and Vong [177] proposed a second-order accurate formula for approximating the Caputo fractional derivative in the case $0 < \alpha < 1$. Additionally, Ji and Sun [75] developed a third-order accurate approximation for the Caputo derivative with $\alpha \in (0,1)$. More recently, Yan et al. [180] proposed fourth-order accurate WSGL difference operators for $0 < \alpha < 1$. Based on these operators, they developed high-order time discretization schemes for time-fractional Schrödinger equations. Their approach achieves improved temporal accuracy by employing higher-order

WSGL formulations for the time-fractional derivatives.These high-order methods are frequently employed in the numerical solution of time-fractional partial differential equations. To summarize the key results and support the derivation of our time-discrete schemes, we present the following three lemmas.

Lemma 3.1 ([120, 121, 166, 170]). *Let $u \in \mathcal{S}^{1+\alpha}(\mathbb{R})$. The first-order Grünwald–Letnikov approximation to estimate the Caputo derivative operator is given by*

$$ {}_0^C\mathcal{D}_t^\alpha u^n = \tau^{-\alpha} \sum_{k=0}^{n} g_k^{(\alpha)} u^{n-k} + \mathrm{T}_n^{(\alpha)}, \qquad n \geq 1, \tag{7} $$

where the coefficients $g_k^{(\alpha)}$ can be calculated by Eq. (5), and

$$ \left| \mathrm{T}_n^{(\alpha)} \right| \leq C\tau. $$

Lemma 3.2 ([166, 172, 177]). *Assume that $u \in \mathcal{S}^{2+\alpha}(\mathbb{R})$. The second-order WSGL formula to approximate the Caputo derivative is introduced as follows*

$$ {}_0^C\mathcal{D}_t^\alpha u^n = \tau^{-\alpha} \sum_{k=0}^{n} w_k^{(\alpha)} u^{n-k} + \mathrm{T}_n^{(\alpha)}, \qquad \alpha \in (0,1), \tag{8} $$

for $n \geq 1$. The coefficients $w_k^{(\alpha)}$ can be found applying the recursive relation

$$ w_0^{(\alpha)} = 1 + \frac{\alpha}{2}, \qquad w_k^{(\alpha)} = \left(1 - \frac{(\alpha+1)(\alpha+2)}{2k}\right) g_{k-1}^{(\alpha)}, \qquad k \geq 1. $$

Besides, it can be shown that

$$ \left| \mathrm{T}_n^{(\alpha)} \right| \leq C\tau^2. $$

Lemma 3.3 ([75, 166, 172]). *The third-order WSGL formula to approximate the Caputo derivative is presented as follows*

$$ {}_0^C\mathcal{D}_t^\alpha u^n = \tau^{-\alpha} \sum_{k=0}^{n} \lambda_k^{(\alpha)} u^{n-k} + \mathrm{T}_n^{(\alpha)}, \qquad \alpha \in (0,1), \tag{9} $$

for $n \geq 1$. The coefficients $\lambda_k^{(\alpha)}$ can be found by the following recursive relation

$$ \lambda_0^{(\alpha)} = \varrho_1 g_0^{(\alpha)}, \quad \lambda_1^{(\alpha)} = \varrho_1 g_1^{(\alpha)} - \varrho_2 g_0^{(\alpha)}, \qquad \lambda_k^{(\alpha)} = \varrho_1 g_k^{(\alpha)} - \varrho_2 g_{k-1}^{(\alpha)} + \varrho_3 g_{k-2}^{(\alpha)}, \quad k \geq 2, $$

in which

$$ \varrho_1 = 1 + \frac{17}{24}\alpha + \frac{1}{8}\alpha^2, \quad \varrho_2 = \frac{11}{12}\alpha + \frac{1}{4}\alpha^2, \quad \varrho_3 = \frac{5}{24}\alpha + \frac{1}{24}\alpha^2. $$

Furthermore, if $u \in \mathcal{S}^{3+\alpha}(\mathbb{R})$, then the following bound is true

$$ \left| \mathrm{T}_n^{(\alpha)} \right| \leq C\tau^3. $$

Lemma 3.4 ([180]). *Suppose that $u \in \mathcal{S}^{4+\alpha}(\mathbb{R})$. The fourth-order WSGD approximation for the Caputo derivative can be obtained using the following formulation*

$$ {}_0^C\mathcal{D}_t^\alpha u^n = \tau^{-\alpha} \sum_{k=0}^{n} \vartheta_k^{(\alpha)} u^{n-k} + \mathrm{T}_n^{(\alpha)}, \qquad \alpha \in (0,1), \tag{10} $$

for $n \geq 1$. The coefficients $\vartheta_k^{(\alpha)}$ can be computed by the following recursive relation

$$ \vartheta_k^{(\alpha)} = \theta_1 g_k^{(\alpha)} - \theta_2 g_{k-1}^{(\alpha)} + \theta_3 g_{k-2}^{(\alpha)} - \theta_4 g_{k-3}^{(\alpha)}, \quad k \geq 3, $$

where

$$ \vartheta_0^{(\alpha)} = \theta_1 g_0^{(\alpha)}, \quad \vartheta_1^{(\alpha)} = \theta_1 g_1^{(\alpha)} - \theta_2 g_0^{(\alpha)}, \qquad \vartheta_2^{(\alpha)} = \theta_1 g_2^{(\alpha)} - \theta_2 g_1^{(\alpha)} + \theta_3 g_0^{(\alpha)}. $$

The coefficients θ_1, θ_2, θ_3 and θ_4 are given by

$$ \theta_1 = \frac{\alpha^3 + 11\alpha^2 + 40\alpha + 48}{48}, \quad \theta_2 = \frac{3\alpha^3 + 27\alpha^2 + 62\alpha}{48}, \quad \theta_3 = \frac{3\alpha^3 + 21\alpha^2 + 28\alpha}{48}, \quad \theta_4 = \frac{\alpha^3 + 5\alpha^2 + 6\alpha}{48}. $$

Additionally, the following estimation holds

$$ \left| \mathrm{T}_n^{(\alpha)} \right| \leq C\tau^4. $$

Another approach is presented in [52], where two different second-order numerical differentiation formulas are derived for the Caputo derivatives ${}_0^C\mathcal{D}_t^\alpha u(x,t)$ $(0<\alpha<1)$ and ${}_0^C\mathcal{D}_t^\beta u(x,t)$ $(1<\beta<2)$ at the point $t_{k+1/2}$. By applying these formulas to time-fractional mixed sub-diffusion and diffusion–wave equations and combining them with a fourth-order compact scheme for the spatial derivative, the author obtains a difference scheme with convergence order $\mathcal{O}(\tau^2+h^4)$, significantly improving the accuracy of existing algorithms for the same type of equations. For further details, the interested reader may refer to [52].

3.2. L–type approximations

A traditional and important approach to approximate the fractional derivatives is to use the interpolation technique. The mentioned idea gives us the *L–type approximations* for fractional derivatives. For instance, consider the Caputo derivative for $0<\alpha<1$ as follows [95, 166]

$$ {}_0^C\mathcal{D}_t^\alpha u\left(x,y,t\right)=\frac{1}{\Gamma\left(1-\alpha\right)}\int_0^t\frac{\partial_\varsigma u\left(x,y,\varsigma\right)}{\left(t-\varsigma\right)^\alpha}d\varsigma. $$

If the function $u\left(x,y,\varsigma\right)$ is approximated on each subinterval $[t_{k-1},t_k]$ by a linear interpolation polynomial, then the *L1 approximations* or *L1 formula* will be obtained. It can be proved that this approximation has the accuracy of $2-\alpha$ [63, 64, 78, 101, 109, 134, 167, 189, 199]. Gao et al. [64] introduced an approximation for the Caputo derivative, known as the *L1-2 formula*, based on a quadratic interpolation over three consecutive time points t_{k-2}, t_{k-1}, and t_k for the function $u(x,y,\varsigma)$ on each subinterval $[t_{k-1},t_k]$. They demonstrated that the resulting approximation achieves an accuracy of order $3-\alpha$. Building on a similar concept, Alikhanov [16] proposed the *L2-1$_\sigma$ formula*, also referred to as the Alikhanov scheme, which considers a time level at $n+\sigma$. He also established that this scheme attains the same accuracy order of $3-\alpha$. Furthermore, Alikhanov developed a second-order difference scheme for TFDEs. Similarly, Lv and Xu [117] employed function interpolation at three points, t_{k-1}, t_k and t_{k+1}, to construct a high-order scheme for the Caputo derivative, which attains a convergence rate of $3-\alpha$. On the other side, Li et al. [92] also developed a high-order approximation for the Caputo derivative, achieving a convergence rate of $3-\alpha$. As a continuation of their research, Cao et al. [33] proposed a $(4-\alpha)$th-order accurate algorithm for approximating the Caputo-type fractional derivative. Subsequently, Li et al. [96] further extended this work by developing a high-order algorithm with a local truncation error of $\mathcal{O}(\tau^{r+1-\alpha})$, where r denotes the degree of interpolation. Mokhtari and Mostajeran [127] proposed a modification of the L1-2 formula by developing a new approximation based on a third-degree interpolation technique at four points: t_{k-3}, t_{k-2}, t_{k-1}, and t_k. The resulting scheme, referred to as the *L1-2-3 formula*, was shown to achieve a local truncation error of order $\mathcal{O}(\tau^{4-\alpha})$. Another class of existing methods in the literature is based on B-spline interpolation. For further details and developments in this direction, the interested reader is referred to [145].

In the following sections, and to summarize the preceding discussion, we focus exclusively on four L–type approximation schemes: the L1, L1-2, L2-1$_\sigma$, and L1-2-3 schemes. The corresponding lemmas for each methodology are presented below.

Lemma 3.5 ([91, 95, 166]). *The L1 formula for approximating Caputo fractional derivative with $0<\alpha<1$, is presented as follows*

$$ {}_0^C\mathcal{D}_t^\alpha u^n=\left(a_0^{(\alpha)}u^n-\sum_{k=1}^{n-1}\left(a_{n-k-1}^{(\alpha)}-a_{n-k}^{(\alpha)}\right)u^k-a_{n-1}^{(\alpha)}u^0\right)+\mathrm{T}_n^{(\alpha)},\qquad n\geq 1, $$

or equivalently

$$ {}_0^C\mathcal{D}_t^\alpha u^n={}_0^C\mathrm{D}_t^\alpha u^n+\mathrm{T}_n^{(\alpha)}, \tag{11} $$

where

$$ {}_0^C\mathrm{D}_t^\alpha u^n:=\sum_{k=1}^{n}a_{n-k}^{(\alpha)}\delta u^k,\qquad \delta u^k:=u^k-u^{k-1}, $$

and the coefficients a_k are given by

$$ a_k^{(\alpha)}=\frac{\tau^{-\alpha}}{\Gamma\left(2-\alpha\right)}\left((k+1)^{1-\alpha}-k^{1-\alpha}\right). \tag{12} $$

Moreover, if $u\in\mathcal{C}^2[0,T]$, then the following bound is true

$$ \left|\mathrm{T}_n^{(\alpha)}\right|\leq C\tau^{2-\alpha}. $$

Lemma 3.6 ([64, 166]). *Let $\alpha \in (0,1)$. The L1-2 formula for estimating Caputo derivative is given as follows*

$$ {}_0^C\mathcal{D}_t^\alpha u^n = \left(c_0^{(\alpha)} u^n - \sum_{k=1}^{n-1} \left(c_{n-k-1}^{(\alpha)} - c_{n-k}^{(\alpha)} \right) u^k - c_{n-1}^{(\alpha)} u^0 \right) + \mathrm{T}_n^{(\alpha)}, $$

or

$$ {}_0^C\mathcal{D}_t^\alpha u^n = {}_0^C\mathrm{D}_t^\alpha u^n + \mathrm{T}_n^{(\alpha)}, \tag{13} $$

where

$$ {}_0^C\mathrm{D}_t^\alpha u^n := \sum_{k=1}^{n} c_{n-k}^{(\alpha)} \delta u^k, \qquad \delta u^k := u^k - u^{k-1}. $$

The coefficients $c_{n-k}^{(\alpha)}$ can be presented as follows

$$ c_k^{(\alpha)} = \frac{\tau^{-\alpha}}{\Gamma(2-\alpha)} \begin{cases} a_0^{(\alpha)} + b_0^{(\alpha)}, & k = 0, \\ a_k^{(\alpha)} + b_k^{(\alpha)} - b_{k-1}^{(\alpha)}, & 1 \le k \le n-2, \\ a_k^{(\alpha)} - b_{k-1}^{(\alpha)}, & k = n-1, \end{cases} $$

for $n \ge 1$, and if $n = 0$, then $c_0^{(\alpha)} = 1$. The coefficients $a_k^{(\alpha)}$ and $b_k^{(\alpha)}$ are given by Eq. (12) and

$$ b_k^{(\alpha)} = \frac{1}{2-\alpha} \left((k+1)^{2-\alpha} - k^{2-\alpha} \right) - \frac{1}{2} \left((k+1)^{1-\alpha} + k^{1-\alpha} \right), \quad k \ge 0, \tag{14} $$

respectively. Additionally, if $u \in \mathcal{C}^3[0,T]$, then

$$ \left| \mathrm{T}_n^{(\alpha)} \right| \le C\tau^{3-\alpha}. $$

Lemma 3.7 ([16, 62, 166]). *Assume that $\sigma = 1 - \frac{\alpha}{2}$ and $\alpha \in (0,1)$. The L2-1$_\sigma$ approximation for Caputo derivative is introduced by*

$$ {}_0^C\mathcal{D}_t^\alpha u^{n+\sigma} = {}_0^C\mathrm{D}_t^\alpha u^{n+\sigma} + \mathrm{T}_{n+\sigma}^{(\alpha)}, \tag{15} $$

in which

$$ {}_0^C\mathrm{D}_t^\alpha u^{n+\sigma} := \sum_{k=0}^{n} c_{n-k}^{(n)} \delta u^k, \qquad \delta u^k := u^{k+1} - u^k. $$

The coefficients $c_{n-k}^{(n)}$ can be presented as follows

$$ c_k^{(n)} = \frac{\tau^{-\alpha}}{\Gamma(2-\alpha)} \begin{cases} a_0^{(\sigma,\alpha)} + b_1^{(\sigma,\alpha)}, & k = 0, \\ a_k^{(\sigma,\alpha)} + b_{k+1}^{(\sigma,\alpha)} - b_k^{(\sigma,\alpha)}, & 1 \le k \le n-1, \\ a_k^{(\sigma,\alpha)} - b_k^{(\sigma,\alpha)}, & k = n, \end{cases} $$

for $n \ge 1$, and for $n = 0$, we have $c_0^{(0)} = \frac{\tau^{-\alpha}}{\Gamma(2-\alpha)} \sigma^{1-\alpha}$. The coefficients $a_k^{(\sigma,\alpha)}$ and $b_k^{(\sigma,\alpha)}$ are also formulated as follows

$$ b_k^{(\sigma,\alpha)} = \frac{1}{2-\alpha} \left[(k+\sigma)^{2-\alpha} - (k-1+\sigma)^{2-\alpha} \right] - \frac{1}{2} \left[(k+\sigma)^{1-\alpha} + (k-1+\sigma)^{1-\alpha} \right], \quad k \ge 1. $$

$$ a_0^{(\sigma,\alpha)} = \sigma^{1-\alpha}, \quad a_k^{(\sigma,\alpha)} = (k+\sigma)^{1-\alpha} - (k-1+\sigma)^{1-\alpha}, \quad k \ge 1. $$

Moreover, if $u \in \mathcal{C}^3[0,T]$, then the following estimate holds for the error term

$$ \left| \mathrm{T}_n^{(\alpha)} \right| \le C\tau^{3-\alpha}. $$

Lemma 3.8 ([16]). *Under the assumptions of Lemma 3.7, the following equality is true*

$$ u(x,y,t_{n+\sigma}) = \sigma u(x,y,t_{n+1}) + (1-\sigma) u(x,y,t_n) + \mathcal{O}\left(\tau^2\right). $$

Lemma 3.9 ([127, 144, 155]). *The L1-2-3 formula for Caputo fractional derivative is defined as follows*

$$ {}_0^C\mathcal{D}_t^\alpha u^n = \left(d_0^{(\alpha)} u^n - \sum_{k=1}^{n-1} \left(d_{n-k-1}^{(\alpha)} - d_{n-k}^{(\alpha)} \right) u^k - d_{n-1}^{(\alpha)} u^0 \right) + \mathrm{T}_n^{(\alpha)}, \qquad n \geq 1, $$

or equivalently

$$ {}_0^C\mathcal{D}_t^\alpha u\left(\mathbf{x}, t_n\right) = {}^C\mathrm{D}_N^\alpha u^n + \mathcal{R}_n^{(\alpha)}, \qquad 0 < \alpha < 1, \tag{16} $$

where the notation ${}^C\mathrm{D}_N^\alpha u^n$ is defined by

$$ {}^C\mathrm{D}_N^\alpha u^n := \sum_{k=0}^{n} d_{n-k}^{(\alpha)} \delta u^k, \qquad \delta u^k := u^k - u^{k-1}. $$

The coefficients $d_{n-k}^{(\alpha)}$ can be computed by

$$ d_k^{(\alpha)} = \frac{\tau^{-\alpha}}{\Gamma(2-\alpha)} \begin{cases} a_k^{(\alpha)} + b_k^{(\alpha)} + \tilde{c}_k^{(\alpha)}, & k = 0, \\ a_k^{(\alpha)} + b_k^{(\alpha)} - b_{k-1}^{(\alpha)} + \tilde{c}_k^{(\alpha)} - 2\tilde{c}_{k-1}^{(\alpha)}, & k = 1, \\ a_k^{(\alpha)} + b_k^{(\alpha)} - b_{k-1}^{(\alpha)} + \tilde{c}_k^{(\alpha)} - 2\tilde{c}_{k-1}^{(\alpha)} + \tilde{c}_{k-2}^{(\alpha)}, & 2 \leq k \leq n-3, \\ a_k^{(\alpha)} + b_k^{(\alpha)} - b_{k-1}^{(\alpha)} - 2\tilde{c}_{k-1}^{(\alpha)} + \tilde{c}_{k-2}^{(\alpha)}, & k = n-2, \\ a_k^{(\alpha)} - b_{k-1}^{(\alpha)} + \tilde{c}_{k-2}^{(\alpha)}, & k = n-1, \end{cases} $$

for $n \geq 4$. For $n = 1$, it is $d_0^{(\alpha)} = \dfrac{\tau^{-\alpha}}{\Gamma(2-\alpha)}$, for $n = 2$

$$ d_0^{(\alpha)} = \frac{\tau^{-\alpha}}{\Gamma(2-\alpha)} \left(a_0^{(\alpha)} + b_0^{(\alpha)} \right), \qquad d_1^{(\alpha)} = \frac{\tau^{-\alpha}}{\Gamma(2-\alpha)} \left(a_1^{(\alpha)} - b_0^{(\alpha)} \right), $$

and then for $n = 3$

$$ d_k^{(\alpha)} = \frac{\tau^{-\alpha}}{\Gamma(2-\alpha)} \begin{cases} a_k^{(\alpha)} + b_k^{(\alpha)} + \tilde{c}_k^{(\alpha)}, & k = 0, \\ a_k^{(\alpha)} + b_k^{(\alpha)} - b_{k-1}^{(\alpha)} - 2\tilde{c}_{k-1}^{(\alpha)}, & k = 1, \\ a_k^{(\alpha)} - b_{k-1}^{(\alpha)} + \tilde{c}_{k-2}^{(\alpha)}, & k = 2, \end{cases} $$

where the coefficients $a_k^{(\alpha)}$ and $b_k^{(\alpha)}$ are given by Eqs. (12) and (14) respectively, and also the coefficients $\tilde{c}_k^{(\alpha)}$ can be calculated as follows

$$ \tilde{c}_k^{(\alpha)} = \frac{1}{(2-\alpha)(3-\alpha)} \left((k+1)^{3-\alpha} + 2k^{3-\alpha} \right) - \frac{1}{2-\alpha} k^{2-\alpha} - \frac{1}{6} \left((k+1)^{1-\alpha} + 2k^{1-\alpha} \right), \quad k \geq 0. $$

Furthermore, if $u \in \mathcal{C}^4[0,T]$, then the following estimate is hold

$$ \left| \mathrm{T}_n^{(\alpha)} \right| \leq C\tau^{4-\alpha}. $$

The table below summarizes typical convergence orders, stability properties, and computational complexity for the mentioned numerical schemes used to discretize Caputo derivative. It includes the L-type temporal methods and WSGL formulas, plus related high-order techniques for comparison.

High-order numerical schemes for non-local fractional operators, such as L-type methods for time-fractional derivatives and Grünwald–Letnikov based operators for space-fractional derivatives, face significant implementation challenges due to their intrinsic history dependence and global coupling. In time-fractional problems, methods like L1, L2-1$_\sigma$, and higher-order L-type schemes require storing all previous time levels to evaluate the fractional derivative, leading to $\mathcal{O}(N^2)$ computational cost and memory usage for N time steps, which becomes particularly burdensome in long-time simulations or multidimensional problems [16, 80]. Similarly, space-fractional operators involve dense or Toeplitz-like matrices, as the fractional Laplacian couples all spatial points, resulting in high memory and computational demands that grow rapidly with the number of grid points in multiple dimensions [163, 172]. Strategies to mitigate these costs include fast convolution techniques such as sum-of-exponentials approximations for temporal history terms, fast fourier transform-based matrix-vector products for Toeplitz structures in space,

Table 1: Comparison of L-type schemes.

Scheme	Convergence	Stability	Computational Complexity
L1	$\mathcal{O}(\tau^{2-\alpha})$ (smooth) / $\mathcal{O}(\tau)$ (nonsmooth)	Unconditional	$\mathcal{O}(N^2)$ direct; $\mathcal{O}(N\log N)$ with fast convolution method.
L1-2	$\mathcal{O}(\tau^{3-\alpha})$ (approximation accuracy) / $\mathcal{O}(\tau^2)$ (PDE solution accuracy)	Unconditional	Same as L1; fast convolution or fast history techniques recommended.
L2-1_σ	$\mathcal{O}(\tau^2)$	Unconditional	Same as L1; sum-of-exponentials reduces memory and complexity.
L1-2-3	$\mathcal{O}(\tau^{4-\alpha})$	Unconditional	Same as L1.

Table 2: Comparison of GL and WSGL schemes.

Scheme	Convergence	Stability	Computational Complexity
Standard Grünwald–Letnikov	$\mathcal{O}(\tau)$	Unstable for $\alpha \in (1,2)$	$\mathcal{O}(N^2)$ direct; $\mathcal{O}(N\log N)$ with fast convolution.
Shifted Grünwald–Letnikov	$\mathcal{O}(\tau)$	Improved stability	$\mathcal{O}(N^2)$ direct; $\mathcal{O}(N)$ with optimized recurrence.
WSGL (2nd order)	$\mathcal{O}(\tau^2)$	Unconditional	Fast convolution yields $\mathcal{O}(N\log N)$.
WSGL (3rd order)	$\mathcal{O}(\tau^3)$	Unconditional	Same as second-order WSGL.
WSGL (4th order)	$\mathcal{O}(\tau^4)$	Unconditional	Same as second-order WSGL.

and low-rank or hierarchical matrix compression [77, 163]. Despite these advances, achieving both high-order accuracy and computational efficiency remains challenging, particularly for multi-dimensional problems with complex geometries and irregular meshes, requiring careful algorithm design and trade-offs between accuracy, stability, and memory usage.

Based on these considerations, the following flowchart guides the selection of an appropriate numerical method.

In the upcoming sections, we investigate the TFDE by applying the aforementioned methods to discretize the Caputo derivative. Additionally, we review various approaches for the spatial discretization.

4. Compact finite difference method for TFDEs

In this section, we employ the lemmas introduced in §3.2 and §3.1 for the temporal discretization, while adopting the fourth-order compact finite difference scheme for the spatial discretization. To this end, we first define uniform partitions in both the temporal and spatial directions as follows

$$t_n = n\tau, \quad \tau = \frac{T}{N}, \quad N \in \mathbb{N}, \quad n = 0, 1, 2, \ldots, N,$$

and

$$x_i = a + ih_x, \quad h_x = \frac{b-a}{M_x}, \quad M_x \in \mathbb{N}, \quad i = 0, 1, 2, \ldots, M_x,$$

$$y_j = a + jh_y, \quad h_y = \frac{b-a}{M_y}, \quad M_y \in \mathbb{N}, \quad j = 0, 1, 2, \ldots, M_y.$$

In addition, the second-order midpoint formulas in x- and y-directions are presented as [29, 65, 140, 164]

$$\partial_x^2 u_{i,j} = \frac{u_{i+1,j} - 2u_{i,j} + u_{i-1,j}}{h_x^2} + \mathcal{O}\left(h_x^2\right), \qquad \partial_y^2 u_{i,j} = \frac{u_{i,j+1} - 2u_{i,j} + u_{i,j-1}}{h_y^2} + \mathcal{O}\left(h_y^2\right), \tag{17}$$

where $u(x_i, y_j, t) = u_{i,j}$. The following compact operators are also introduced by

$$H_x u_{i,j} := \left(I + \frac{h_x^2}{12}\partial_x^2\right) u_{i,j}, \quad H_y u_{i,j} := \left(I + \frac{h_y^2}{12}\partial_x^2\right) u_{i,j}, \tag{18}$$

and also denote

$$H u_{i,j} = H_x H_y u_{i,j}, \quad L u_{i,j} = \left(\partial_x^2 H_y + \partial_y^2 H_x\right) u_{i,j}. \tag{19}$$

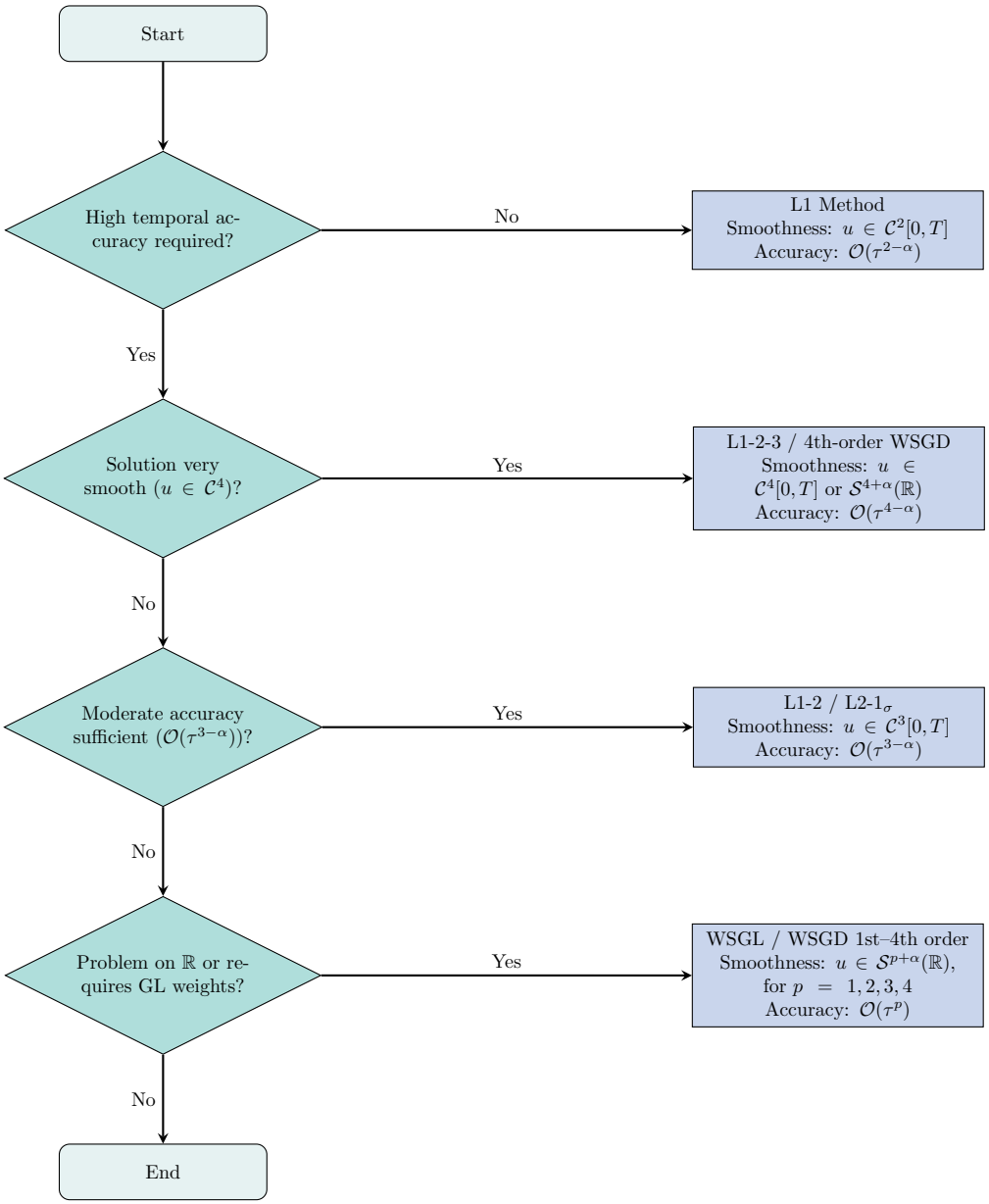

Figure 1: Flowchart guiding the selection of numerical methods for approximating Caputo fractional derivatives based on desired accuracy, solution smoothness, and computational considerations.

Now, suppose that $u \in \mathcal{C}_{x,y}^{6,6}(\Omega)$. Then, as shown in [73, 198], the following fourth-order accurate compact finite difference approximations hold:

$$H_x \frac{\partial^2 u_{i,j}}{\partial x^2} = \partial_x^2 u_{i,j} + \mathcal{O}\left(h_x^4\right), \quad H_y \frac{\partial^2 u_{i,j}}{\partial y^2} = \partial_y^2 u_{i,j} + \mathcal{O}\left(h_y^4\right). \tag{20}$$

With these results and the notations previously introduced, we are now prepared to derive the matrix formulation of the compact difference scheme.

4.1. Numerical methodologies

4.1.1. Grünwald–Letnikov based schemes

Let us consider Eq. (1). By applying the first-order accurate Grünwald–Letnikov approximation from Eq. (7) to the time-fractional derivative, and utilizing the second-order finite difference formula given in Eq. (17) for the spatial direction, one obtains

$$\tau^{-\alpha} g_0^{(\alpha)} u_{i,j}^n - \varepsilon \left(\partial_x^2 I_y + \partial_y^2 I_x\right) u_{i,j}^n + \mathcal{O}(\tau) + \mathcal{O}\left(h_x^2\right) + \mathcal{O}\left(h_y^2\right) = f_{i,j}^n - \tau^{-\alpha} \sum_{k=1}^{n} g_k^{(\alpha)} u_{i,j}^{n-k}.$$

Utilizing the compact difference operator results

$$\tau^{-\alpha} g_0^{(\alpha)} H u_{i,j}^n - \varepsilon L u_{i,j}^n + \mathrm{T}^{(n)} = H f_{i,j}^n - \tau^{-\alpha} \sum_{k=1}^{n} g_k^{(\alpha)} H u_{i,j}^{n-k}, \tag{21}$$

where

$$\left|\mathrm{T}^{(n)}\right| \leq C\left(\tau + h_x^4 + h_y^4\right).$$

Dropping the truncation error and rewriting Eq. (21) in the matrix form, concludes

$$\mathcal{A} U^n = \mathcal{F}^{(n)}, \qquad 1 \leq n \leq N, \tag{22}$$

in which

$$\mathcal{A} = \tau^{-\alpha} g_0^{(\alpha)} H - \varepsilon L,$$

$$\mathcal{F}^{(n)} = H F^n - \tau^{-\alpha} \sum_{k=1}^{n} g_k^{(\alpha)} H U^{n-k},$$

and

$$L = \left(D_x \otimes \bar{H}\right) + \left(\bar{H} \otimes D_y\right), \quad H = \bar{H} \otimes \bar{H}. \tag{23}$$

Also,

$$\bar{H} = \begin{bmatrix} \frac{10}{12} & \frac{1}{12} & 0 & \cdots & 0 \\ \frac{1}{12} & \frac{10}{12} & \frac{1}{12} & \ddots & \vdots \\ 0 & \frac{1}{12} & \frac{10}{12} & \ddots & 0 \\ \vdots & \ddots & \ddots & \ddots & \frac{1}{12} \\ 0 & \cdots & 0 & \frac{1}{12} & \frac{10}{12} \end{bmatrix}, D_x = \frac{1}{h_x^2} \begin{bmatrix} -2 & 1 & 0 & \cdots & 0 \\ 1 & -2 & 1 & \ddots & \vdots \\ 0 & 1 & -2 & \ddots & 0 \\ \vdots & \ddots & \ddots & \ddots & 1 \\ 0 & \cdots & 0 & 1 & -2 \end{bmatrix}, D_y = \frac{1}{h_y^2} \begin{bmatrix} -2 & 1 & 0 & \cdots & 0 \\ 1 & -2 & 1 & \ddots & \vdots \\ 0 & 1 & -2 & \ddots & 0 \\ \vdots & \ddots & \ddots & \ddots & 1 \\ 0 & \cdots & 0 & 1 & -2 \end{bmatrix}.$$

Applying the second-order WSGL approximation Eq. (8), along with the spatial discretizations given in Eqs. (17)–(20), to Eq. (1), yields

$$\tau^{-\alpha} \sum_{k=0}^{n} w_k^{(\alpha)} H u_{i,j}^{n-k} - \varepsilon L u_{i,j}^n + \mathrm{T}^{(n)} = H f_{i,j}^n, \tag{24}$$

with the error term

$$\left|\mathrm{T}^{(n)}\right| \leq C\left(\tau^2 + h_x^4 + h_y^4\right).$$

Neglecting the error and rewriting Eq. (24) in the following matrix form

$$\mathcal{A} U^n = \mathcal{F}^{(n)}, \qquad 1 \leq n \leq N, \tag{25}$$

where

$$\mathcal{A} = \tau^{-\alpha} w_0^{(\alpha)} H - \varepsilon L,$$

$$\mathcal{F}^{(n)} = H F^n - \tau^{-\alpha} \sum_{k=1}^{n} w_k^{(\alpha)} H U^{n-k},$$

and the matrices H and L are presented by Eq. (23). Similarly, for the third-order WSGL formula, one has

$$\tau^{-\alpha} \sum_{k=0}^{n} \lambda_k^{(\alpha)} H u_{i,j}^{n-k} - \varepsilon L u_{i,j}^n + \mathrm{T}^{(n)} = H f_{i,j}^n,$$

where

$$\left|\mathrm{T}^{(n)}\right| \leq C\left(\tau^3 + h_x^4 + h_y^4\right),$$

and by omitting the error the following matrix form can be obtained

$$\mathcal{A} U^n = \mathcal{F}^{(n)}, \qquad 1 \leq n \leq N, \tag{26}$$

in which

$$\mathcal{A} = \tau^{-\alpha}\lambda_0^{(\alpha)} H - \varepsilon L,$$

$$\mathcal{F}^{(n)} = HF^n - \tau^{-\alpha}\sum_{k=1}^{n} \lambda_k^{(\alpha)} HU^{n-k}.$$

Applying fourth-order WSGL approximation gives the following scheme

$$\tau^{-\alpha}\sum_{k=0}^{n} \vartheta_k^{(\alpha)} Hu_{i,j}^{n-k} - \varepsilon L u_{i,j}^n + \mathrm{T}^{(n)} = Hf_{i,j}^n,$$

where the truncation error can be estimated as

$$\left|\mathrm{T}^{(n)}\right| \leq C\left(\tau^4 + h_x^4 + h_y^4\right),$$

and if we drop the truncation error, the following system can be concluded

$$\mathcal{A}U^n = \mathcal{F}^{(n)}, \qquad 1 \leq n \leq N, \tag{27}$$

with the following LHS matrix and RHS vector

$$\mathcal{A} = \tau^{-\alpha}\vartheta_0^{(\alpha)} H - \varepsilon L,$$

$$\mathcal{F}^{(n)} = HF^n - \tau^{-\alpha}\sum_{k=1}^{n} \vartheta_k^{(\alpha)} HU^{n-k}.$$

4.1.2. L–type schemes

In this section, we focus on the derivation of difference schemes based on the L–type approximations. By substituting Eq. (11) and Eqs. (17)–(20) into Eq. (1), we obtain

$$\sum_{k=1}^{n} b_{n-k}^{(\alpha)} \delta H u_{i,j}^k - \varepsilon L u_{i,j}^n + \mathrm{T}^{(n)} = Hf_{i,j}^n,$$

where the truncation error satisfies

$$\left|\mathrm{T}^{(n)}\right| \leq \mathcal{C}\left(\tau^{2-\alpha} + h_x^4 + h_y^4\right).$$

Neglecting the truncation error and performing standard algebraic manipulations, we arrive at the following matrix formulation

$$\mathcal{A}U^n = \mathcal{F}^{(n)}, \qquad 1 \leq n \leq N, \tag{28}$$

where

$$\mathcal{A} = a_0^{(\alpha)} H - \varepsilon L,$$

$$\mathcal{F}^{(n)} = a_0^{(\alpha)} HU^{n-1} - \sum_{k=1}^{n-1} a_{n-k}^{(\alpha)} \delta HU^k + HF^n,$$

and matrices H and L are previously defined by Eq. (23). Following a similar procedure as in the previous case, we derive a difference scheme based on the L1-2 approximation. By substituting Eq. (13) and Eqs. (17)–(20) into Eq. (1), we obtain

$$\sum_{k=1}^{n} c_{n-k}^{(\alpha)} \delta H u_{i,j}^k - \varepsilon L u_{i,j}^n + \mathrm{T}^{(n)} = Hf_{i,j}^n,$$

where the truncation error satisfies

$$\left|\mathrm{T}^{(n)}\right| \leq \mathcal{C}\left(\tau^{3-\alpha} + h_x^4 + h_y^4\right).$$

Dropping the truncation error term, the resulting matrix formulation becomes

$$\mathcal{A}U^n = \mathcal{F}^{(n)}, \qquad 1 \leq n \leq N, \tag{29}$$

where

$$\mathcal{A} = c_0^{(\alpha)} H - \varepsilon L,$$

$$\mathcal{F}^{(n)} = c_0^{(\alpha)} H U^{n-1} - \sum_{k=1}^{n-1} c_{n-k}^{(\alpha)} \delta H U^k + H F^n.$$

The matrices H and L are defined as in Eq. (23). Similarly, for the L2-1_σ scheme, by substituting the corresponding relations into Eq. (1), we obtain

$$\sum_{k=0}^{n} c_{n-k}^{(n)} \delta H u_{i,j}^k - \varepsilon L u_{i,j}^{n+\sigma} + \mathrm{T}^{(n+\sigma)} = H f_{i,j}^{n+\sigma},$$

where the truncation error satisfies

$$\left|\mathrm{T}^{(n+\sigma)}\right| \leq \mathcal{C}\left(\tau^2 + h_x^4 + h_y^4\right).$$

Discarding the truncation error term, the matrix form of the scheme becomes

$$\mathcal{A} U^{n+1} = \mathcal{F}^{(n+\sigma)}, \quad 0 \leq n \leq N-1, \tag{30}$$

with

$$\mathcal{A} = c_0^{(n)} H - \varepsilon \sigma L,$$

$$\mathcal{F}^{(n+\sigma)} = c_0^{(n)} H U^n - \sum_{k=0}^{n-1} c_{n-k}^{(n)} \delta H U^k + \varepsilon\left(1-\sigma\right) L U^n + \sigma H F^{n+1} + \left(1-\sigma\right) H F^n.$$

Now, using the L1-2-3 formula to approximate the Caputo derivative in Eq. (1), one concludes

$$\sum_{k=1}^{n} d_{n-k}^{(\alpha)} \delta H u_{i,j}^k - \varepsilon L u_{i,j}^n + \mathrm{T}^{(n)} = H f_{i,j}^n,$$

with the associated truncation error bounded by

$$\left|\mathrm{T}^{(n)}\right| \leq \mathcal{C}\left(\tau^{4-\alpha} + h_x^4 + h_y^4\right).$$

Omitting the truncation error, the scheme can be expressed in matrix form as

$$\mathcal{A} U^n = \mathcal{F}^{(n)}, \quad 1 \leq n \leq N, \tag{31}$$

where

$$\mathcal{A} = d_0^{(\alpha)} H - \varepsilon L,$$

$$\mathcal{F}^{(n)} = d_0^{(\alpha)} H U^{n-1} - \sum_{k=1}^{n-1} d_{n-k}^{(\alpha)} \delta H U^k + H F^n.$$

4.2. Theoretical claims

In this section, we present the stability and convergence theorems corresponding to the derived numerical schemes. Since the proofs of these theorems are well-established in the literature and the underlying ideas are similar across various works, we omit the detailed proofs and instead refer the reader to the relevant references. It is important to note that the solvability of these compact differences schemes can be found in the corresponding references.

Theorem 4.1 ([35, 38]). *The compact difference scheme (22) is unconditionally stable.*

Following the same idea, given in Refs. [35, 38, 76, 166], the following theorems can also be proved.

Theorem 4.2 ([76, 166, 180]). *The compact difference schemes (25), (26) and (27) are unconditionally stable to the initial values.*

Theorem 4.3 ([35, 38]). *Let U^n be the approximate solution of exact solution u^n, obtained by scheme (22), and $u(x,y,t) \in \mathcal{S}^{1+\alpha}(\mathbb{R})$. Hence, there exists a constant $C > 0$, independent of τ, h_x and h_y such that*

$$\|u^n - U^n\| \leq C\left(\tau + h_x^4 + h_y^4\right), \qquad 1 \leq n \leq N.$$

Theorem 4.4 ([166]). *Assume that U^n is the estimation of the analytic solution u^n, computed by scheme (25), and $u(x,y,t) \in \mathcal{S}^{2+\alpha}(\mathbb{R})$. Therefore, there exists a positive constant C, independent of τ, h_x and h_y with*

$$\|u^n - U^n\| \leq C\left(\tau^2 + h_x^4 + h_y^4\right), \qquad 1 \leq n \leq N.$$

Theorem 4.5 ([75, 76]). *If U^n is obtained by solving the system, given in Eq. (26), and $u(x,y,t) \in \mathcal{S}^{3+\alpha}(\mathbb{R})$, then there exists a $C > 0$, independent of τ, h_x and h_y such that*

$$\|u^n - U^n\| \leq C\left(\tau^3 + h_x^4 + h_y^4\right), \qquad 1 \leq n \leq N.$$

Theorem 4.6 ([75, 180]). *Suppose that U^n is the numerical solution generated by the scheme described in Eq. (27), and let $u(x,y,t) \in \mathcal{S}^{4+\alpha}(\mathbb{R})$. Then, there exists a constant $C > 0$, independent of τ, h_x, and h_y, such that*

$$\|u^n - U^n\| \leq C\left(\tau^4 + h_x^4 + h_y^4\right), \qquad 1 \leq n \leq N.$$

In what follows, we present the stability and convergence theorems of L–type schemes.

Theorem 4.7 ([63, 166, 205]). *The implicit difference scheme, given by (28) is unconditionally stable.*

Theorem 4.8 ([16, 95, 142, 166]). *The implicit difference schemes, introduced by (29), (30) and (31) are unconditionally stable.*

Theorem 4.9 ([63, 166, 205]). *Suppose U^n is computed by Eq. (28), and $u \in \mathcal{C}^2[0,T]$. Therefore, there exists a $C > 0$, independent of τ, h_x and h_y such that*

$$\|u^n - U^n\| \leq C\left(\tau^{2-\alpha} + h_x^4 + h_y^4\right), \qquad 1 \leq n \leq N.$$

Theorem 4.10 ([166]). *Let $u \in \mathcal{C}^3[0,T]$ and U^n, which is obtained by Eq. (29) is the approximation of u^n. Then, there exists a positive constant, say C, independent of τ, h_x and h_y subject to*

$$\|u^n - U^n\| \leq C\left(\tau^{3-\alpha} + h_x^4 + h_y^4\right), \qquad 1 \leq n \leq N.$$

Theorem 4.11 ([16, 166]). *If $u \in \mathcal{C}^3[0,T]$ and U^n, found by Eq. (30) is the estimation of u^n, then there exists a positive C, independent of τ, h_x and h_y with*

$$\|u^n - U^n\| \leq C\left(\tau^2 + h_x^4 + h_y^4\right), \qquad 1 \leq n \leq N.$$

Theorem 4.12. *Assume $u \in \mathcal{C}^4[0,T]$ and U^n is the solution of system (31). Thus, there exists a positive constant C, independent of τ, h_x and h_y such that*

$$\|u^n - U^n\| \leq C\left(\tau^{4-\alpha} + h_x^4 + h_y^4\right), \qquad 1 \leq n \leq N.$$

4.3. Numerical tests

This section presents a series of numerical experiments to validate the theoretical results established in §4.2. All simulations are performed using MATLAB R2024b on a Windows 11 Pro (64-bit) system equipped with an Intel(R) Core i5 (11th generation) processor running at 2.40 GHz and 8 GB of RAM. In all tests of this manuscript, the temporal and spatial discretizations are chosen such that the number of time steps and spatial nodes are equal, i.e., $N = M$. To evaluate the accuracy of the numerical scheme, the computational order (CO) is computed using the following formula

$$\mathrm{CO} \approx \frac{\log\left(\dfrac{\mathcal{E}_i}{\mathcal{E}_{i+1}}\right)}{\log\left(\dfrac{h_i}{h_{i+1}}\right)},$$

where $\mathcal{E}_i$ and $\mathcal{E}_{i+1}$ denote the $\mathcal{L}^2$-errors corresponding to successive spatial step sizes h_i and h_{i+1}, respectively.

Example 4.1. In this test, we consider the spatial domain $\Omega = [-5,5]^2$ with spatial step size $h = \dfrac{10}{M}$, where $M_x = M_y = M$, and set $T = 1$. The exact solution is given by

$$u(x,y,t) = t^p \operatorname{sech}(x)\operatorname{sech}(y),$$

and the corresponding source term is

$$f(x,y,t) = \left(\frac{\Gamma(p+1)}{\Gamma(p+1-\alpha)} t^{p-\alpha} - 2t^p \left[\tanh^2(x) + \tanh^2(y) - 1 \right] \right) \operatorname{sech}(x) \operatorname{sech}(y).$$

Tables 3–10 report the numerical results for different scenarios. Table 3 presents the results for Eq. (1) solved using scheme (22) for $\alpha = 0.1, 0.5, 0.9$, demonstrating agreement with the theoretical convergence order (TCO) predicted by Theorem 4.3. Table 4 shows the results for scheme (25) with $\alpha = 0.2, 0.5, 0.8$, also confirming the TCO from Theorem 4.4. Table 5 reports the results for scheme (26) with $\alpha = 0.25, 0.5, 0.75$, achieving the expected third-order accuracy predicted by Theorem 4.5; a visual illustration corresponding to $M = 64$ and $\alpha = 0.25$ is provided in Fig. 2. There is also Table 6 which reports the findings for scheme (27) with $\alpha = 0.3, 0.6, 0.9$, achieving the expected fourth-order accuracy provided by Theorem 4.6.

Table 3: Numerical findings for Example 4.1 with $p = 2$ and $\varepsilon = 0.1$.

	$\alpha = 0.1$		$\alpha = 0.5$		$\alpha = 0.9$	
M	$\mathcal{L}^2$	CO	$\mathcal{L}^2$	CO	$\mathcal{L}^2$	CO
4	2.6256×10^{-2}	–	4.1362×10^{-2}	–	5.7732×10^{-2}	–
8	5.3295×10^{-3}	2.3006	1.2608×10^{-2}	1.7140	2.0770×10^{-2}	1.4749
16	1.1147×10^{-3}	2.2573	5.5879×10^{-3}	1.1739	1.0208×10^{-2}	1.0248
32	5.5717×10^{-4}	1.0005	2.8829×10^{-3}	0.9548	5.2633×10^{-3}	0.9557
64	2.8600×10^{-4}	0.9621	1.4669×10^{-3}	0.9747	2.6743×10^{-3}	0.9768
TCO		1.0000		1.0000		1.0000

Table 4: Numerical findings for Example 4.1 with $p = 3$ and $\varepsilon = \frac{1}{\sqrt{4\pi^2}}$.

	$\alpha = 0.2$		$\alpha = 0.5$		$\alpha = 0.8$	
M	$\mathcal{L}^2$	CO	$\mathcal{L}^2$	CO	$\mathcal{L}^2$	CO
4	3.3368×10^{-2}	–	3.0165×10^{-2}	–	3.0561×10^{-2}	–
8	6.0465×10^{-3}	2.4643	5.5323×10^{-3}	2.4469	5.8105×10^{-3}	2.3949
16	4.1030×10^{-4}	3.8813	6.3130×10^{-4}	3.1315	1.0289×10^{-3}	2.4975
32	5.2135×10^{-5}	2.9763	1.4282×10^{-4}	2.1441	2.6047×10^{-4}	1.9819
64	1.2460×10^{-5}	2.0650	3.6234×10^{-5}	1.9788	6.6613×10^{-5}	1.9673
TCO		2.0000		2.0000		2.0000

Table 5: Numerical findings for Example 4.1 with $p = 4$ and $\varepsilon = 0.01$.

	$\alpha = 0.25$		$\alpha = 0.5$		$\alpha = 0.75$	
M	$\mathcal{L}^2$	CO	$\mathcal{L}^2$	CO	$\mathcal{L}^2$	CO
4	4.1107×10^{-3}	–	6.5936×10^{-3}	–	9.9828×10^{-3}	–
8	6.1895×10^{-4}	2.7315	8.5852×10^{-4}	2.9411	1.2825×10^{-3}	2.9605
16	6.0885×10^{-5}	3.3457	1.0044×10^{-4}	3.0955	1.6746×10^{-4}	2.9371
32	5.8256×10^{-6}	3.3856	1.2677×10^{-5}	2.9862	2.2104×10^{-5}	2.9214
64	6.9579×10^{-7}	3.0657	1.6185×10^{-6}	2.9695	2.8482×10^{-6}	2.9562
TCO		3.0000		3.0000		3.0000

Similarly, Table 7 displays results for scheme (28) with $\alpha = 0.35, 0.65, 0.95$, verifying the TCO from Theorem 4.9. Table 8 shows results for scheme (29) with $\alpha = 0.25, 0.45, 0.65$, matching the TCO of Theorem 4.10. Table 9 presents results for scheme (31) with $\alpha = 0.01, 0.45, 0.99$, confirming the TCO predicted by Theorem 4.12. Finally, Table 10 contains results for scheme (30) with $\alpha = 0.2, 0.4, 0.7$, achieving the second-order accuracy predicted by Theorem 4.11.

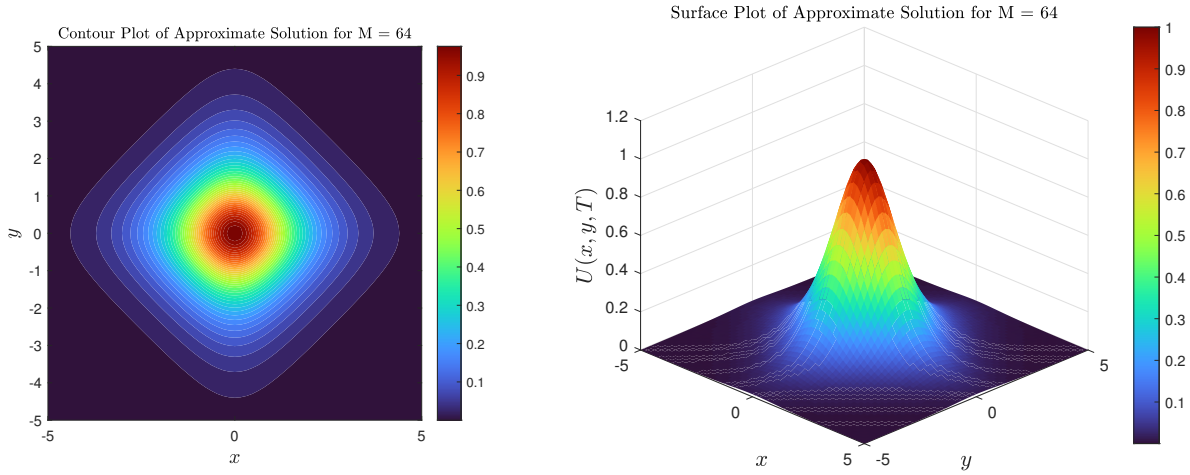

Figure 2: Visual representation of solution density and surface linked to Table 5 for $\alpha = 0.25$ and $M = 64$.

Table 6: Numerical results for Example 4.1 with $p = 4$ and $\varepsilon = 0.5$.

	$\alpha = 0.3$		$\alpha = 0.6$		$\alpha = 0.9$	
M	$\mathcal{L}^2$	CO	$\mathcal{L}^2$	CO	$\mathcal{L}^2$	CO
4	7.0142×10^{-2}	–	4.7846×10^{-2}	–	3.3093×10^{-2}	–
8	1.0585×10^{-2}	2.7282	7.9172×10^{-3}	2.5953	5.6603×10^{-3}	2.5476
16	4.8579×10^{-4}	4.4456	4.2758×10^{-4}	4.2107	3.6083×10^{-4}	3.9715
32	2.2685×10^{-5}	4.4205	1.9959×10^{-5}	4.4211	1.6897×10^{-5}	4.4164
64	1.3927×10^{-6}	4.0258	1.2236×10^{-6}	4.0278	1.0343×10^{-6}	4.0300
TCO		4.0000		4.0000		4.0000

Table 7: Numerical findings for Example 4.1 with $p = 1 + \alpha$ and $\varepsilon = 0.01$.

	$\alpha = 0.3$		$\alpha = 0.6$		$\alpha = 0.9$	
M	$\mathcal{L}^2$	CO	$\mathcal{L}^2$	CO	$\mathcal{L}^2$	CO
4	4.6011×10^{-3}	–	1.5292×10^{-2}	–	4.5476×10^{-2}	–
8	1.1595×10^{-3}	1.9885	5.1159×10^{-3}	1.5797	1.8614×10^{-2}	1.2887
16	3.0344×10^{-4}	1.9340	2.0957×10^{-3}	1.2876	9.4081×10^{-3}	0.9844
32	9.8452×10^{-5}	1.6239	8.6466×10^{-4}	1.2772	4.7015×10^{-3}	1.0008
64	3.1962×10^{-5}	1.6231	3.4899×10^{-4}	1.3089	2.3115×10^{-3}	1.0243
TCO		1.6500		1.3500		1.0500

Table 8: Numerical findings for Example 4.1 with $p = 3 - \alpha$ and $\varepsilon = \dfrac{25}{10000}$.

	$\alpha = 0.25$		$\alpha = 0.45$		$\alpha = 0.65$	
M	$\mathcal{L}^2$	CO	$\mathcal{L}^2$	CO	$\mathcal{L}^2$	CO
4	1.9138×10^{-3}	–	3.1471×10^{-3}	–	3.8156×10^{-3}	–
8	2.6012×10^{-4}	2.8792	4.7143×10^{-4}	2.7389	7.1920×10^{-4}	2.4074
16	3.1110×10^{-5}	3.0637	7.4464×10^{-5}	2.6624	1.4467×10^{-4}	2.3137
32	4.3412×10^{-6}	2.8412	1.2695×10^{-5}	2.5523	2.9439×10^{-5}	2.2969
64	6.5231×10^{-7}	2.7345	2.1662×10^{-6}	2.5510	5.8734×10^{-6}	2.3255
TCO		2.7500		2.5500		2.3500

5. Meshless method for TFDEs

Numerous studies have explored the application of meshless methods for solving PDEs and FPDEs; refer to, for example, [3, 4, 5, 11, 40, 44, 45, 46, 59, 112, 125, 126]. In this section, we focus on the implementation of a meshless method for solving Eq. (1) using radial basis functions (RBFs).

Table 9: Numerical findings for Example 4.1 with $p = 4 - \alpha$ and $\varepsilon = \frac{1}{4000}$.

	$\alpha = 0.1$		$\alpha = 0.45$		$\alpha = 0.99$	
M	$\mathcal{L}^2$	CO	$\mathcal{L}^2$	CO	$\mathcal{L}^2$	CO
4	8.4326×10^{-5}	–	7.5087×10^{-4}	–	2.2129×10^{-3}	–
8	1.6230×10^{-5}	2.3773	9.8080×10^{-5}	2.9365	4.0400×10^{-4}	2.4535
16	1.7239×10^{-6}	3.2350	9.3646×10^{-6}	3.3887	5.0797×10^{-5}	2.9915
32	9.1887×10^{-8}	4.2296	8.5887×10^{-7}	3.4467	6.3779×10^{-6}	2.9936
64	5.6248×10^{-9}	4.0300	7.6390×10^{-8}	3.4910	7.9004×10^{-7}	3.0131
TCO		3.9900		3.5500		3.0100

Table 10: Numerical findings for Example 4.1 with $p = 3 - \alpha$ and $\varepsilon = 0.1$.

	$\alpha = 0.2$		$\alpha = 0.4$		$\alpha = 0.7$	
M	$\mathcal{L}^2$	CO	$\mathcal{L}^2$	CO	$\mathcal{L}^2$	CO
4	2.2081×10^{-2}	–	1.9384×10^{-2}	–	1.4906×10^{-2}	–
8	4.2221×10^{-3}	2.3868	3.6825×10^{-3}	2.3961	2.8461×10^{-3}	2.3888
16	3.2138×10^{-4}	3.7156	3.2843×10^{-4}	3.4870	2.8517×10^{-4}	3.3191
32	4.0535×10^{-5}	2.9870	5.6413×10^{-5}	2.5415	5.3335×10^{-5}	2.4186
64	9.8450×10^{-6}	2.0417	1.4246×10^{-5}	1.9855	1.3708×10^{-5}	1.9600
TCO		2.0000		2.0000		2.0000

A meshless method is characterized by the absence of a predefined mesh to discretize the domain. Instead, it constructs a system of algebraic equations over the entire problem domain using scattered nodes [112]. According to [112], meshless methods employ sets of nodes distributed within the interior and along the boundaries of the domain to represent the problem domain and its boundary. These nodes are not connected by any mesh structure, and no prior information about the connectivity among nodes is required for interpolation or approximation of unknown field variables.

Among the various types of RBFs discussed in the literature [45, 161], we employ the *multiquadric* (MQ) RBF in this study, defined by

$$\phi(r) = \sqrt{1 + (cr)^2},$$

where $c > 0$ is a shape parameter and r is the Euclidean distance between nodes [162].

5.1. Numerical schemes

In this section, we implement the meshless method for solving Eq. (1) based on the Grünwald–Letnikov approximation and L–type formulas. Beginning with the application of Eq. (7), the time-fractional differential equation takes the form

$$\tau^{-\alpha} \sum_{k=0}^{n} g_k^{(\alpha)} u^{n-k} - \varepsilon \Delta u^n + \mathrm{T}_n^{(\alpha)} = f^n, \tag{32}$$

where τ is the time step size, and $\mathrm{T}_n^{(\alpha)}$ accounts for the truncation error. To approximate the solution using a meshless RBF approach (Kansa method), we define the MQ–RBF as [45, 82, 83]

$$\varphi_j(\mathbf{x}) = \sqrt{\|\mathbf{x} - \mathbf{x}_j\|^2 + c^2},$$

and equivalently in terms of the distance r_{ij} between the node $\mathbf{x}_i$ and center $\mathbf{x}_j$

$$\varphi(r_{ij}) = \sqrt{\|\mathbf{x}_i - \mathbf{x}_j\|^2 + c^2} = \sqrt{1 + r^2 c^2},$$

where $c > 0$ is the shape parameter. Using the RBF approximation, the numerical scheme becomes

$$\tau^{-\alpha} \sum_{k=0}^{n} g_k^{(\alpha)} \sum_{j=1}^{M} c_j^{n-k} \varphi(r_{ij}) - \varepsilon \sum_{j=1}^{M} c_j^n \Delta\varphi(r_{ij}) = f^n.$$

After rearranging and isolating the unknown coefficients at the current time level n, we obtain the following discrete scheme

$$\tau^{-\alpha} g_0^{(\alpha)} \sum_{j=1}^{M} c_j^n \varphi(r_{ij}) - \varepsilon \sum_{j=1}^{M} c_j^n \Delta\varphi(r_{ij}) = f^n - \tau^{-\alpha} \sum_{k=1}^{n} g_k^{(\alpha)} \sum_{j=1}^{M} c_j^{n-k} \varphi(r_{ij}).$$

This system can be compactly written in matrix form as

$$\mathcal{A}\mathbf{C}^n = \mathcal{F}^{(n)}, \qquad 1 \le n \le N, \tag{33}$$

where $\mathcal{A}$ is the coefficient matrix composed of RBF and Laplace evaluations, $\mathbf{C}^n$ is the vector of unknown coefficients at time step n, and $\mathcal{F}^{(n)}$ is the modified RHS incorporating both the source term and the memory contributions from previous time steps. Similarly, if one applies second-order WSGL, then

$$\sum_{j=1}^{M} c_j^n \left(\tau^{-\alpha} w_0^{(\alpha)} \varphi\left(r_{ij}\right) - \varepsilon \Delta\varphi\left(r_{ij}\right) \right) = f^n - \tau^{-\alpha} \sum_{k=1}^{n} w_k^{(\alpha)} \sum_{j=1}^{M} c_j^{n-k} \varphi\left(r_{ij}\right),$$

or equivalently in matrix form

$$\mathcal{A}\mathbf{C}^n = \mathcal{F}^{(n)}, \quad 1 \le n \le N. \tag{34}$$

Moreover, for third-order WSGL, one obtains

$$\sum_{j=1}^{M} c_j^n \left(\tau^{-\alpha} \lambda_0^{(\alpha)} \varphi\left(r_{ij}\right) - \varepsilon \Delta\varphi\left(r_{ij}\right) \right) = f^n - \tau^{-\alpha} \sum_{k=1}^{n} \lambda_k^{(\alpha)} \sum_{j=1}^{M} c_j^{n-k} \varphi\left(r_{ij}\right),$$

or in matrix form

$$\mathcal{A}\mathbf{C}^n = \mathcal{F}^{(n)}, \quad 1 \le n \le N. \tag{35}$$

Additionally, by employing fourth-order WSGL, one concludes

$$\sum_{j=1}^{M} c_j^n \left(\tau^{-\alpha} \vartheta_0^{(\alpha)} \varphi\left(r_{ij}\right) - \varepsilon \Delta\varphi\left(r_{ij}\right) \right) = f^n - \tau^{-\alpha} \sum_{k=1}^{n} \vartheta_k^{(\alpha)} \sum_{j=1}^{M} c_j^{n-k} \varphi\left(r_{ij}\right),$$

or in its compact form

$$\mathcal{A}\mathbf{C}^n = \mathcal{F}^{(n)}, \quad 1 \le n \le N. \tag{36}$$

By substituting Eq. (11) into Eq. (1) and using the Kansa method, we get the following discretization

$$\sum_{j=1}^{M} c_j^n \left(a_0^{(\alpha)} \varphi\left(r_{ij}\right) - \varepsilon \Delta\varphi\left(r_{ij}\right) \right) = a_0^{(\alpha)} \sum_{j=1}^{M} c_j^{n-1} \varphi\left(r_{ij}\right) - \sum_{k=1}^{n-1} a_{n-k}^{(\alpha)} \sum_{j=1}^{M} \delta c_j^k \varphi\left(r_{ij}\right) + f^n,$$

and its corresponding matrix form is

$$\mathcal{A}\mathbf{C}^n = \mathcal{F}^{(n)}, \quad 1 \le n \le N. \tag{37}$$

Now, using L1-2 method gives

$$c_0^{(\alpha)} \sum_{j=1}^{M} c_j^n \varphi\left(r_{ij}\right) - \varepsilon \sum_{j=1}^{M} c_j^n \Delta\varphi\left(r_{ij}\right) = c_0^{(\alpha)} \sum_{j=1}^{M} c_j^{n-1} \varphi\left(r_{ij}\right) - \sum_{k=1}^{n-1} c_{n-k}^{(\alpha)} \sum_{j=1}^{M} \delta c_j^k \varphi\left(r_{ij}\right) + f^n,$$

which implies the following matrix form

$$\mathcal{A}\mathbf{C}^n = \mathcal{F}^{(n)}, \quad 1 \le n \le N. \tag{38}$$

Following the same procedure for L2-1$_\sigma$ approximation and utilizing Lemma 3.8 yield

$$\begin{aligned} c_0^{(n)} \sum_{j=1}^{M} c_j^{n+1} \varphi\left(r_{ij}\right) - \varepsilon\sigma \sum_{j=1}^{M} c_j^{n+1} \Delta\varphi\left(r_{ij}\right) = c_0^{(n)} \sum_{j=1}^{M} c_j^n \varphi\left(r_{ij}\right) - \sum_{k=0}^{n-1} c_{n-k}^{(n)} \sum_{j=1}^{M} \delta c_j^k \varphi\left(r_{ij}\right) \\ + \varepsilon\left(1-\sigma\right) \sum_{j=1}^{M} c_j^n \Delta\varphi\left(r_{ij}\right) + \sigma f^{n+1} + \left(1-\sigma\right) f^n. \end{aligned} \tag{39}$$

The compact matrix form of Eq. (39) can be presented as follows

$$\mathcal{A}\mathbf{C}^{n+1} = \mathcal{F}^{(n+\sigma)}, \quad 0 \le n \le N-1. \tag{40}$$

Finally, for L1-2-3 approximation one obtains

$$\sum_{j=1}^{M} c_j^n \left(c_0^{(\alpha)} \varphi(r_{ij}) - \varepsilon \Delta \varphi(r_{ij}) \right) = c_0^{(\alpha)} \sum_{j=1}^{M} c_j^{n-1} \varphi(r_{ij}) - \sum_{k=1}^{n-1} c_{n-k}^{(\alpha)} \sum_{j=1}^{M} \delta c_j^k \varphi(r_{ij}) + f^n,$$

with the matrix form

$$\mathcal{A}\mathbf{C}^{n} = \mathcal{F}^{(n)}, \quad 1 \le n \le N. \tag{41}$$

5.2. Numerical examples

Example 5.1. We now perform a second test on the spatial domain $\Omega = [-5,5]^2$ with step size $h = \frac{10}{M}$, where $M_x = M_y = M$, and set $T = 1$. The exact solution is

$$u(x,y,t) = t^p \sin(x+y),$$

with corresponding source term

$$f(x,y,t) = \left(\frac{\Gamma(p+1)}{\Gamma(p+1-\alpha)} t^{p-\alpha} + 2t^p \right) \sin(x+y).$$

Tables 11–18 summarize the numerical results for various schemes and parameter settings. For the Grünwald–Letnikov formula (22), we take $p = 2$, $\varepsilon = 1$, and $\alpha = 0.2, 0.5, 0.75$ (Table 11). For the second-order WSGL scheme (25), we use $p = 3$, $\varepsilon = 0.1$, and $\alpha = 0.1, 0.5, 0.8$ (Table 12). For the third-order WSGL scheme (26), we set $p = 4$, $\varepsilon = 0.01$, and $\alpha = 0.15, 0.55, 0.85$ (Table 13); and for the variant (27), we choose $p = 5$, $\varepsilon = 0.001$, and $\alpha = 0.25, 0.55, 0.85$ (Table 14).

For the L1 method (28), we choose $p = 2 - \alpha$, $\varepsilon = 1/\sqrt{4\pi^2}$, and $\alpha = 0.3, 0.5, 0.8$ (Table 15). For the L1-2 approximation (29), we select $p = 2 + \alpha$, $\varepsilon = 1/\sqrt{8\pi^2}$, and $\alpha = 0.3, 0.6, 0.9$ (Table 16). For the L2-1σ formula (30), the parameters are taken as $p = 3 + \alpha$, $\varepsilon = 1/\sqrt{16\pi^2}$, and $\alpha = 0.25, 0.5, 0.75$ (Table 17). At the end, for the L1-2-3 scheme (31), we put $p = 4 - \alpha$, $\varepsilon = 0.01$, and $\alpha = 0.1, 0.5, 0.9$ (Table 18). Fig. 3 illustrates the results from Table 18 for $\alpha = 0.5$ and $M = 40$.

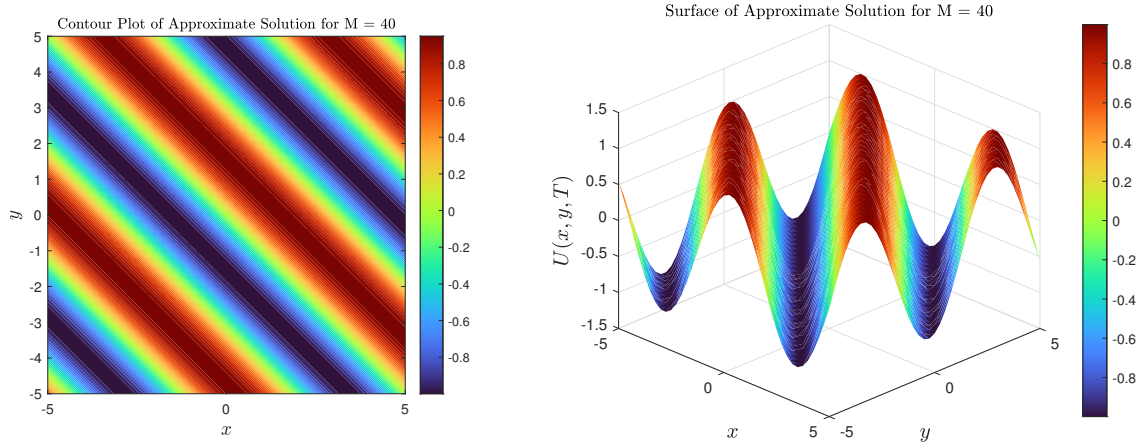

Figure 3: Representation of density and surface of approximate solution associated with Table 18 for $\alpha = 0.5$ and $M = 40$.

6. Finite element method for TFDEs

In this section, we present the FEM for solving Eq. (1). To begin, it is essential to define the finite element space used in the formulation [41, 42, 81, 95].

Suppose $\mathcal{T}_h$ is a quasi-uniform triangulation of the domain Ω, such that

$$\bar{\Omega} = \bigcup_{\mathfrak{K} \in \mathcal{T}_h} \mathfrak{K},$$

Table 11: Errors for Example 5.1 with $p = 2$ and $\varepsilon = 1$.

	$\alpha = 0.2$	$\alpha = 0.5$	$\alpha = 0.75$
M	$\mathcal{L}^2$	$\mathcal{L}^2$	$\mathcal{L}^2$
10	1.8390×10^{-2}	1.2186×10^{-2}	1.0823×10^{-2}
20	3.0385×10^{-3}	5.5427×10^{-3}	7.9493×10^{-3}
30	1.3470×10^{-3}	3.8676×10^{-3}	5.6337×10^{-3}
40	9.6419×10^{-4}	3.0322×10^{-3}	4.3831×10^{-3}

Table 12: Errors for Example 5.1 with $p = 3$ and $\varepsilon = 0.1$.

	$\alpha = 0.1$	$\alpha = 0.5$	$\alpha = 0.8$
M	$\mathcal{L}^2$	$\mathcal{L}^2$	$\mathcal{L}^2$
10	2.8778×10^{-2}	7.0118×10^{-3}	9.9216×10^{-3}
20	1.2380×10^{-2}	4.2786×10^{-3}	5.1830×10^{-3}
30	2.3297×10^{-3}	2.0059×10^{-3}	2.9367×10^{-3}
40	4.1180×10^{-4}	4.8339×10^{-4}	7.9861×10^{-4}

Table 13: Errors for Example 5.1 with $p = 4$ and $\varepsilon = 0.01$.

	$\alpha = 0.15$	$\alpha = 0.55$	$\alpha = 0.85$
M	$\mathcal{L}^2$	$\mathcal{L}^2$	$\mathcal{L}^2$
10	1.1098×10^{-3}	8.4495×10^{-3}	1.7309×10^{-2}
20	1.0771×10^{-3}	1.5891×10^{-3}	3.7762×10^{-3}
30	3.7592×10^{-4}	3.6697×10^{-4}	6.3488×10^{-4}
40	9.1784×10^{-5}	6.7768×10^{-5}	9.2121×10^{-5}

Table 14: Errors for Example 5.1 with $p = 5$ and $\varepsilon = 0.001$.

	$\alpha = 0.25$	$\alpha = 0.55$	$\alpha = 0.85$
M	$\mathcal{L}^2$	$\mathcal{L}^2$	$\mathcal{L}^2$
10	1.3064×10^{-4}	4.3496×10^{-4}	8.7019×10^{-4}
20	2.5874×10^{-5}	3.5319×10^{-5}	6.6263×10^{-5}
30	1.0949×10^{-5}	9.1292×10^{-6}	1.4149×10^{-5}
40	4.7564×10^{-6}	3.4935×10^{-6}	4.7196×10^{-6}

Table 15: Errors for Example 5.1 with $p = 2 - \alpha$ and $\varepsilon = \frac{1}{\sqrt{4\pi^2}}$.

	$\alpha = 0.3$	$\alpha = 0.5$	$\alpha = 0.8$
M	$\mathcal{L}^2$	$\mathcal{L}^2$	$\mathcal{L}^2$
10	7.2273×10^{-3}	5.6233×10^{-3}	5.0851×10^{-3}
20	1.7065×10^{-3}	1.8590×10^{-3}	3.3024×10^{-3}
30	5.9611×10^{-4}	8.4713×10^{-4}	2.1210×10^{-3}
40	2.4712×10^{-4}	5.1089×10^{-4}	1.5650×10^{-3}

Table 16: Errors for Example 5.1 with $p = 2 + \alpha$ and $\varepsilon = \frac{1}{\sqrt{8\pi^2}}$.

	$\alpha = 0.3$	$\alpha = 0.6$	$\alpha = 0.9$
M	$\mathcal{L}^2$	$\mathcal{L}^2$	$\mathcal{L}^2$
10	6.0139×10^{-3}	3.7952×10^{-3}	4.1994×10^{-3}
20	1.4410×10^{-3}	1.1328×10^{-3}	1.5947×10^{-3}
30	5.0032×10^{-4}	4.0747×10^{-4}	7.0118×10^{-4}
40	1.8430×10^{-4}	1.5442×10^{-4}	3.7996×10^{-4}

Table 17: Errors for Example 5.1 with $p = 3 + \alpha$ and $\varepsilon = \frac{1}{\sqrt{16\pi^2}}$.

	$\alpha = 0.25$	$\alpha = 0.5$	$\alpha = 0.75$
M	$\mathcal{L}^2$	$\mathcal{L}^2$	$\mathcal{L}^2$
10	1.5276×10^{-2}	3.0009×10^{-3}	7.3277×10^{-3}
20	6.9786×10^{-3}	2.8942×10^{-3}	3.5375×10^{-3}
30	1.7735×10^{-3}	1.7887×10^{-3}	2.1211×10^{-3}
40	3.6042×10^{-4}	4.5759×10^{-4}	5.8550×10^{-4}

Table 18: Errors for Example 5.1 with $p = 4 - \alpha$ and $\varepsilon = 0.01$.

	$\alpha = 0.1$	$\alpha = 0.5$	$\alpha = 0.9$
M	$\mathcal{L}^2$	$\mathcal{L}^2$	$\mathcal{L}^2$
10	8.4475×10^{-4}	4.0935×10^{-4}	4.3396×10^{-4}
20	2.8827×10^{-4}	1.7096×10^{-4}	1.0846×10^{-4}
30	1.1786×10^{-4}	7.2538×10^{-5}	4.5843×10^{-5}
40	4.8458×10^{-5}	3.0551×10^{-5}	1.9532×10^{-5}

where h denotes the mesh size, defined as

$$h := \max_{\mathfrak{K} \in \mathcal{T}_h} \{\operatorname{diam}(\mathfrak{K})\}.$$

We then define the finite element space as

$$\mathcal{S}_M^h := \left\{ s \in \mathcal{C}\left(\bar{\Omega}\right) \middle| \, s|_{\mathfrak{K}} \in \mathcal{P}_M^h\left(\mathfrak{K}\right), \forall \mathfrak{K} \in \mathcal{T}_h, \, s|_{\partial\Omega} = 0 \right\},$$

where $\mathcal{P}_M^h(\mathfrak{K})$ denotes the space of polynomials of degree at most M on each element $\mathfrak{K}$, and $\mathcal{S}_M^h \subset \mathcal{H}_0^1(\Omega)$.

6.1. Variational weak forms

In the current section, we apply the notations given above to derive the weak form. By substituting Eq. (7) into Eq. (1), we arrive at Eq. (32). The variational weak formulation of Eq. (32) is: find a $u^n \in \mathcal{H}_0^1(\Omega)$, such that

$$\left(\tau^{-\alpha} \sum_{k=0}^{n} g_k^{(\alpha)} u^{n-k}, s^n\right) - \varepsilon\left(\Delta u^n, s^n\right) + \left(\mathrm{T}_n^{(\alpha)}, s^n\right) = \left(f^n, s^n\right), \qquad \forall s^n \in \mathcal{S}_M^h.$$

Then there exists a $U^n \in \mathcal{P}_M^h(\Omega)$ with

$$\left(\tau^{-\alpha} \sum_{k=0}^{n} g_k^{(\alpha)} U^{n-k}, s^n\right) - \varepsilon\left(\Delta U^n, s^n\right) = \left(f^n, s^n\right), \qquad \forall s^n \in \mathcal{S}_M^h. \tag{42}$$

On the other hand, for second-order WSGL approximation, one can conclude

$$\left(\tau^{-\alpha} \sum_{k=0}^{n} w_k^{(\alpha)} U^{n-k}, s^n\right) - \varepsilon\left(\Delta U^n, s^n\right) = \left(f^n, s^n\right), \qquad \forall s^n \in \mathcal{S}_M^h. \tag{43}$$

Substituting Eq. (9) into Eq. (1) results

$$\tau^{-\alpha} \sum_{k=0}^{n} \lambda_k^{(\alpha)} u^{n-k} - \varepsilon \Delta u^n + \mathrm{T}_n^{(\alpha)} = f^n. \tag{44}$$

The weak formulation of Eq. (44) is: finding a $u^n \in \mathcal{H}_0^1(\Omega)$, such that

$$\left(\tau^{-\alpha} \sum_{k=0}^{n} \lambda_k^{(\alpha)} u^{n-k}, s^n\right) - \varepsilon\left(\Delta u^n, s^n\right) + \left(\mathrm{T}_n^{(\alpha)}, s^n\right) = \left(f^n, s^n\right), \qquad \forall s^n \in \mathcal{S}_M^h. \tag{45}$$

Therefore, there exists a $U^n \in \mathcal{P}_M^h(\Omega)$ subject to

$$\left(\tau^{-\alpha} \sum_{k=0}^{n} \lambda_k^{(\alpha)} U^{n-k}, s^n\right) - \varepsilon\left(\Delta U^n, s^n\right) = \left(f^n, s^n\right), \qquad \forall s^n \in \mathcal{S}_M^h. \tag{46}$$

The same reasoning for the fourth-order WSGL results the following scheme

$$\left(\tau^{-\alpha}\sum_{k=0}^{n}\vartheta_k^{(\alpha)}U^{n-k},s^n\right)-\varepsilon\left(\Delta U^n,s^n\right)=\left(f^n,s^n\right),\qquad\forall s^n\in\mathcal{S}_M^h. \tag{47}$$

Next, we will find the weak forms for L–type schemes. Using L1 formula for Eq. (1) gives

$$\sum_{k=1}^{n}a_{n-k}^{(\alpha)}\delta u^k-\varepsilon\Delta u^n+\mathrm{T}_n^{(\alpha)}=f^n, \tag{48}$$

The weak form of Eq. (48) is to **find** a $u^n\in\mathcal{H}_0^1(\Omega)$, **such that**

$$\left(\sum_{k=1}^{n}a_{n-k}^{(\alpha)}\delta u^k,s^n\right)-\varepsilon\left(\Delta u^n,s^n\right)+\left(\mathrm{T}_n^{(\alpha)},s^n\right)=\left(f^n,s^n\right),\qquad\forall s^n\in\mathcal{S}_M^h, \tag{49}$$

thus there exists a $U^n\in\mathcal{P}_M^h(\Omega)$, with

$$\left(\sum_{k=1}^{n}a_{n-k}^{(\alpha)}\delta u^k,s^n\right)-\varepsilon\left(\Delta U^n,s^n\right)=\left(f^n,s^n\right),\qquad\forall s^n\in\mathcal{S}_M^h. \tag{50}$$

Similarly, if one applies the L1-2 approximation (13), then the following scheme can be obtained

$$\left(\sum_{k=1}^{n}c_{n-k}^{(\alpha)}\delta u^k,s^n\right)-\varepsilon\left(\Delta U^n,s^n\right)=\left(f^n,s^n\right),\qquad\forall s^n\in\mathcal{S}_M^h. \tag{51}$$

Using Eq. (15) for Eq. (1) leads to

$$\sum_{k=0}^{n}c_{n-k}^{(n)}\delta u^k-\varepsilon\Delta u^{n+\sigma}+\mathrm{T}_{n+\sigma}^{(\alpha)}=f^{n+\sigma}, \tag{52}$$

The weak form of Eq. (52) is to **find** a $u^{n+\sigma}\in\mathcal{H}_0^1(\Omega)$, **such that**

$$\left(\sum_{k=0}^{n}c_{n-k}^{(n)}\delta u^k,s^{n+\sigma}\right)-\varepsilon\left(\Delta u^{n+\sigma},s^{n+\sigma}\right)+\left(\mathrm{T}_{n+\sigma}^{(\alpha)},s^{n+\sigma}\right)=\left(f^{n+\sigma},s^{n+\sigma}\right),\qquad\forall s^{n+\sigma}\in\mathcal{S}_M^h. \tag{53}$$

Then, one has

$$\exists U^{n+\sigma}\in\mathcal{P}_M^h(\Omega)\quad\ni\quad\left(\sum_{k=0}^{n}c_{n-k}^{(n)}\delta U^k,s^{n+\sigma}\right)-\varepsilon\left(\Delta U^{n+\sigma},s^{n+\sigma}\right)=\left(f^{n+\sigma},s^{n+\sigma}\right),\qquad\forall s^{n+\sigma}\in\mathcal{S}_M^h. \tag{54}$$

Applying the same procedure to the L1-2-3 formula yields the scheme below

$$\left(\sum_{k=1}^{n}d_{n-k}^{(\alpha)}\delta u^k,s^n\right)-\varepsilon\left(\Delta U^n,s^n\right)=\left(f^n,s^n\right),\qquad\forall s^n\in\mathcal{S}_M^h. \tag{55}$$

6.2. Stability and error analysis

There are some key lemmas presented as follows. These lemmas will be useful for further analysis in upcoming sections.

Lemma 6.1 ([75, 172, 177]). *For the set of coefficients* $\left\{\lambda_k^{(\alpha)}\right\}_{k=0}^{\infty}$, *appeared in Eq.* (9), $N\in\mathbb{N}$ *and* $\begin{bmatrix}u_0 & u_1 & \dots & u_N\end{bmatrix}^T\in\mathbb{R}^{N+1}$, *the following property holds*

$$\sum_{n=0}^{N}\left(\sum_{k=0}^{n}\lambda_k^{(\alpha)}u^{n-k}\right)u^n\geq 0.$$

Moreover, the mentioned property is true for $\left\{g_k^{(\alpha)}\right\}_{k=0}^{\infty}$, $\left\{w_k^{(\alpha)}\right\}_{k=0}^{\infty}$ *and* $\left\{\vartheta_k^{(\alpha)}\right\}_{k=0}^{\infty}$ *in Eqs.* (7), (8) *and* (10), *respectively.*

Lemma 6.2 ([15, 62, 176]). *The following inequality can be easily concluded for any* $\mathcal{V}^n \in \mathcal{P}(\lambda)$,

$$\left({}^{C}\mathrm{D}_N^{\alpha}\mathcal{V}^n, \mathcal{V}^n\right) \geq \frac{1}{2}{}^{C}\mathrm{D}_N^{\alpha}\|\mathcal{V}^n\|^2.$$

Lemma 6.3 ([60, 107, 108]). *Suppose that* $T > 0$ *and there is a constant* ϑ, *independent of* τ, *with* $\vartheta \geq \sum_{l=0}^{N-1}\vartheta_l$, *in which* $\{\vartheta_l\}_{l=0}^{N-1}$, *is a nonnegative sequence. Let the sequences* $\{u^n\}_{n=0}^{N}$, $\{w^n\}_{n=1}^{N}$ *and* $\{v^n\}_{n=1}^{N}$ *be nonnegative and satisfy the following relation*

$${}^{C}\mathrm{D}_N^{\alpha}\left(u^n\right)^2 \leq u^n\left(v^n + w^n\right) + \sum_{l=1}^{n}\vartheta_{n-l}\left(u^l\right)^2, \quad n \geq 1,$$

then

$$u^n \leq E_{\alpha}\left(2\vartheta t_n^{\alpha}\right)\left(2u^0 + 2\max_{1\leq k\leq n}\sum_{l=1}^{k}\kappa_{k-l}^{(k)}v^l + \frac{2t_n^{\alpha}}{\Gamma\left(1+\alpha\right)}\max_{1\leq k\leq n}w^k\right), \quad n \geq 1,$$

where the coefficients $\kappa_{k-l}^{(k)}$ *are the discrete kernels and* E_{α} *is the Mittag–Leffler function.*

Lemma 6.4 ([108, 113, 176]). *Let* $\{\upsilon^n\}_{n=0}^{N}$ *and* $\{\nu^n\}_{n=0}^{N}$ *be two nonnegative sequences, satisfying*

$$\begin{cases} {}_0^{C}\mathrm{D}_t^{\alpha}\upsilon^{\sigma} \leq \zeta_1\upsilon^1 + \zeta_2\upsilon^0 + \nu^0, \\ {}_0^{C}\mathrm{D}_t^{\alpha}\upsilon^{n+\sigma} \leq \zeta_1\upsilon^{n+1} + \zeta_2\upsilon^n + \zeta_3\upsilon^{n-1} + \nu^n, \end{cases}$$

where ζ_1, ζ_2 *and* ζ_3 *denote three positive constants that are independent of* τ. *Then there exists* $\tau^* > 0$, *such that* $0 < \tau \leq \tau^*$, *and*

$$\upsilon^n \leq E_{\alpha}\left(2\zeta t_n^{\alpha}\right)\left(6\upsilon^0 + \frac{12t_n^{\alpha}}{\Gamma\left(1+\alpha\right)}\max_{0\leq l\leq n}\nu^l\right), \qquad \zeta = 6\zeta_1 + \frac{c_0^{(n)}\zeta_2}{c_0^{(n)} - c_1^{(n)}} + \frac{c_0^{(n)}\zeta_3}{c_1^{(n)} - c_2^{(n)}},$$

for $n \geq 1$.

To establish the convergence of the FEM, we require the $\mathcal{H}^1$–orthogonal projection operator. Specifically, we define the projection operator $\Psi_M : \mathcal{H}^{q+1}(\Omega) \to \mathcal{S}_M^h(\Omega)$, such that [46, 78, 192]

$$\left(\nabla u^n, \nabla s^n\right) = \left(\nabla\Psi_M u^n, \nabla s^n\right), \quad \forall u^n \in \mathcal{H}^{q+1}(\Omega), \quad q \geq 1, \quad \forall s^n \in \mathcal{S}_M^h. \tag{56}$$

Lemma 6.5 ([171, 175, 192, 194]). *For the defined orthogonal projection operator* (56), *the following estimate holds*

$$\|u - \Psi_M u\| \leq Ch^{l+1}\|u\|, \quad \forall u \in \mathcal{H}_0^1(\Omega) \cap \mathcal{H}^{q+1}(\Omega),$$

in which $l := \min\{M, q\}$, *and* C *is a constant depending on* u *and its derivatives but independent of the mesh size* h.

We are now ready to study the theorems associated with the obtained schemes.

Theorem 6.6. *Let* $\tilde{U}^n \in \mathcal{P}_M^h(\Omega)$ *be an approximation of* U^n. *The fully-discrete schemes* (42), (43), (46) *and* (47) *are unconditionally stable.*

Proof. The proof is presented only for (46); the same reasoning applies to (42), (43) and (47).First, it is required to introduce the following round-off error equation

$$\mathcal{E}^n := U^n - \tilde{U}^n. \tag{57}$$

Subtracting

$$\left(\tau^{-\alpha}\sum_{k=0}^{n}\lambda_k^{(\alpha)}\tilde{U}^{n-k}, s^n\right) - \varepsilon\left(\Delta\tilde{U}^n, s^n\right) = \left(f^n, s^n\right),$$

from Eq. (46) yields

$$\left(\tau^{-\alpha}\sum_{k=0}^{n}\lambda_k^{(\alpha)}\mathcal{E}^{n-k}, s^n\right) - \varepsilon\left(\Delta\mathcal{E}^n, s^n\right) = 0.$$

Set $s^n = \mathcal{E}^n$, then one has

$$\left(\tau^{-\alpha}\sum_{k=0}^{n}\lambda_k^{(\alpha)}\mathcal{E}^{n-k},\mathcal{E}^n\right)-\varepsilon\left(\Delta\mathcal{E}^n,\mathcal{E}^n\right)=0.$$

By using the Green's theorem, it can be concluded that

$$\left(\tau^{-\alpha}\sum_{k=0}^{n}\lambda_k^{(\alpha)}\mathcal{E}^{n-k},\mathcal{E}^n\right)+\varepsilon\left(\nabla\mathcal{E}^n,\nabla\mathcal{E}^n\right)=0. \tag{58}$$

Summing Eq. (58) over n from 1 to N yields

$$\tau^{-\alpha}\sum_{n=1}^{N}\left(\sum_{k=0}^{n}\lambda_k^{(\alpha)}\mathcal{E}^{n-k},\mathcal{E}^n\right)+\varepsilon\sum_{n=1}^{N}\left(\nabla\mathcal{E}^n,\nabla\mathcal{E}^n\right)=0. \tag{59}$$

Adding $\tau^{-\alpha}\lambda_0^{(\alpha)}\left(\mathcal{E}^0,\mathcal{E}^0\right)$ to both sides of Eq. (59) leads to

$$\tau^{-\alpha}\sum_{n=0}^{N}\left(\sum_{k=0}^{n}\lambda_k^{(\alpha)}\mathcal{E}^{n-k},\mathcal{E}^n\right)+\varepsilon\sum_{n=1}^{N}\left(\nabla\mathcal{E}^n,\nabla\mathcal{E}^n\right)=\tau^{-\alpha}\lambda_0^{(\alpha)}\left(\mathcal{E}^0,\mathcal{E}^0\right). \tag{60}$$

From Lemma 6.1, the first term on the LHS of (60) is nonnegative, so dropping it and by setting $\varrho_1=\tau^{-\alpha}\lambda_0^{(\alpha)}$, we obtain

$$\varepsilon\sum_{n=1}^{N}\|\nabla\mathcal{E}^n\|^2\le\varrho_1\left\|\mathcal{E}^0\right\|^2.$$

The use of Poincaré inequality results in

$$\varepsilon\|\nabla\mathcal{E}^n\|^2\ge\frac{\varepsilon}{C_\Omega}\|\mathcal{E}^n\|^2.$$

Finally, simplifying the recent result gives

$$\|\mathcal{E}^n\|\le\sqrt{\frac{\varrho_1 C_\Omega}{\varepsilon}}\left\|\mathcal{E}^0\right\|,$$

and the proof is finished. □

Theorem 6.7. *Let $\tilde{U}^n\in\mathcal{P}_M^h(\Omega)$ be the estimate solution of the fully-discrete schemes (50), (51) and (55). Then these schemes are unconditionally stable.*

Proof. The proof is given only for (50). Others follow the same idea. By considering (57) and subtracting

$$\left({}_0^C\mathrm{D}_t^\alpha\tilde{U}^n,s^n\right)-\varepsilon\left(\Delta\tilde{U}^n,s^n\right)=\left(f^n,s^n\right),$$

from Eq. (48) results in

$$\left({}_0^C\mathrm{D}_t^\alpha\mathcal{E}^n,s^n\right)-\varepsilon\left(\Delta\mathcal{E}^n,s^n\right)=0.$$

By following the same argument given in the proof of Theorem 6.6, it is evident that

$$\left({}_0^C\mathrm{D}_t^\alpha\mathcal{E}^n,\mathcal{E}^n\right)+\varepsilon\left(\nabla\mathcal{E}^n,\nabla\mathcal{E}^n\right)=0. \tag{61}$$

By employing Lemma 6.2 for the first term, we deduce that

$$\frac{1}{2}{}_0^C\mathrm{D}_t^\alpha\|\mathcal{E}^n\|^2+\varepsilon\|\nabla\mathcal{E}^n\|^2\le0.$$

An application of the Poincaré inequality implies

$${}_0^C\mathrm{D}_t^\alpha\|\mathcal{E}^n\|^2\le\frac{2\varepsilon}{C_\Omega}\|\mathcal{E}^n\|^2,$$

and the use of Lemma 6.3 leads to

$$\|\mathcal{E}^n\|\le\frac{4\varepsilon}{C_\Omega}\mathcal{E}^0E_\alpha\left(2\zeta t_n^\alpha\right)\le\frac{4\varepsilon}{C_\Omega}\mathcal{E}^0E_\alpha\left(2\zeta T\right),$$

which finishes the proof. □

Theorem 6.8. *Suppose that $\tilde{U}^n \in \mathcal{P}_M^h(\Omega)$ is the estimate solution of the fully-discrete scheme (54). Hence this scheme is unconditionally stable.*

Proof. This proof follows the same steps as in the proof of Theorem 6.7 at the $n+\sigma$ level, up to the point where the following relation is derived

$$ {}_0^C\mathrm{D}_t^\alpha \left\|\mathcal{E}^{n+\sigma}\right\|^2 \leq \frac{2\varepsilon}{C_\Omega}\left\|\mathcal{E}^{n+\sigma}\right\|^2. $$

Then by utilizing Lemma 6.4, we obtain

$$ \|\mathcal{E}^n\| \leq \frac{12\varepsilon}{C_\Omega}\mathcal{E}^0 E_\alpha\left(2\zeta t_n^\alpha\right) \leq \frac{12\varepsilon}{C_\Omega}\mathcal{E}^0 E_\alpha\left(2\zeta T\right), $$

which fulfills the proof. □

Theorem 6.9. *Assume that $U^n \in \mathcal{P}_M^h(\Omega)$ is the approximation of u^n, obtained by Eq. (46), and $u(x,y,t) \in \mathcal{S}^{3+\alpha}(\mathbb{R})$ with $U^0 = \Psi_M u^0$. Therefore, there exists a positive constant C, independent of τ and h such that*

$$ \|u^n - U^n\| \leq C\left(\tau^3 + h^{l+1}\right), \qquad 1 \leq n \leq N. $$

Proof. Subtracting Eq. (46) from Eq. (45) and denoting

$$ v^n := u^n - \Psi_M u^n, \quad w^n := U^n - \Psi_M u^n, $$

then it follows that

$$ \left(\tau^{-\alpha}\sum_{k=0}^{n}\lambda_k^{(\alpha)}\left(v^{n-k} - w^{n-k}\right), s^n\right) - \varepsilon\left(\Delta\left(v^n - w^n\right), s^n\right) + \left(\mathrm{T}_n^{(\alpha)}, s^n\right) = 0. $$

By using the Green's theorem, one has

$$ \left(\tau^{-\alpha}\sum_{k=0}^{n}\lambda_k^{(\alpha)}\left(v^{n-k} - w^{n-k}\right), s^n\right) + \varepsilon\left(\nabla\left(v^n - w^n\right), \nabla s^n\right) + \left(\mathrm{T}_n^{(\alpha)}, s^n\right) = 0. $$

Considering Eq. (56) and rearranging the terms, the following expression is obtained

$$ \left(\tau^{-\alpha}\sum_{k=0}^{n}\lambda_k^{(\alpha)} w^{n-k}, w^n\right) + \varepsilon\left(\nabla w^n, \nabla w^n\right) = \left(\tau^{-\alpha}\sum_{k=0}^{n}\lambda_k^{(\alpha)} v^{n-k}, w^n\right) + \left(\mathrm{T}_n^{(\alpha)}, w^n\right). \tag{62} $$

Summing Eq. (62) for n from 1 to N results

$$ \tau^{-\alpha}\sum_{n=1}^{N}\left(\sum_{k=0}^{n}\lambda_k^{(\alpha)} w^{n-k}, w^n\right) + \varepsilon\sum_{n=1}^{N}\left(\nabla w^n, \nabla w^n\right) = \tau^{-\alpha}\sum_{n=1}^{N}\left(\sum_{k=0}^{n}\lambda_k^{(\alpha)} v^{n-k}, w^n\right) + \sum_{n=1}^{N}\left(\mathrm{T}_n^{(\alpha)}, w^n\right). \tag{63} $$

By adding $\tau^{-\alpha}\left(\lambda_0^{(\alpha)} w^0, w^0\right)$ to both sides of Eq. (63), we can deduce that

$$ \begin{aligned} \tau^{-\alpha}\sum_{n=0}^{N}\left(\sum_{k=0}^{n}\lambda_k^{(\alpha)} w^{n-k}, w^n\right) + \varepsilon\sum_{n=1}^{N}\left(\nabla w^n, \nabla w^n\right) &= \tau^{-\alpha}\left(\lambda_0^{(\alpha)} w^0, w^0\right) + \tau^{-\alpha}\sum_{n=1}^{N}\left(\sum_{k=0}^{n}\lambda_k^{(\alpha)} v^{n-k}, w^n\right) \\ &\quad + \sum_{n=1}^{N}\left(\mathrm{T}_n^{(\alpha)}, w^n\right). \end{aligned} \tag{64} $$

By using Lemma 6.1, one can conclude that the first term on the LHS of Eq. (64) is nonnegative. Since $w^0 = 0$, Eq. (64) can be rewritten as follows

$$ \varepsilon\sum_{n=1}^{N}\|\nabla w^n\|^2 \leq \sum_{n=1}^{N}\left\|\tau^{-\alpha}\sum_{k=0}^{n}\lambda_k^{(\alpha)} v^{n-k}\right\|\|w^n\| + \sum_{n=1}^{N}\left\|\mathrm{T}_n^{(\alpha)}\right\|\|w^n\|. $$

Employing the Poincaré and ε–Young inequalities leads to

$$ \frac{\varepsilon}{C_\Omega}\sum_{n=1}^{N}\|w^n\|^2 \leq \frac{1}{2\varepsilon_1^2}\sum_{n=1}^{N}\left\|\tau^{-\alpha}\sum_{k=0}^{n}\lambda_k^{(\alpha)} v^{n-k}\right\|^2 + \frac{\varepsilon_1^2}{2}\sum_{n=1}^{N}\|w^n\|^2 + \frac{1}{2\varepsilon_2^2}\sum_{n=1}^{N}\left\|\mathrm{T}_n^{(\alpha)}\right\|^2 + \frac{\varepsilon_2^2}{2}\sum_{n=1}^{N}\|w^n\|^2. \tag{65} $$

By putting $\varepsilon_1^2 = \varepsilon_2^2 = \dfrac{2\varepsilon}{3C_\Omega}$, Eq. (65) can be presented as follows

$$\frac{\varepsilon}{3C_\Omega}\sum_{n=1}^{N}\|w^n\|^2 \le \frac{3C_\Omega}{4\varepsilon}\sum_{n=1}^{N}\left(\left\|\tau^{-\alpha}\sum_{k=0}^{n}\lambda_k^{(\alpha)}v^{n-k}\right\|^2 + \left\|\mathrm{T}_n^{(\alpha)}\right\|^2\right).$$

A direct application of Lemma 6.5 results

$$\|w^n\|^2 \le \frac{9C_\Omega^2}{4\varepsilon^2}\left(\tilde{C}^2h^{2l+2}\max_{1\le n\le N}\left\|{}_0^C\mathcal{D}_t^\alpha u^n\right\|^2 + \max_{1\le n\le N}\left\|\mathrm{T}_n^{(\alpha)}\right\|^2\right),$$

which implies the following result

$$\|w^n\| \le C\left(\tau^3 + h^{l+1}\right).$$

Finally, by utilizing the triangle inequality, one can easily complete the proof. □

Theorem 6.10. *If U^n is obtained by solving the system, presented by Eq. (42) (Eq. (43)) ((Eq. (47))), and $u \in \mathcal{S}^{1+\alpha}(\mathbb{R})$ ($u \in \mathcal{S}^{2+\alpha}(\mathbb{R})$) (($u \in \mathcal{S}^{4+\alpha}(\mathbb{R})$)) with $U^0 = \Psi_M u^0$, then there exists a $C > 0$, independent of τ and h for $n \ge 1$*

$$\|u^n - U^n\| \le C\left(\tau + h^{l+1}\right). \ \left(\|u^n - U^n\| \le C\left(\tau^2 + h^{l+1}\right).\right) \ \left(\left(\|u^n - U^n\| \le C\left(\tau^4 + h^{l+1}\right).\right)\right)$$

Proof. The proof of this theorem is similar to the proof of Theorem 6.9. □

In the following, we give the convergence theorems of L–type formulations.

Theorem 6.11. *Assume $u \in \mathcal{C}^2[0,T]$, and $U^n \in \mathcal{P}_M^h(\Omega)$ is the approximation of exact solution of Eq. (1), obtained by Eq. (50) with $U^0 = \Psi_M u^0$. Therefore, there exists a positive constant C, independent of τ and h such that*

$$\|u^n - U^n\| \le C\left(\tau^{2-\alpha} + h^{l+1}\right), \qquad n = 1, 2, \ldots, N.$$

Proof. By subtracting Eq. (50) from Eq. (49) and introducing

$$v^n := u^n - \Psi_M u^n, \quad w^n := U^n - \Psi_M u^n,$$

then one has

$$\left({}_0^C\mathrm{D}_t^\alpha\left(v^n - w^n\right), s^n\right) - \varepsilon\left(\Delta\left(v^n - w^n\right), s^n\right) + \left(\mathrm{T}_n^{(\alpha)}, s^n\right) = 0.$$

Using the projection operator, defined by Eq. (56) and assuming $s^n = w^n$, then one can obtain the following expression

$$\left({}_0^C\mathrm{D}_t^\alpha w^n, w^n\right) + \varepsilon\left(\nabla w^n, \nabla w^n\right) = \left({}_0^C\mathrm{D}_t^\alpha v^n, w^n\right) + \left(\mathrm{T}_n^{(\alpha)}, w^n\right).$$

Employing Lemma 6.2 and applying the Cauchy and ε–Young inequalities lead to

$$\frac{1}{2}{}_0^C\mathrm{D}_t^\alpha\|w^n\|^2 + \varepsilon\|\nabla w^n\|^2 \le \frac{1}{2\varepsilon_1^2}\left\|{}_0^C\mathrm{D}_t^\alpha v^n\right\|^2 + \frac{\varepsilon_1^2}{2}\|w^n\|^2 + \frac{1}{2\varepsilon_2^2}\left\|\mathrm{T}_n^{(\alpha)}\right\|^2 + \frac{\varepsilon_2^2}{2}\|w^n\|^2. \tag{66}$$

Multiplying both sides of Eq. (66) by 2 and setting $\varepsilon_1^2 = 1$ and $\varepsilon_2^2 = \dfrac{2\varepsilon}{C_\Omega}$, then Eq. (66) can be given as

$${}_0^C\mathrm{D}_t^\alpha\|w^n\|^2 \le \|w^n\|^2 + \left\|{}_0^C\mathrm{D}_t^\alpha v^n\right\|^2 + \frac{C_\Omega}{2\varepsilon}\left\|\mathrm{T}_n^{(\alpha)}\right\|^2.$$

From Lemmas 6.5 and 6.3, it can be deduced that

$$\|w^n\| \le C\left(\tau^{2-\alpha} + h^{l+1}\right),$$

and an application of triangle inequality fulfills the proof. □

Theorem 6.12. *Suppose U^n is computed by Eq. (51), and (Eq. (55)), and $u \in \mathcal{C}^3[0,T]$ ($u \in \mathcal{C}^4[0,T]$), $U^0 = \Psi_M u^0$. Then there exists a $C > 0$, independent of τ and h for $n \ge 1$*

$$\|u^n - U^n\| \le C\left(\tau^{3-\alpha} + h^{l+1}\right). \ \left(\|u^n - U^n\| \le C\left(\tau^{4-\alpha} + h^{l+1}\right).\right)$$

Proof. The argument proceeds in the same manner as the proof of Theorem 6.11, and is therefore neglected. □

Theorem 6.13. *Let $u \in \mathcal{C}^2[0,T]$ and U^n be the solution of system (54) such that $U^0 = \Psi_M u^0$. Thus, there exists a positive constant C, independent of τ and h such that*

$$\|u^n - U^n\| \leq C\left(\tau^2 + h^{l+1}\right), \qquad 1 \leq n \leq N.$$

Proof. A similar procedure to that in the proof of Theorem 6.11 is followed at the $n+\sigma$ level, resulting in the following relation

$${}_0^C\mathrm{D}_t^\alpha \left\|w^{n+\sigma}\right\|^2 \leq \left\|w^{n+\sigma}\right\|^2 + \left\|{}_0^C\mathrm{D}_t^\alpha v^{n+\sigma}\right\|^2 + \frac{C_\Omega}{2\varepsilon}\left\|\mathrm{T}_{n+\sigma}^{(\alpha)}\right\|^2.$$

By invoking Lemmas 6.5 and 6.4, we obtain

$$\|w^n\| \leq C\left(\tau^2 + h^{l+1}\right).$$

The proof is then completed by an application of the triangle inequality. □

6.3. Numerical simulations

Example 6.1. We now consider Eq. (1) on the domain $[0,1]^2$ with final time $T = 1$ and parameter $\varepsilon = 0.01$. The source term is defined by

$$f(x,y,t) = \left(\frac{\Gamma(p+1)}{\Gamma(p+1-\alpha)}t^{p-\alpha} + 2\pi^2 t^p\right)\sin(\pi x)\sin(\pi y),$$

corresponding to the exact solution $u(x,y,t) = t^p \sin(\pi x)\sin(\pi y)$.

Tables 19–26 present the numerical results for different parameter settings. In Table 19, with $\alpha = 0.2, 0.5, 0.8$ and $p = 2$, the CO approaches 1, confirming the theoretical prediction. Table 20, for $\alpha = 0.25, 0.5, 0.75$ and $p = 3$, shows the CO approaching 2, again in agreement with theory.

In Table 21, for $\alpha = 0.3, 0.5, 0.7$ and $p = 4$, the CO approaches 2. This behavior is expected since $M = 1$, and consequently $l = 1$; with $M = N$, the theoretical order is 2. Similarly, in Table 22, for $\alpha = 0.35, 0.55, 0.85$ and $p = 5$, the CO also approaches 2, which is again consistent with the fact that $M = 1$ and thus $l = 1$; with $M = N$, the theoretical order remains 2.

Table 23, with $\alpha = 0.2, 0.5, 0.7$ and $p = 2 - \alpha$, shows the CO approaching $2 - \alpha$, matching the theoretical order. Similarly, Table 24 for $\alpha = 0.1, 0.5, 0.9$ and $p = 3 - \alpha$ demonstrates the CO approaching 2 as predicted.

Furthermore, Table 25 for $\alpha = 0.25, 0.5, 0.75$ and $p = 4 - \alpha$, and Table 26 for $\alpha = 0.3, 0.6, 0.9$ and $p = 3 + \alpha$ both confirm the second-order convergence, consistent with theoretical expectations. Fig. 4 provides graphical illustrations of the error and solution surface from Table 26 for $\alpha = 0.9$ and $M = 20$.

Table 19: Numerical outcomes, obtained by Grünwald–Letnikov formula for Example 6.1 with $p = 2$.

	$\alpha = 0.2$		$\alpha = 0.5$		$\alpha = 0.8$	
M	$\mathcal{L}^2$	CO	$\mathcal{L}^2$	CO	$\mathcal{L}^2$	CO
10	7.4589×10^{-3}	–	2.0601×10^{-2}	–	3.4424×10^{-2}	–
20	3.9719×10^{-3}	0.9091	1.0602×10^{-2}	0.9583	1.7580×10^{-2}	0.9695
30	2.7218×10^{-3}	0.9322	7.1668×10^{-3}	0.9659	1.1846×10^{-2}	0.9736
40	2.0497×10^{-3}	0.9858	5.3591×10^{-3}	1.0103	8.8436×10^{-3}	1.0160
TCO		1.0000		1.0000		1.0000

Table 20: Numerical outcomes, computed by second-order WSGL for Example 6.1 with $p = 3$.

	$\alpha = 0.25$		$\alpha = 0.5$		$\alpha = 0.75$	
M	$\mathcal{L}^2$	CO	$\mathcal{L}^2$	CO	$\mathcal{L}^2$	CO
10	1.2906×10^{-3}	–	2.8287×10^{-3}	–	5.1385×10^{-3}	–
20	3.6906×10^{-4}	1.8061	7.4264×10^{-4}	1.9294	1.3380×10^{-3}	1.9413
30	1.6950×10^{-4}	1.9191	3.3815×10^{-4}	1.9403	6.0685×10^{-4}	1.9500
40	9.4480×10^{-5}	2.0316	1.9047×10^{-4}	1.9953	3.4167×10^{-4}	1.9967
TCO		2.0000		2.0000		2.0000

Table 21: Numerical outcomes, computed by third-order WSGL for Example 6.1 with $p = 4$.

	$\alpha = 0.3$		$\alpha = 0.5$		$\alpha = 0.7$	
M	$\mathcal{L}^2$	CO	$\mathcal{L}^2$	CO	$\mathcal{L}^2$	CO
10	1.1838×10^{-3}	–	1.1152×10^{-3}	–	1.3512×10^{-3}	–
20	3.7558×10^{-4}	1.6562	3.4285×10^{-4}	1.7016	3.3154×10^{-4}	2.0270
30	1.7474×10^{-4}	1.8872	1.6176×10^{-4}	1.8527	1.5385×10^{-4}	1.8936
40	9.7511×10^{-5}	2.0276	9.1149×10^{-5}	1.9939	8.6845×10^{-5}	1.9877
TCO		2.0000		2.0000		2.0000

Table 22: Numerical outcomes, computed using the fourth-order WSGL scheme for Example 6.1 with $p = 5$.

	$\alpha = 0.35$		$\alpha = 0.55$		$\alpha = 0.85$	
M	$\mathcal{L}^2$	CO	$\mathcal{L}^2$	CO	$\mathcal{L}^2$	CO
10	1.2310×10^{-3}	–	1.0890×10^{-3}	–	1.0207×10^{-3}	–
20	3.8638×10^{-4}	1.6717	3.6104×10^{-4}	1.5927	3.3061×10^{-4}	1.6263
30	1.7770×10^{-4}	1.9157	1.6854×10^{-4}	1.8789	1.5802×10^{-4}	1.8206
40	9.8566×10^{-5}	2.0486	9.4204×10^{-5}	2.0221	8.9542×10^{-5}	1.9745
TCO		2.0000		2.0000		2.0000

Table 23: Numerical outcomes, obtained by L1 scheme for Example 6.1 with $p = 2 - \alpha$.

	$\alpha = 0.2$		$\alpha = 0.5$		$\alpha = 0.7$	
M	$\mathcal{L}^2$	CO	$\mathcal{L}^2$	CO	$\mathcal{L}^2$	CO
10	1.2710×10^{-3}	–	8.4966×10^{-3}	–	2.2044×10^{-2}	–
20	3.9732×10^{-4}	1.6776	3.2390×10^{-3}	1.3914	9.3911×10^{-3}	1.2310
30	1.9562×10^{-4}	1.7475	1.8299×10^{-3}	1.4083	5.6712×10^{-3}	1.2439
40	1.1624×10^{-4}	1.8095	1.2023×10^{-3}	1.4601	3.9113×10^{-3}	1.2915
TCO		1.8000		1.5000		1.3000

Table 24: Numerical outcomes, by L1-2 formula for Example 6.1 with $p = 3 - \alpha$.

	$\alpha = 0.1$		$\alpha = 0.5$		$\alpha = 0.9$	
M	$\mathcal{L}^2$	CO	$\mathcal{L}^2$	CO	$\mathcal{L}^2$	CO
10	1.4745×10^{-3}	–	1.1273×10^{-3}	–	1.0889×10^{-3}	–
20	4.2754×10^{-4}	1.7860	3.5171×10^{-4}	1.6804	3.3574×10^{-4}	1.6974
30	1.9370×10^{-4}	1.9527	1.6371×10^{-4}	1.8861	1.5498×10^{-4}	1.9067
40	1.0671×10^{-4}	2.0725	9.1469×10^{-5}	2.0233	8.6300×10^{-5}	2.0350
TCO		2.0000		2.0000		2.0000

Table 25: Numerical outcomes, obtained by L1-2-3 method for Example 6.1 with $p = 4 - \alpha$.

	$\alpha = 0.25$		$\alpha = 0.5$		$\alpha = 0.75$	
M	$\mathcal{L}^2$	CO	$\mathcal{L}^2$	CO	$\mathcal{L}^2$	CO
10	1.3819×10^{-3}	–	1.2298×10^{-3}	–	1.1489×10^{-3}	–
20	4.0868×10^{-4}	1.7576	3.8026×10^{-4}	1.6934	3.6121×10^{-4}	1.6693
30	1.8577×10^{-4}	1.9444	1.7482×10^{-4}	1.9165	1.6727×10^{-4}	1.8987
40	1.0251×10^{-4}	2.0667	9.7055×10^{-5}	2.0456	9.3337×10^{-5}	2.0279
TCO		2.0000		2.0000		2.0000

7. Spectral element method for TFDEs

Recently, considerable attention has been devoted to the spectral element method (SEM) for the numerical solution of both PDEs and FPDEs [1, 6, 7, 8, 10, 43, 47, 48, 136]. SEM offers a powerful framework that blends the flexibility of the FEM with the high-order accuracy of spectral methods. This hybrid approach enables the resolution of

Table 26: Numerical outcomes, computed by L2-1_σ formula for Example 6.1 with $p = 3 + \alpha$.

	$\alpha = 0.3$		$\alpha = 0.6$		$\alpha = 0.9$	
M	$\mathcal{L}^2$	CO	$\mathcal{L}^2$	CO	$\mathcal{L}^2$	CO
10	1.5179×10^{-3}	–	3.1418×10^{-3}	–	4.2634×10^{-3}	–
20	4.2607×10^{-4}	1.8329	8.3686×10^{-4}	1.9085	1.0996×10^{-3}	1.9551
30	1.9685×10^{-4}	1.9044	3.8537×10^{-4}	1.9125	4.9973×10^{-4}	1.9449
40	1.1087×10^{-4}	1.9956	2.1907×10^{-4}	1.9633	2.8242×10^{-4}	1.9838
TCO		2.0000		2.0000		2.0000

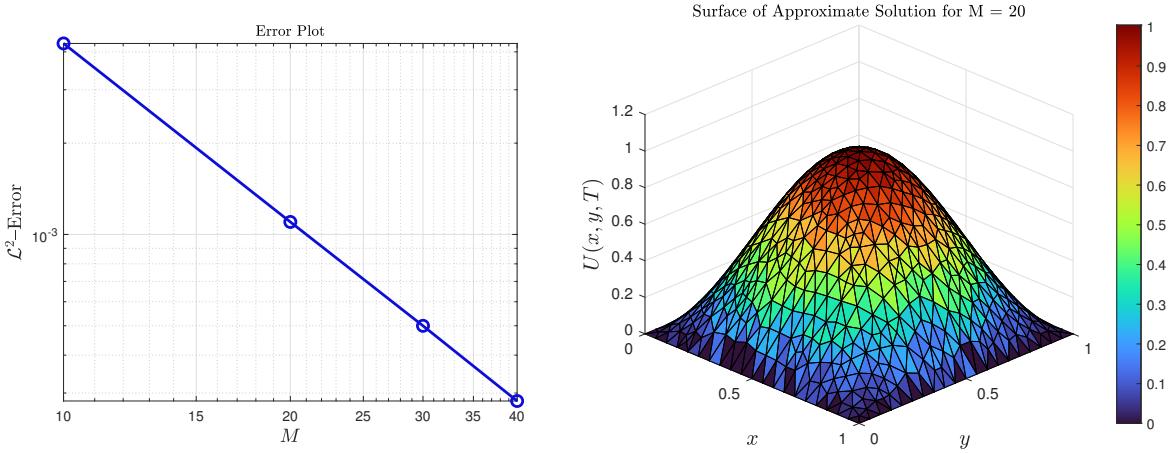

Figure 4: Graphical illustration of error and surface plots for Table 26 with $\alpha = 0.9$ and $M = 20$.

complex geometries and boundary conditions while achieving spectral convergence rates for smooth solutions. In the current section, we explore the implementation of SEM for solving Eq. (1) using Legendre polynomials as basis functions, which are particularly suitable due to their orthogonality and excellent approximation properties on bounded domains [158]. Moreover, there are some initial tips and important lemmas in Refs. [19, 43, 158] which can be useful for the interested reader.

Originally introduced by Patera [136], the SEM is constructed by partitioning the domain into non-overlapping elements, within which high-degree spectral polynomials are employed for spatial approximation. This structure retains the local approximation flexibility of FEM while achieving the superior convergence characteristics of spectral methods. When applied to fractional models, SEM is particularly advantageous due to its ability to accurately capture nonlocal behaviors and singularities inherent in fractional operators. By leveraging SEM in the current work, we aim to obtain highly accurate numerical solutions for Eq. (1), particularly in scenarios where traditional low-order methods may suffer from reduced efficiency or accuracy [32, 85, 136].

Before proceeding to the next section, we introduce the notation $\mathbb{S}_M^0(\Omega)$, which denotes the spectral element approximation space, defined as

$$\mathbb{S}_M^0(\Omega) := \left\{ u \in \mathcal{H}_0^1(\Omega) \;\middle|\; u|_{\Omega_k} \in \mathcal{P}_M(\Omega_k),\ 1 \le k \le m_k \right\}. \tag{67}$$

where $\mathcal{P}_M(\Omega_k)$ represents the space of polynomials of degree at most M on Ω_k.

7.1. Weak formulations

To derive the weak forms corresponding to SEM, we follow the same procedures as utilized in §6.1. The variational weak form of Eq. (32) is presented as follows

$$\left(\tau^{-\alpha} \sum_{k=0}^{n} g_k^{(\alpha)} u^{n-k}, \varsigma^n \right) - \varepsilon \left(\Delta u^n, \varsigma^n \right) + \left(\mathrm{T}_n^{(\alpha)}, \varsigma^n \right) = \left(f^n, \varsigma^n \right), \qquad \forall \varsigma^n \in \mathbb{S}_M^0.$$

Then by dropping the truncation error, one has

$$\exists U^n \in \mathbb{S}_M^0(\Omega) \quad \ni \quad \left(\tau^{-\alpha} \sum_{k=0}^{n} g_k^{(\alpha)} U^{n-k}, \varsigma^n \right) - \varepsilon \left(\Delta U^n, \varsigma^n \right) = \left(f^n, \varsigma^n \right), \qquad \forall \varsigma^n \in \mathbb{S}_M^0. \tag{68}$$

Obviously, for the second-order WSGL and Eq. (44), it can be deduced that

$$\left(\tau^{-\alpha}\sum_{k=0}^{n} w_k^{(\alpha)} U^{n-k}, \varsigma^n\right) - \varepsilon\left(\Delta U^n, \varsigma^n\right) = \left(f^n, \varsigma^n\right), \qquad \forall \varsigma^n \in \mathbb{S}_M^0, \tag{69}$$

and

$$\left(\tau^{-\alpha}\sum_{k=0}^{n} \lambda_k^{(\alpha)} U^{n-k}, \varsigma^n\right) - \varepsilon\left(\Delta U^n, \varsigma^n\right) = \left(f^n, \varsigma^n\right), \qquad \forall \varsigma^n \in \mathbb{S}_M^0. \tag{70}$$

Additionally, for the fourth-order WSGL formula, we have

$$\left(\tau^{-\alpha}\sum_{k=0}^{n} \vartheta_k^{(\alpha)} U^{n-k}, \varsigma^n\right) - \varepsilon\left(\Delta U^n, \varsigma^n\right) = \left(f^n, \varsigma^n\right), \qquad \forall \varsigma^n \in \mathbb{S}_M^0. \tag{71}$$

To derive the schemes based on L–type approximations and Legendre SEM, we should present the weak formulations. The weak form of Eq. (48) can be obtained as follows

$$\left(\sum_{k=1}^{n} a_{n-k}^{(\alpha)} \delta u^k, \varsigma^n\right) - \varepsilon\left(\Delta u^n, \varsigma^n\right) + \left(\mathrm{T}_n^{(\alpha)}, \varsigma^n\right) = \left(f^n, \varsigma^n\right), \qquad \forall \varsigma^n \in \mathbb{S}_M^0.$$

Then there exists a $U^n \in \mathbb{S}_M^0(\Omega)$ such that

$$\left(\sum_{k=1}^{n} a_{n-k}^{(\alpha)} \delta U^k, \varsigma^n\right) - \varepsilon\left(\Delta U^n, \varsigma^n\right) = \left(f^n, \varsigma^n\right), \qquad \forall \varsigma^n \in \mathbb{S}_M^0. \tag{72}$$

In the same manner, the corresponding spectral element schemes for formulations based on various L–type discretizations are derived as follows. For the L1-2 formula, the scheme is given by

$$\left(\sum_{k=1}^{n} c_{n-k}^{(\alpha)} \delta U^k, \varsigma^n\right) - \varepsilon\left(\Delta U^n, \varsigma^n\right) = \left(f^n, \varsigma^n\right), \quad \forall \varsigma^n \in \mathbb{S}_M^0. \tag{73}$$

For the L1-2-3 scheme, the corresponding formulation is

$$\left(\sum_{k=1}^{n} d_{n-k}^{(\alpha)} \delta U^k, \varsigma^n\right) - \varepsilon\left(\Delta U^n, \varsigma^n\right) = \left(f^n, \varsigma^n\right), \quad \forall \varsigma^n \in \mathbb{S}_M^0. \tag{74}$$

Finally, for the L2-1_σ scheme, the formulation becomes

$$\left(\sum_{k=1}^{n} c_{n-k}^{(n)} \delta U^k, \varsigma^{n+\sigma}\right) - \varepsilon\left(\Delta U^{n+\sigma}, \varsigma^{n+\sigma}\right) = \left(f^{n+\sigma}, \varsigma^{n+\sigma}\right), \qquad \forall \varsigma^{n+\sigma} \in \mathbb{S}_M^0. \tag{75}$$

7.2. Theoretical findings

To present the convergence analysis of the SEM, we need an orthogonal projection operator. Thus, we define the projection operator $\Phi_M : \mathcal{H}_0^1(\Omega) \to \mathbb{S}_M^0(\Omega)$ such that [31]

$$\left(\nabla\left(u^n - \Phi_M u^n\right), \nabla\varsigma^n\right) = 0, \quad \forall \varsigma^n \in \mathbb{S}_M^0, \tag{76}$$

where $\mathbb{S}_M^0(\Omega)$ denotes the spectral element approximation space, defined by Eq. (67). Here, $\mathcal{P}_M(\Omega_k)$ represents the space of polynomials of degree at most M on the subdomain Ω_k, and m_k is the total number of elements.

Lemma 7.1 ([31, 32, 141]). *Let Φ_M be the orthogonal projection operator defined in Eq. (76). Then, the following approximation estimate holds*

$$\left\|u - \Phi_M u\right\|_{\mathcal{L}^2(\Omega)} \leq C M^{-\xi} \left\|u\right\|_{\mathcal{H}^\xi(\Omega)}, \quad \forall u \in \mathcal{H}_0^1(\Omega) \cap \mathcal{H}^\xi(\Omega),$$

where $\xi > 0$ is a regularity parameter and C is a constant independent of M.

We are now in a position to present and analyze the stability and convergence theorems corresponding to the proposed numerical schemes.

Theorem 7.2. *Assume $\tilde{U}^n \in \mathbb{S}_M^0(\Omega)$ is an estimation of approximate solution U^n. The discrete schemes (68)–(75) are unconditionally stable.*

Proof. The proof follows a similar structure to those given in Theorems 6.6 and 6.7. □

Theorem 7.3. *If $U^n \in \mathbb{S}_M^0(\Omega)$ is the approximate solution of u^n, given by Eq. (70), and $u \in \mathcal{S}^{3+\alpha}(\mathbb{R})$, provided $U^0 = \Phi_M u^0$, then there exists a $C > 0$, independent of τ and M such that*

$$\|u^n - U^n\| \leq C\left(\tau^3 + M^{-\xi}\right),$$

for $n \geq 1$.

Proof. Introducing the following notations

$$v^n := u^n - \Phi_M u^n, \quad w^n := U^n - \Phi_M u^n,$$

then we have

$$\left(\tau^{-\alpha}\sum_{k=0}^{n}\lambda_k^{(\alpha)} v^{n-k}, \varsigma^n\right) - \left(\tau^{-\alpha}\sum_{k=0}^{n}\lambda_k^{(\alpha)} w^{n-k}, \varsigma^n\right) - \varepsilon\left(\nabla w^n, \nabla\varsigma^n\right) + \left(\mathrm{T}_n^{(\alpha)}, \varsigma^n\right) = 0.$$

Setting $\varsigma^n = w^n$, and following the same argument as presented in the proof of Theorem 6.9 leads to

$$\frac{\varepsilon}{3C_\Omega}\sum_{n=1}^{N}\|w^n\|^2 \leq \frac{3C_\Omega}{4\varepsilon}\sum_{n=1}^{N}\left(\left\|\tau^{-\alpha}\sum_{k=0}^{n}\lambda_k^{(\alpha)} v^{n-k}\right\|^2 + \left\|\mathrm{T}_n^{(\alpha)}\right\|^2\right).$$

The use of Lemma 7.1 results

$$\|w^n\|^2 \leq \frac{9C_\Omega^2}{4\varepsilon^2}\left(\tilde{C}^2 M^{-2\xi}\max_{1\leq n\leq N}\left\|{}_0^C\mathcal{D}_t^\alpha u^n\right\|^2 + \max_{1\leq n\leq N}\left\|\mathrm{T}_n^{(\alpha)}\right\|^2\right).$$

Assuming $C = \dfrac{3C_\Omega}{2\varepsilon}\max\left\{\tilde{C}\max_{1\leq n\leq N}\left\|{}_0^C\mathcal{D}_t^\alpha u^n\right\|, \hat{C}\right\}$, and then one obtains the following relation

$$\|w^n\| \leq C\left(\tau^3 + M^{-\xi}\right).$$

An application of the triangle inequality completes the proof. □

Theorem 7.4. *Suppose $U^n \in \mathbb{S}_M^0(\Omega)$ is the solution of the system, presented by Eq. (68) (Eq. (69)) ((Eq. (71))), and $u \in \mathcal{S}^{1+\alpha}(\mathbb{R})$ ($u \in \mathcal{S}^{2+\alpha}(\mathbb{R})$) ((($u \in \mathcal{S}^{4+\alpha}(\mathbb{R})$))), such that $U^0 = \Phi_M u^0$, then*

$$\|u^n - U^n\| \leq C\left(\tau + M^{-\xi}\right), \quad \left(\|u^n - U^n\| \leq C\left(\tau^2 + M^{-\xi}\right),\right) \quad \left(\left(\|u^n - U^n\| \leq C\left(\tau^4 + M^{-\xi}\right),\right)\right)$$

in which C is a positive constant independent of τ and M.

Proof. The proof is similar to the proof of Theorem 7.3. □

Theorem 7.5. *Let $u \in \mathcal{C}^2[0,T]$, and $U^n \in \mathcal{P}_M^h(\Omega)$ be the approximate solution of Eq. (1), given by Eq. (72), and $U^0 = \Phi_M u^0$. Hence*

$$\|u^n - U^n\| \leq C\left(\tau^{2-\alpha} + M^{-\xi}\right), \qquad 1 \leq n \leq N,$$

where $C > 0$ and it is independent of τ and M.

Proof. Denoting

$$v^n := u^n - \Phi_M u^n, \quad w^n := U^n - \Phi_M u^n,$$

then one obtains

$$\left({}_0^C\mathrm{D}_t^\alpha w^n, \varsigma^n\right) + \varepsilon\left(\nabla w^n, \nabla\varsigma^n\right) = \left({}_0^C\mathrm{D}_t^\alpha v^n, \varsigma^n\right) + \left(\mathrm{T}_n^{(\alpha)}, \varsigma^n\right).$$

By choosing $\varsigma^n = w^n$ and proceeding with the argument analogous to that in the proof of Theorem 6.11, we obtain

$${}_0^C\mathrm{D}_t^\alpha\|w^n\|^2 \leq \|w^n\|^2 + \left\|{}_0^C\mathrm{D}_t^\alpha v^n\right\|^2 + \frac{C_\Omega}{2\varepsilon}\left\|\mathrm{T}_n^{(\alpha)}\right\|^2.$$

The use of Lemmas 7.1 and 6.3 holds

$$\|w^n\| \leq C\left(\tau^{2-\alpha} + M^{-\xi}\right).$$

Finally, employing the triangle inequality finishes the proof. □

Since the proof of the following theorem is essentially the same as that of the previous one, it is omitted for brevity.

Theorem 7.6. *Let U^n be the estimate solution obtained from Eq. (73) (or Eq. (74)), and suppose that the exact solution satisfies $u \in \mathcal{C}^3[0,T]$ for Eq. (73), and $u \in \mathcal{C}^4[0,T]$ for Eq. (74). In addition, let $U^0 = \Phi_M u^0$. Then, there exists a constant $C > 0$, independent of τ and M, such that for all $n \geq 1$, the following error estimates hold for Eq. (73)*

$$\|u^n - U^n\| \leq C\left(\tau^{3-\alpha} + M^{-\xi}\right),$$

and for Eq. (74)

$$\|u^n - U^n\| \leq C\left(\tau^{4-\alpha} + M^{-\xi}\right).$$

Theorem 7.7. *If U^n is the solution of Eq. (75), and $u \in \mathcal{C}^3[0,T]$ with $U^0 = \Phi_M u^0$, then there exists a constant $C > 0$, independent of τ and M, such that $\forall n \geq 1$, the following error estimate holds*

$$\|u^n - U^n\| \leq C\left(\tau^2 + M^{-\xi}\right).$$

Proof. First defining

$$v^{n+\sigma} := u^{n+\sigma} - \Phi_M u^{n+\sigma}, \quad w^{n+\sigma} := U^{n+\sigma} - \Phi_M u^{n+\sigma}.$$

Similar to the proof of Theorem 6.11, we arrive at the following result

$$ {}_0^C\mathrm{D}_t^\alpha \left\|w^{n+\sigma}\right\|^2 \leq \left\|w^{n+\sigma}\right\|^2 + \left\|{}_0^C\mathrm{D}_t^\alpha v^{n+\sigma}\right\|^2 + \frac{C_\Omega}{2\varepsilon}\left\|\mathrm{T}_{n+\sigma}^{(\alpha)}\right\|^2.$$

Applying Lemmas 7.1 and 6.4 gives the following estimate

$$\|w^n\| \leq C\left(\tau^2 + M^{-\xi}\right),$$

and using the triangle inequality completes the proof. □

7.3. Numerical results

Example 7.1. For this experiment, we consider the exact solution of Eq. (1) as

$$u(x,y,t) = t^p x^2(1-x)^2 y^2(1-y)^2,$$

with the corresponding source term given by

$$f(x,y,t) = \frac{\Gamma(p+1)}{\Gamma(p+1-\alpha)} t^{p-\alpha} x^2(1-x)^2 y^2(1-y)^2 - t^p\left(2 - 12x + 12x^2\right)\left(y^2 - 2y^3 + y^4\right) + \left(2 - 12y + 12y^2\right)\left(x^2 - 2x^3 + x^4\right).$$

The spatial domain is set as $\Omega = [0,1]^2$ and the final time as $T = 1$.

In one scenario, with $\varepsilon = 0.1$, Table 27 presents the results using the first-order Grünwald–Letnikov scheme for fractional orders $\alpha = 0.2, 0.5, 0.8$ with $p = 1$. The CO approaches 1, consistent with Theorem 7.4. Table 28 reports the results obtained by applying the second-order WSGL scheme for $\alpha = 0.2, 0.5, 0.7$ and $p = 2$, where the CO approaches 2 as predicted by Theorem 7.4. Moreover, Table 29 shows that using scheme (70) with $p = 3$ and $\alpha = 0.3, 0.6, 0.8$ achieves third-order convergence, in agreement with Theorem 7.3. Similarly, Table 30 shows that scheme (71) with $p = 3$ and $\alpha = 0.25, 0.5, 0.85$ achieves fourth-order convergence, consistent with Theorem 7.4.

Table 27: Numerical results for Example 7.1 with $p = 1$.

	$\alpha = 0.2$		$\alpha = 0.5$		$\alpha = 0.8$	
M	$\mathcal{L}^2$	CO	$\mathcal{L}^2$	CO	$\mathcal{L}^2$	CO
10	3.4056×10^{-6}	–	6.7901×10^{-6}	–	6.1159×10^{-6}	–
20	1.6723×10^{-6}	1.0261	3.3770×10^{-6}	1.0077	3.1488×10^{-6}	0.9578
30	1.1092×10^{-6}	1.0124	2.2535×10^{-6}	0.9976	2.1398×10^{-6}	0.9528
40	8.3001×10^{-7}	1.0080	1.6925×10^{-6}	0.9952	1.6267×10^{-6}	0.9530
TCO		1.0000		1.0000		1.0000

In a different scenario, setting $\varepsilon = \frac{1}{4\pi^2}$, Table 31 displays results obtained by the L1 scheme for fractional orders $\alpha = 0.35, 0.65, 0.85$ with $p = 1 + \alpha$, achieving an accuracy order of $2 - \alpha$. Table 32 presents results for the L1-2 scheme with $\alpha = 0.1, 0.5, 0.9$ and $p = 2 + \alpha$, where the convergence order is $3 - \alpha$. Using scheme (75) for $\alpha = 0.25, 0.5, 0.75$ and $p = 2$, Table 33 demonstrates second-order accuracy. Finally, Table 34 reports the results of the L1-2-3 scheme with $\alpha = 0.3, 0.5, 0.9$ and $p = 3+\alpha$, showing an accuracy order of $4-\alpha$. Fig. 5 is an illustration of the error plot in logarithmic scale and the surface of approximate solution, corresponding to Table 34 with $M = 40$ and the derivative order $\alpha = 0.3$.

Table 28: Numerical results for Example 7.1 with $p = 2$.

	$\alpha = 0.2$		$\alpha = 0.5$		$\alpha = 0.7$	
M	$\mathcal{L}^2$	CO	$\mathcal{L}^2$	CO	$\mathcal{L}^2$	CO
10	7.9716×10^{-7}	–	1.9341×10^{-6}	–	2.4521×10^{-6}	–
20	2.1809×10^{-7}	1.8699	5.2566×10^{-7}	1.8795	6.6048×10^{-7}	1.8924
30	9.9988×10^{-8}	1.9234	2.4052×10^{-7}	1.9283	3.0154×10^{-7}	1.9337
40	5.7134×10^{-8}	1.9454	1.3732×10^{-7}	1.9484	1.7202×10^{-7}	1.9512
TCO		2.0000		2.0000		2.0000

Table 29: Numerical results for Example 7.1 with $p = 3$.

	$\alpha = 0.3$		$\alpha = 0.6$		$\alpha = 0.8$	
M	$\mathcal{L}^2$	CO	$\mathcal{L}^2$	CO	$\mathcal{L}^2$	CO
10	2.1266×10^{-7}	–	4.3651×10^{-7}	–	5.5199×10^{-7}	–
20	3.0251×10^{-8}	2.8135	6.1025×10^{-8}	2.8385	7.5408×10^{-8}	2.8719
30	9.3707×10^{-9}	2.8904	1.8789×10^{-8}	2.9053	2.3031×10^{-8}	2.9252
40	4.0431×10^{-9}	2.9218	8.0821×10^{-9}	2.9325	9.8659×10^{-9}	2.9468
TCO		3.0000		3.0000		3.0000

Table 30: Numerical results for Example 7.1 with $p = 3$.

	$\alpha = 0.25$		$\alpha = 0.5$		$\alpha = 0.85$	
M	$\mathcal{L}^2$	CO	$\mathcal{L}^2$	CO	$\mathcal{L}^2$	CO
10	2.1523×10^{-9}	–	1.1090×10^{-8}	–	5.1748×10^{-8}	–
20	1.4735×10^{-10}	3.8685	7.4695×10^{-10}	3.8920	3.2226×10^{-9}	4.0052
30	2.9920×10^{-11}	3.9320	1.4921×10^{-10}	3.9723	6.2749×10^{-10}	4.0354
40	9.5764×10^{-12}	3.9601	4.7147×10^{-11}	4.0048	1.9420×10^{-10}	4.0768
TCO		4.0000		4.0000		4.0000

Table 31: Numerical results for Example 7.1 with $p = 1 + \alpha$.

	$\alpha = 0.35$		$\alpha = 0.65$		$\alpha = 0.85$	
M	$\mathcal{L}^2$	CO	$\mathcal{L}^2$	CO	$\mathcal{L}^2$	CO
10	5.6250×10^{-7}	–	4.7661×10^{-6}	–	1.5313×10^{-5}	–
20	1.8250×10^{-7}	1.6240	1.8554×10^{-6}	1.3610	6.7951×10^{-6}	1.1722
30	9.4381×10^{-8}	1.6262	1.0718×10^{-6}	1.3534	4.2436×10^{-6}	1.1611
40	5.9070×10^{-8}	1.6289	7.2658×10^{-7}	1.3514	3.0418×10^{-6}	1.1574
TCO		1.6500		1.3500		1.1500

Table 32: Numerical results for Example 7.1 with $p = 2 + \alpha$.

	$\alpha = 0.1$		$\alpha = 0.5$		$\alpha = 0.9$	
M	$\mathcal{L}^2$	CO	$\mathcal{L}^2$	CO	$\mathcal{L}^2$	CO
10	2.3407×10^{-8}	–	2.7646×10^{-7}	–	3.4473×10^{-6}	–
20	3.0448×10^{-9}	2.9425	4.8251×10^{-8}	2.5185	8.2640×10^{-7}	2.0606
30	9.1053×10^{-10}	2.9772	1.7391×10^{-8}	2.5167	3.5631×10^{-7}	2.0749
40	3.8508×10^{-10}	2.9914	8.4364×10^{-9}	2.5146	1.9578×10^{-7}	2.0815
TCO		2.9000		2.5000		2.1000

Table 33: Numerical results for Example 7.1 with $p = 2$.

	$\alpha = 0.25$		$\alpha = 0.5$		$\alpha = 0.75$	
M	$\mathcal{L}^2$	CO	$\mathcal{L}^2$	CO	$\mathcal{L}^2$	CO
10	2.3774×10^{-7}	–	3.2706×10^{-7}	–	2.5952×10^{-7}	–
20	6.0454×10^{-8}	1.9755	8.3425×10^{-8}	1.9710	6.6981×10^{-8}	1.9540
30	2.7051×10^{-8}	1.9833	3.7389×10^{-8}	1.9794	3.0212×10^{-8}	1.9636
40	1.5271×10^{-8}	1.9875	2.1128×10^{-8}	1.9840	1.7147×10^{-8}	1.9690
TCO		2.0000		2.0000		2.0000

Table 34: Numerical results for Example 7.1 with $p = 3 + \alpha$.

	$\alpha = 0.3$		$\alpha = 0.5$		$\alpha = 0.9$	
M	$\mathcal{L}^2$	CO	$\mathcal{L}^2$	CO	$\mathcal{L}^2$	CO
10	1.1206×10^{-8}	–	5.4157×10^{-8}	–	8.8036×10^{-7}	–
20	8.9163×10^{-10}	3.6516	5.1760×10^{-9}	3.3872	1.1241×10^{-7}	2.9693
30	2.0001×10^{-10}	3.6863	1.2855×10^{-9}	3.4353	3.2947×10^{-8}	3.0268
40	6.9058×10^{-11}	3.6966	4.7605×10^{-10}	3.4530	1.3707×10^{-8}	3.0484
TCO		3.7000		3.5000		3.1000

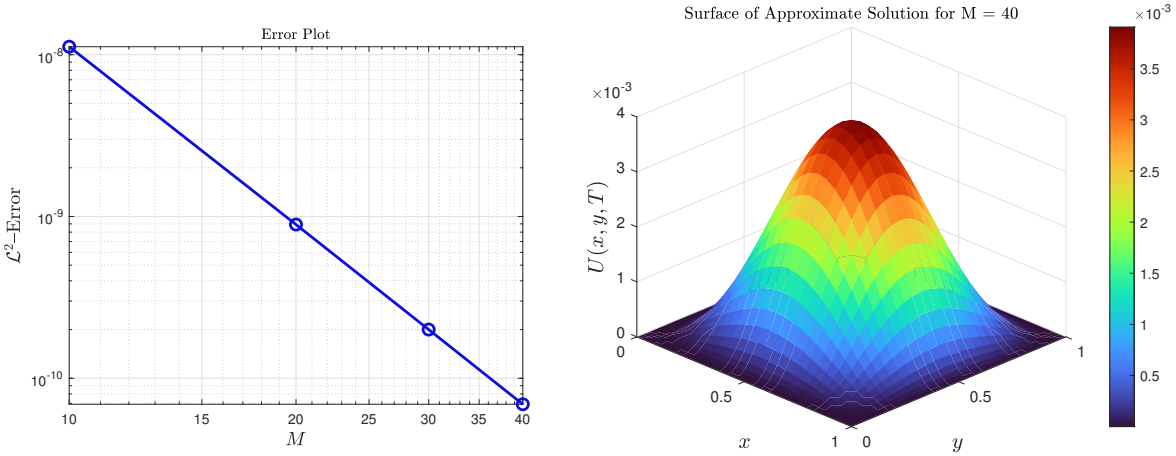

Figure 5: Graphs of error and surface plots for Table 34 with $\alpha = 0.3$ and $M = 40$.

8. Chebyshev spectral method for TFDEs

The Chebyshev spectral method (CSM) is a classic approach for solving PDEs. Its main idea is to employ the Chebyshev nodes (2) as collocation points in the Lagrange interpolation process. The method is employed by many researchers for solving FPDEs [32, 57, 58, 67, 68, 159, 169, 173]. Before presenting the schemes based on CSM, we need the following definition.

Definition 8.1 ([32, 71, 159, 173]). *Assume that $M \in \mathbb{N}$. The $(M+1) \times (M+1)$ Chebyshev derivative matrix* $\mathbf{D}$*, with both rows and columns indexed from 0 to M, is defined by its entries as follows*

$$\mathbf{D}_{ij} = \begin{cases} \dfrac{2M^2+1}{6}, & i = j = 0, \\ \dfrac{c_i(-1)^{i+j}}{c_j\,(x_i - x_j)}, & i \neq j,\ i, j = 0, 1, \ldots, M, \\ -\dfrac{x_j}{2(1-x_j^2)}, & i = j = 1, 2, \ldots, M-1, \\ -\dfrac{2M^2+1}{6}, & i = j = M, \end{cases}$$

in which $c_i = 1$ for $i = 1, 2, \ldots, M-1$, and $c_0 = c_M = 2$.

8.1. Compact matrix forms

To establish the numerical schemes based on CSM, we use Definition 8.1 and Eq. (3). Firstly, considering Eq. (32), we assume that $U^n \in \mathcal{P}(\omega)$ and neglect the error term. This yields

$$\tau^{-\alpha}\sum_{k=0}^{n} g_k^{(\alpha)} U^{n-k} - \varepsilon \Delta U^n = f^n. \tag{77}$$

By rearranging the terms, Eq. (77) can be rewritten as follows

$$\tau^{-\alpha} g_0^{(\alpha)} U^n - \varepsilon \Delta U^n = f^n - \tau^{-\alpha}\sum_{k=1}^{n} g_k^{(\alpha)} U^{n-k}.$$

Now, approximating Δ using the differentiation matrix in Definition 8.1 and in the compact matrix form, one obtains

$$\mathcal{A}U^n = \mathcal{F}^{(n)}, \qquad 1 \le n \le N, \tag{78}$$

with

$$\mathcal{A} = \tau^{-\alpha} g_0^{(\alpha)} \mathcal{I} - \varepsilon \left(\left(\mathbf{D}^2 \otimes I \right) + \left(I \otimes \mathbf{D}^2 \right) \right), \quad \mathcal{I} = I \otimes I,$$

$$\mathcal{F}^{(n)} = f^n - \tau^{-\alpha}\sum_{k=1}^{n} g_k^{(\alpha)} U^{n-k}.$$

The same process can be applied to the second-, third- and fourth-order WSGL schemes, yielding

$$\mathcal{A}U^n = \mathcal{F}^{(n)}, \qquad 1 \le n \le N, \tag{79}$$

in which

$$\mathcal{A} = \tau^{-\alpha} w_0^{(\alpha)} \mathcal{I} - \varepsilon \left(\left(\mathbf{D}^2 \otimes I \right) + \left(I \otimes \mathbf{D}^2 \right) \right),$$

$$\mathcal{F}^{(n)} = f^n - \tau^{-\alpha}\sum_{k=1}^{n} w_k^{(\alpha)} U^{n-k},$$

and

$$\mathcal{A}U^n = \mathcal{F}^{(n)}, \qquad 1 \le n \le N, \tag{80}$$

where

$$\mathcal{A} = \tau^{-\alpha} \lambda_0^{(\alpha)} \mathcal{I} - \varepsilon \left(\left(\mathbf{D}^2 \otimes I \right) + \left(I \otimes \mathbf{D}^2 \right) \right),$$

$$\mathcal{F}^{(n)} = f^n - \tau^{-\alpha}\sum_{k=1}^{n} \lambda_k^{(\alpha)} U^{n-k}.$$

Moreover,

$$\mathcal{A}U^n = \mathcal{F}^{(n)}, \qquad 1 \le n \le N, \tag{81}$$

with the following coefficient matrix and RHS vector

$$\mathcal{A} = \tau^{-\alpha} \vartheta_0^{(\alpha)} \mathcal{I} - \varepsilon \left(\left(\mathbf{D}^2 \otimes I \right) + \left(I \otimes \mathbf{D}^2 \right) \right),$$

$$\mathcal{F}^{(n)} = f^n - \tau^{-\alpha}\sum_{k=1}^{n} \vartheta_k^{(\alpha)} U^{n-k}.$$

On the other side, we consider Eq. (48). Let $U^n \in \mathcal{P}(\omega)$. By dropping the truncation error, Eq. (48) can be rearranged as follows

$$a_0^{(\alpha)} U^n - \varepsilon \Delta U^n = a_0^{(\alpha)} U^{n-1} - \sum_{k=1}^{n-1} a_{n-k}^{(\alpha)} \delta U^k + f^n,$$

which leads to the following compact matrix scheme

$$\mathcal{A}U^n = \mathcal{F}^{(n)}, \qquad 1 \le n \le N, \tag{82}$$

where the LHS matrix and RHS vector is introduced as follows

$$\mathcal{A} = a_0^{(\alpha)}\mathcal{I} - \varepsilon\left(\left(\mathbf{D}^2 \otimes I\right) + \left(I \otimes \mathbf{D}^2\right)\right),$$

$$\mathcal{F}^{(n)} = a_0^{(\alpha)} U^{n-1} - \sum_{k=1}^{n-1} a_{n-k}^{(\alpha)} \delta U^k + f^n,$$

Similarly, one can easily obtain the following matrix schemes for L1-2

$$\mathcal{A}U^n = \mathcal{F}^{(n)}, \qquad 1 \le n \le N, \tag{83}$$

in which

$$\mathcal{A} = c_0^{(\alpha)}\mathcal{I} - \varepsilon\left(\left(\mathbf{D}^2 \otimes I\right) + \left(I \otimes \mathbf{D}^2\right)\right),$$

$$\mathcal{F}^{(n)} = c_0^{(\alpha)} U^{n-1} - \sum_{k=1}^{n-1} c_{n-k}^{(\alpha)} \delta U^k + f^n,$$

and for L1-2-3

$$\mathcal{A}U^n = \mathcal{F}^{(n)}, \qquad 1 \le n \le N, \tag{84}$$

where

$$\mathcal{A} = d_0^{(\alpha)}\mathcal{I} - \varepsilon\left(\left(\mathbf{D}^2 \otimes I\right) + \left(I \otimes \mathbf{D}^2\right)\right),$$

$$\mathcal{F}^{(n)} = d_0^{(\alpha)} U^{n-1} - \sum_{k=1}^{n-1} d_{n-k}^{(\alpha)} \delta U^k + f^n.$$

Moreover, in a similar manner, at the $n+\sigma$ step one obtains

$$\mathcal{A}U^{n+1} = \mathcal{F}^{(n+\sigma)}, \quad 0 \le n \le N-1, \tag{85}$$

in which

$$\mathcal{A} = c_0^{(n)}\mathcal{I} - \varepsilon\sigma\left(\left(\mathbf{D}^2 \otimes I\right) + \left(I \otimes \mathbf{D}^2\right)\right),$$

$$\mathcal{F}^{(n+\sigma)} = c_0^{(n)} U^n - \sum_{k=0}^{n-1} c_{n-k}^{(n)} \delta U^k + \varepsilon(1-\sigma)\left(\left(\mathbf{D}^2 \otimes I\right) + \left(I \otimes \mathbf{D}^2\right)\right) U^n + \sigma f^{n+1} + (1-\sigma) f^n.$$

8.2. Theoretical results

In this section, our target is to establish the stability and convergence theorems for the obtained schemes. In order to investigate the convergence, it is required to introduce the following projection operator $\mathrm{P}_M : \mathcal{H}_0^1(\Omega) \to \mathcal{P}(\omega)$, such that

$$\Delta u^n = \Delta \mathrm{P}_M u^n, \tag{86}$$

where $\mathcal{P}(\omega)$ is given by Eq. (3) in §2.2.

Lemma 8.2 ([31, 32, 141]). *Assume that $\mathrm{P}_M u^n \in \mathcal{P}(\omega)$ denotes a projection operator. For any function $u^n \in \mathcal{H}_0^1(\Omega) \cap \mathcal{H}^\rho(\Omega)$ with $\rho \ge 1$ and the Chebyshev nodes (2), the following relation is hold*

$$\|u^n - \mathrm{P}_M u^n\|_{\mathcal{L}^2(\Omega)} \le C M^{-\rho} \|u^n\|_{\mathcal{H}^\rho(\Omega)}.$$

With the preceding lemmas established, we are now equipped to formulate and rigorously analyze the stability and convergence theorems corresponding to the proposed numerical schemes.

Theorem 8.3. *Assume $\tilde{U}^n \in \mathcal{P}(\omega)$ is an approximation for U^n, in Eqs. (78)–(81). Therefore, the discrete schemes (78)–(81) are unconditionally stable.*

Proof. We first consider Eq. (57), then

$$\tau^{-\alpha} \sum_{k=0}^{n} \lambda_k^{(\alpha)} \mathcal{E}^{n-k} - \varepsilon \Delta \mathcal{E}^n = 0. \tag{87}$$

An inner product of Eq. (87) by $\mathcal{E}^n$ gives

$$\left(\tau^{-\alpha} \sum_{k=0}^{n} \lambda_k^{(\alpha)} \mathcal{E}^{n-k}, \mathcal{E}^n\right) - \varepsilon\left(\Delta \mathcal{E}^n, \mathcal{E}^n\right) = 0.$$

The proof is completed by applying the argument of Theorem 6.6, as the cases are identical. □

Theorem 8.4. *If $\tilde{U}^n \in \mathcal{P}(\omega)$ is an approximation for U^n, in Eqs. (82)–(84), then the schemes (82)–(84) are unconditionally stable.*

Proof. Considering Eq. (57) holds

$$ {}_0^C\mathrm{D}_t^\alpha \mathcal{E}^n - \varepsilon \Delta \mathcal{E}^n = 0. \tag{88}$$

Taking an inner product of Eq. (88) with $\mathcal{E}^n$ contributes to

$$ \left({}_0^C\mathrm{D}_t^\alpha \mathcal{E}^n, \mathcal{E}^n\right) - \varepsilon \left(\Delta \mathcal{E}^n, \mathcal{E}^n\right) = 0, $$

and the remaining steps of this proof follow similarly to those in the proof of Theorem 6.7. □

Theorem 8.5. *Let $\tilde{U}^{n+\sigma} \in \mathcal{P}(\omega)$ be an estimate of $U^{n+\sigma}$, in Eqs. (85), then this scheme is unconditionally stable.*

Proof. The proof is completed by the contributions from Theorems 8.4 and 6.8. □

Theorem 8.6. *If $U^n \in \mathcal{P}(\omega)$ is the approximation of u^n, given by Eq. (80), and $u \in \mathcal{S}^{3+\alpha}(\mathbb{R})$, such that $U^0 = \mathrm{P}_M u^0$, then*

$$ \|u^n - U^n\| \leq C\left(\tau^3 + M^{-\rho}\right), $$

for $n \geq 1$ and C is a positive constant independent of τ and M.

Proof. By subtracting

$$ \tau^{-\alpha} \sum_{k=0}^{n} \lambda_k^{(\alpha)} U^{n-k} - \varepsilon \Delta U^n = f^n, $$

form Eq. (44), we have

$$ \tau^{-\alpha} \sum_{k=0}^{n} \lambda_k^{(\alpha)} \left(u^{n-k} - U^{n-k}\right) - \varepsilon \Delta \left(u^n - U^n\right) + \mathrm{T}_n^{(\alpha)} = 0. $$

Denoting

$$ v^n := u^n - \mathrm{P}_M u^n, \quad w^n := U^n - \mathrm{P}_M u^n, \tag{89}$$

and restructuring the expressions yield

$$ \tau^{-\alpha} \sum_{k=0}^{n} \lambda_k^{(\alpha)} w^{n-k} - \varepsilon \Delta w^n = \tau^{-\alpha} \sum_{k=0}^{n} \lambda_k^{(\alpha)} v^{n-k} + \mathrm{T}_n^{(\alpha)}. \tag{90}$$

Now, taking an inner product of Eq. (90) with w^n produces

$$ \left(\tau^{-\alpha} \sum_{k=0}^{n} \lambda_k^{(\alpha)} w^{n-k}, w^n\right) - \varepsilon \left(\Delta w^n, w^n\right) = \left(\tau^{-\alpha} \sum_{k=0}^{n} \lambda_k^{(\alpha)} v^{n-k}, w^n\right) + \left(\mathrm{T}_n^{(\alpha)}, w^n\right). $$

Using the same argument as in the proof of Theorem 6.9, we obtain

$$ \frac{\varepsilon}{3C_\Omega} \sum_{n=1}^{N} \|w^n\|^2 \leq \frac{3C_\Omega}{4\varepsilon} \sum_{n=1}^{N} \left(\left\| \tau^{-\alpha} \sum_{k=0}^{n} \lambda_k^{(\alpha)} v^{n-k} \right\|^2 + \left\| \mathrm{T}_n^{(\alpha)} \right\|^2 \right). $$

By employing Lemma 8.2, one concludes

$$ \|w^n\|^2 \leq \frac{9C_\Omega^2}{4\varepsilon^2} \left(\tilde{C}^2 M^{-2\rho} \max_{1 \leq n \leq N} \left\| {}_0^C\mathcal{D}_t^\alpha u^n \right\|^2 + \max_{1 \leq n \leq N} \left\| \mathrm{T}_n^{(\alpha)} \right\|^2 \right), $$

and obviously

$$ \|w^n\| \leq C\left(\tau^3 + M^{-\rho}\right). $$

Now, the use of triangle inequality completes the proof. □

Theorem 8.7. *If $U^n \in \mathcal{P}(\omega)$ is the approximation of u^n, presented by Eq. (78) (Eq. (79)) ((Eq. (81))), and $u \in \mathcal{S}^{1+\alpha}(\mathbb{R})$ ($u \in \mathcal{S}^{2+\alpha}(\mathbb{R})$) (($u \in \mathcal{S}^{4+\alpha}(\mathbb{R})$)), such that $U^0 = \mathrm{P}_M u^0$, then*

$$ \|u^n - U^n\| \leq C\left(\tau + M^{-\rho}\right), \quad \left(\|u^n - U^n\| \leq C\left(\tau^2 + M^{-\rho}\right),\right) \quad \left(\left(\|u^n - U^n\| \leq C\left(\tau^4 + M^{-\rho}\right),\right)\right) $$

for $1 \leq n \leq N$, and C is a positive which is independent of τ and M.

Proof. The proof follows directly from Theorem 8.6. □

Theorem 8.8. *Suppose that $U^n \in \mathcal{P}(\omega)$ is the approximation of u^n, given by Eq. (82), and $u \in \mathcal{C}^2[0,T]$, such that $U^0 = \mathrm{P}_M u^0$, then*

$$\|u^n - U^n\| \leq C\left(\tau^{2-\alpha} + M^{-\rho}\right).$$

Proof. Subtracting

$$ {}_0^C\mathrm{D}_t^\alpha U^n - \varepsilon \Delta U^n = f^n,$$

from Eq. (48), using the notation in Eq. (89) and a simplification give

$$ {}_0^C\mathrm{D}_t^\alpha w^n - \varepsilon \Delta w^n = {}_0^C\mathrm{D}_t^\alpha v^n + \mathrm{T}_n^{(\alpha)}.$$

Now, $\forall \eta^n \in \mathcal{P}(\omega)$ we have

$$\left({}_0^C\mathrm{D}_t^\alpha w^n, \eta^n\right) - \varepsilon\left(\Delta w^n, \eta^n\right) = \left({}_0^C\mathrm{D}_t^\alpha v^n, \eta^n\right) + \left(\mathrm{T}_n^{(\alpha)}, \eta^n\right),$$

and hence, putting $\eta^n = w^n$,

$$\left({}_0^C\mathrm{D}_t^\alpha w^n, w^n\right) - \varepsilon\left(\Delta w^n, w^n\right) = \left({}_0^C\mathrm{D}_t^\alpha v^n, w^n\right) + \left(\mathrm{T}_n^{(\alpha)}, w^n\right).$$

Then from the proof of Theorem 6.11, it can be inferred that

$$ {}_0^C\mathrm{D}_t^\alpha \|w^n\|^2 \leq \|w^n\|^2 + \left\|{}_0^C\mathrm{D}_t^\alpha v^n\right\|^2 + \frac{C_\Omega}{2\varepsilon}\left\|\mathrm{T}_n^{(\alpha)}\right\|^2.$$

The use of Lemmas 8.2 and 6.3 implies that

$$\|w^n\| \leq C\left(\tau^{2-\alpha} + M^{-\rho}\right),$$

and consequently

$$\|u^n - U^n\| \leq C\left(\tau^{2-\alpha} + M^{-\rho}\right),$$

which completes the proof. □

Theorem 8.9. *Assume that U^n is the approximate solution obtained from Eq. (83) (or Eq. (84)), and suppose that the exact solution satisfies $u \in \mathcal{C}^3[0,T]$ for Eq. (83), and $u \in \mathcal{C}^4[0,T]$ for Eq. (84). Additionally, suppose $U^0 = \mathrm{P}_M u^0$. Then, there exists a $C > 0$, independent of τ and M, such that the following error bounds hold for Eq. (83)*

$$\|u^n - U^n\| \leq C\left(\tau^{3-\alpha} + M^{-\rho}\right), \qquad \forall n \geq 1,$$

and for Eq. (84)

$$\|u^n - U^n\| \leq C\left(\tau^{4-\alpha} + M^{-\rho}\right), \qquad \forall n \geq 1.$$

Proof. The proof is carried out similarly to the proof of Theorem 8.8. □

Theorem 8.10. *Let U^n be the solution of Eq. (75), and suppose $u \in \mathcal{C}^3[0,T]$ provided the condition $U^0 = \mathrm{P}_M u^0$. Then, there exists a constant $C > 0$, independent of τ and M, such that for all $n \geq 1$, the following error estimate holds*

$$\|u^n - U^n\| \leq C\left(\tau^2 + M^{-\rho}\right).$$

Proof. By utilizing the same argument used in the proof of Theorem 8.8 at the $n+\sigma$ step, we conclude

$$ {}_0^C\mathrm{D}_t^\alpha \left\|w^{n+\sigma}\right\|^2 \leq \left\|w^{n+\sigma}\right\|^2 + \left\|{}_0^C\mathrm{D}_t^\alpha v^{n+\sigma}\right\|^2 + \frac{C_\Omega}{2\varepsilon}\left\|\mathrm{T}_{n+\sigma}^{(\alpha)}\right\|^2.$$

Utilizing Lemmas 8.2 and 6.4 yields the following expression

$$\|w^n\| \leq C\left(\tau^2 + M^{-\rho}\right),$$

which leads to

$$\|u^n - U^n\| \leq C\left(\tau^2 + M^{-\rho}\right),$$

and the proof is fulfilled. □

8.3. Numerical findings

Example 8.1. For this example, we consider Eq. (1) with the following analytic solution

$$u(x,y,t) = t^p \cos(x)\cos(y),$$

with the following inhomogeneous term

$$f(x,y,t) = \left(\frac{\Gamma(p+1)}{\Gamma(p+1-\alpha)}t^{p-\alpha} + 2t^p\right)\cos(x)\cos(y).$$

We also put $\Omega = [0,1]^2$, $\varepsilon = 1$, $p = 4$ and the final time is set as $T = 1$.

Table 35 presents the results obtained using Grünwald–Letnikov type schemes for $\alpha = 0.25, 0.5, 0.75$. As observed from the results, the CO of scheme (78) approaches 1, scheme (79) approaches 2, and scheme (80) achieves third-order convergence. This confirms that scheme (80) is the most accurate among the three, in agreement with the theoretical predictions. Furthermore, Table 36 reports the results found utilizing scheme (81). As it can be seen the CO tends to 4 which is consistent with the theoretical result of Theorem 8.7.

For the L-type approximations, we consider fractional orders $\alpha = 0.3, 0.6, 0.9$. In Table 37, with $p = 1+\alpha$, the observed convergence rate for the L1 scheme is approximately $2-\alpha$. Table 38 presents results for $p = 3-\alpha$, showing a convergence rate of about $3-\alpha$ for the L1-2 scheme. In Table 39, with $p = 4-\alpha$, the convergence rate for the L1-2-3 scheme approaches $4-\alpha$. Finally, Table 40 displays results for $p = 2$, where the L2-1_σ scheme exhibits a convergence rate of 2. Fig. 5 illustrates the surface plot and the density of the approximate solution corresponding to the results in Table 39, with $M = 32$ and fractional derivative order $\alpha = 0.6$.

Table 35: Computational findings in Example 8.1.

		Scheme (78)		**Scheme (79)**		**Scheme (80)**	
α	M	$\mathcal{L}^2$	CO	$\mathcal{L}^2$	CO	$\mathcal{L}^2$	CO
0.25	4	2.4990×10^{-3}	–	7.2804×10^{-4}	–	2.1089×10^{-4}	–
	8	1.4510×10^{-3}	0.7843	2.2585×10^{-4}	1.6887	3.2269×10^{-5}	2.7083
	16	7.8702×10^{-4}	0.8826	6.3220×10^{-5}	1.8369	4.4776×10^{-6}	2.8493
	32	4.1035×10^{-4}	0.9396	1.6737×10^{-5}	1.9173	5.8980×10^{-7}	2.9244
0.5	4	6.3798×10^{-3}	–	1.9601×10^{-3}	–	5.4901×10^{-4}	–
	8	3.7530×10^{-3}	0.7655	6.1192×10^{-4}	1.6795	8.2341×10^{-5}	2.7372
	16	2.0489×10^{-3}	0.8732	1.7164×10^{-4}	1.8340	1.1304×10^{-5}	2.8648
	32	1.0718×10^{-3}	0.9348	4.5477×10^{-5}	1.9161	1.4811×10^{-6}	2.9320
0.75	4	1.2060×10^{-2}	–	3.8552×10^{-3}	–	1.0306×10^{-3}	–
	8	7.1687×10^{-3}	0.7504	1.2050×10^{-3}	1.6778	1.4920×10^{-4}	2.7882
	16	3.9344×10^{-3}	0.8656	3.3777×10^{-4}	1.8349	2.0171×10^{-5}	2.8869
	32	2.0636×10^{-3}	0.9310	8.9447×10^{-5}	1.9169	2.6237×10^{-6}	2.9426

Table 36: Computational findings in Example 8.1 for $p = 4$ using scheme (81).

	$\alpha = 0.25$		$\alpha = 0.5$		$\alpha = 0.75$	
M	$\mathcal{L}^2$	CO	$\mathcal{L}^2$	CO	$\mathcal{L}^2$	CO
4	3.9838×10^{-5}	–	7.8048×10^{-5}	–	7.6659×10^{-5}	–
8	2.5431×10^{-6}	3.9695	4.7611×10^{-6}	4.0350	4.7152×10^{-6}	4.0231
16	1.6431×10^{-7}	3.9521	2.9857×10^{-7}	3.9951	2.9144×10^{-7}	4.0161
32	1.0464×10^{-8}	3.9728	1.8756×10^{-8}	3.9926	1.7983×10^{-8}	4.0185
TCO		4.0000		4.0000		4.0000

9. Finite block method for TFDEs

The finite block method (FBM) was first proposed by Li and Wen [100], where its effectiveness was demonstrated through numerical experiments on various geometries. The method constructs a differentiation matrix based on polynomial approximation at equally spaced nodes in one dimension. In two dimensions, an eight-seed mapping

Table 37: Computational findings in Example 8.1 for $p = 1 + \alpha$.

	$\alpha = 0.3$		$\alpha = 0.6$		$\alpha = 0.9$	
M	$\mathcal{L}^2$	CO	$\mathcal{L}^2$	CO	$\mathcal{L}^2$	CO
4	9.6838×10^{-5}	–	6.6996×10^{-4}	–	2.8334×10^{-3}	–
8	3.3165×10^{-5}	1.5459	2.7899×10^{-4}	1.2639	1.4598×10^{-3}	0.9567
16	1.0955×10^{-5}	1.5981	1.1170×10^{-4}	1.3206	7.2032×10^{-4}	1.0191
32	3.5105×10^{-6}	1.6418	4.3575×10^{-5}	1.3580	3.4605×10^{-4}	1.0576
TCO		1.7000		1.4000		1.1000

Table 38: Computational findings in Example 8.1 for $p = 3 - \alpha$.

	$\alpha = 0.3$		$\alpha = 0.6$		$\alpha = 0.9$	
M	$\mathcal{L}^2$	CO	$\mathcal{L}^2$	CO	$\mathcal{L}^2$	CO
4	1.2160×10^{-4}	–	2.0991×10^{-4}	–	9.1583×10^{-5}	–
8	1.8878×10^{-5}	2.6873	3.6927×10^{-5}	2.5070	2.2581×10^{-5}	2.0199
16	2.9668×10^{-6}	2.6698	6.7204×10^{-6}	2.4581	4.8920×10^{-6}	2.2066
32	4.6574×10^{-7}	2.6713	1.2418×10^{-6}	2.4361	1.0943×10^{-6}	2.1605
TCO		2.7000		2.4000		2.1000

Table 39: Computational findings in Example 8.1 for $p = 4 - \alpha$.

	$\alpha = 0.3$		$\alpha = 0.6$		$\alpha = 0.9$	
M	$\mathcal{L}^2$	CO	$\mathcal{L}^2$	CO	$\mathcal{L}^2$	CO
4	1.9211×10^{-5}	–	1.1913×10^{-4}	–	6.2927×10^{-4}	–
8	5.6085×10^{-6}	1.7763	1.0047×10^{-5}	3.5676	6.7398×10^{-6}	6.5448
16	4.5092×10^{-7}	3.6367	9.5869×10^{-7}	3.3896	6.3600×10^{-7}	3.4056
32	3.5842×10^{-8}	3.6532	9.0234×10^{-8}	3.4093	7.3583×10^{-8}	3.1116
TCO		3.7000		3.4000		3.1000

Table 40: Computational findings in Example 8.1 for $p = 2$.

	$\alpha = 0.3$		$\alpha = 0.6$		$\alpha = 0.9$	
M	$\mathcal{L}^2$	CO	$\mathcal{L}^2$	CO	$\mathcal{L}^2$	CO
4	1.0544×10^{-4}	–	1.0040×10^{-4}	–	1.8963×10^{-5}	–
8	2.8747×10^{-5}	1.8749	2.8879×10^{-5}	1.7977	8.0723×10^{-6}	1.2322
16	7.5811×10^{-6}	1.9229	7.6271×10^{-6}	1.9208	2.1823×10^{-6}	1.8871
32	1.9491×10^{-6}	1.9596	1.9623×10^{-6}	1.9586	5.6348×10^{-7}	1.9534
TCO		2.0000		2.0000		2.0000

scheme was developed to transform a block from physical coordinates to normalized coordinates. Since its introduction, FBM has been applied in diverse areas, including elasticity [178], interface crack analysis [98], and functionally graded materials [100], as well as other applications [90, 99, 97, 104, 181, 182, 200, 202]. Recently, the FBM has also been extended to FPDEs, one can see [9, 67, 68] for further details.

9.1. Mapping strategy

The shape functions are presented as follows [13, 178]

$$M_i = \frac{1}{4}\left(1+\xi_i\xi\right)\left(1+\eta_i\eta\right)\left(\xi_i\xi+\eta_i\eta-1\right), \quad i = 1,2,3,4,$$

$$M_i = \frac{1}{2}\left(1-\xi^2\right)\left(1+\eta_i\eta\right), \quad i = 5,7, \qquad M_i = \frac{1}{2}\left(1-\eta^2\right)\left(1+\xi_i\xi\right), \quad i = 6,8.$$

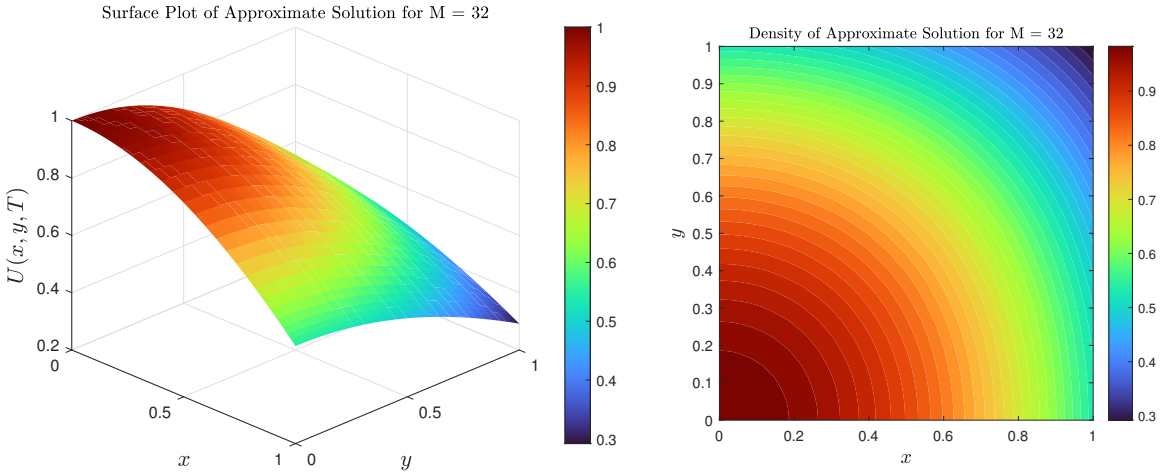

Figure 6: Graphs of surface and density plots for Table 39 with $\alpha = 0.6$ and $M = 32$.

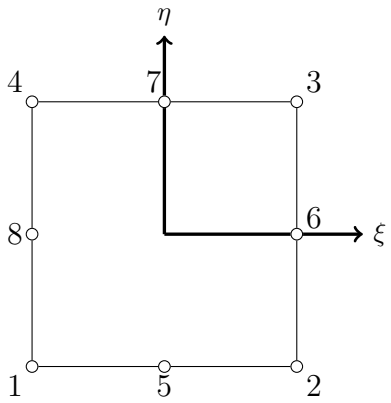

Figure 7: Isoparametric mapping in two dimensions [90].

Then, the coordinate transform is defined by

$$x = \sum_{j=1}^{8} M_j x_j, \qquad y = \sum_{j=1}^{8} M_j y_j.$$

Taking partial derivatives of u in the Cartesian coordinate, one obtains [178]

$$\frac{\partial u}{\partial x} = \frac{1}{\mathcal{J}} \left(\gamma_{11} \frac{\partial u}{\partial \xi} + \gamma_{12} \frac{\partial u}{\partial \eta} \right), \qquad \frac{\partial u}{\partial y} = \frac{1}{\mathcal{J}} \left(\gamma_{21} \frac{\partial u}{\partial \xi} + \gamma_{22} \frac{\partial u}{\partial \eta} \right),$$

and

$$\mathcal{J} = \begin{vmatrix} \dfrac{\partial x}{\partial \xi} & \dfrac{\partial x}{\partial \eta} \\ \dfrac{\partial y}{\partial \xi} & \dfrac{\partial y}{\partial \eta} \end{vmatrix}, \qquad \begin{cases} \gamma_{11} = \dfrac{\partial y}{\partial \eta}, & \gamma_{12} = -\dfrac{\partial y}{\partial \xi}, \\ \gamma_{21} = -\dfrac{\partial x}{\partial \eta}, & \gamma_{22} = \dfrac{\partial x}{\partial \xi}. \end{cases} \tag{91}$$

Now, one finds [178]

$$\mathbf{U}_x = \mathcal{V}_{11} \mathbf{U}_\xi^{(1)} + \mathcal{V}_{12} \mathbf{U}_\eta^{(1)} = \left(\mathcal{V}_{11} \mathbf{D}_\xi + \mathcal{V}_{12} \mathbf{D}_\eta \right) \mathbf{u} = \mathbf{D}_x \mathbf{u}, \tag{92}$$

$$\mathbf{U}_y = \mathcal{V}_{21} \mathbf{U}_\xi^{(1)} + \mathcal{V}_{22} \mathbf{U}_\eta^{(1)} = \left(\mathcal{V}_{21} \mathbf{D}_\xi + \mathcal{V}_{22} \mathbf{D}_\eta \right) \mathbf{u} = \mathbf{D}_y \mathbf{u}, \tag{93}$$

provided that

$$\mathcal{V}_{ik} = \begin{bmatrix} \dfrac{\gamma_{ik}^{(1)}}{\mathcal{J}^{(1)}} & 0 & \dots & 0 \\ 0 & \dfrac{\gamma_{ik}^{(2)}}{\mathcal{J}^{(2)}} & \dots & 0 \\ \vdots & \vdots & \ddots & \vdots \\ 0 & 0 & \dots & \dfrac{\gamma_{ik}^{(M^2)}}{\mathcal{J}^{(M^2)}} \end{bmatrix}, \tag{94}$$

and $\dfrac{\gamma_{ik}^{(j)}}{\mathcal{J}^{(j)}}$ can be computed by (91) at collocation nodes (ξ_j, η_j) [178].

9.2. Irregular regions

Two irregular regions are considered in the numerical illustrations

- *A quarter square plate with a circular hole* of radius 1, introduced in [178],

$$\Omega_1 := \left\{(x,y) \in \mathbb{R}^2 \,\middle|\, 0 \le x \le 2,\ 0 \le y \le 2,\ x^2+y^2 > 1\right\},$$

- *A pipe-shaped domain* presented in [67, 68],

$$\Omega_2 := \left\{(x,y) \in \mathbb{R}^2_+ \,\middle|\, 1 \le x^2+y^2 \le 2\right\}.$$

The geometrical configurations of these domains are shown in Fig. 8.

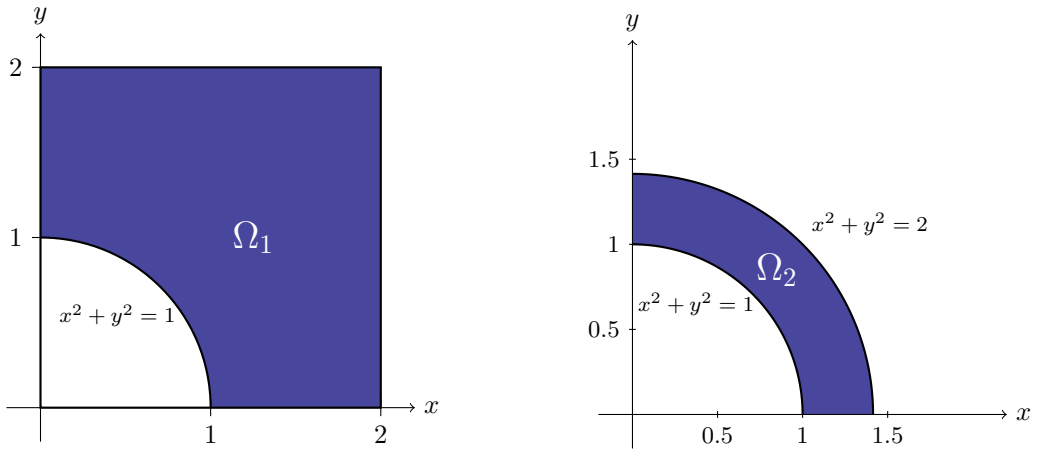

Figure 8: Square plate and pipe-shaped geometries [67, 68, 178].

9.3. Strong forms

Since the algebraic manipulations are identical to those presented in §8.1, we directly present the matrix schemes in this section. It is worth noting that the only difference between the following matrix forms and those obtained in §8.1 lies in the approximation of Δ. The schemes are given as follows

- First-order Grünwald–Letnikov approximation

$$\mathcal{A}U^n = \mathcal{F}^{(n)}, \qquad \begin{cases} \mathcal{A} = \tau^{-\alpha} g_0^{(\alpha)} \mathbf{I} - \varepsilon \left(\mathbf{D}_x^2 + \mathbf{D}_y^2\right), \\ \mathcal{F}^{(n)} = f^n - \tau^{-\alpha} \displaystyle\sum_{k=1}^{n} g_k^{(\alpha)} U^{n-k}, \end{cases} \quad 1 \le n \le N. \tag{95}$$

- Second-order WSGL

$$\mathcal{A}U^n = \mathcal{F}^{(n)}, \qquad \begin{cases} \mathcal{A} = \tau^{-\alpha} w_0^{(\alpha)} \mathbf{I} - \varepsilon \left(\mathbf{D}_x^2 + \mathbf{D}_y^2\right), \\ \mathcal{F}^{(n)} = f^n - \tau^{-\alpha} \displaystyle\sum_{k=1}^{n} w_k^{(\alpha)} U^{n-k}, \end{cases} \quad 1 \le n \le N. \tag{96}$$

- Third-order WSGL

$$\mathcal{A}U^n = \mathcal{F}^{(n)}, \qquad \begin{cases} \mathcal{A} = \tau^{-\alpha}\lambda_0^{(\alpha)}\mathbf{I} - \varepsilon\left(\mathbf{D}_x^2 + \mathbf{D}_y^2\right), \\ \mathcal{F}^{(n)} = f^n - \tau^{-\alpha}\sum_{k=1}^{n}\lambda_k^{(\alpha)}U^{n-k}, \end{cases} \quad 1 \le n \le N. \tag{97}$$

- Fourth-order WSGL

$$\mathcal{A}U^n = \mathcal{F}^{(n)}, \qquad \begin{cases} \mathcal{A} = \tau^{-\alpha}\vartheta_0^{(\alpha)}\mathbf{I} - \varepsilon\left(\mathbf{D}_x^2 + \mathbf{D}_y^2\right), \\ \mathcal{F}^{(n)} = f^n - \tau^{-\alpha}\sum_{k=1}^{n}\vartheta_k^{(\alpha)}U^{n-k}, \end{cases} \quad 1 \le n \le N. \tag{98}$$

- L1 scheme

$$\mathcal{A}U^n = \mathcal{F}^{(n)}, \qquad \begin{cases} \mathcal{A} = a_0^{(\alpha)}\mathbf{I} - \varepsilon\left(\mathbf{D}_x^2 + \mathbf{D}_y^2\right), \\ \mathcal{F}^{(n)} = a_0^{(\alpha)}U^{n-1} - \sum_{k=1}^{n-1}a_{n-k}^{(\alpha)}\delta U^k + f^n, \end{cases} \quad 1 \le n \le N. \tag{99}$$

- L1-2 formula

$$\mathcal{A}U^n = \mathcal{F}^{(n)}, \qquad \begin{cases} \mathcal{A} = c_0^{(\alpha)}\mathbf{I} - \varepsilon\left(\mathbf{D}_x^2 + \mathbf{D}_y^2\right), \\ \mathcal{F}^{(n)} = c_0^{(\alpha)}U^{n-1} - \sum_{k=1}^{n-1}c_{n-k}^{(\alpha)}\delta U^k + f^n, \end{cases} \quad 1 \le n \le N. \tag{100}$$

- L1-2-3 approximation

$$\mathcal{A}U^n = \mathcal{F}^{(n)}, \qquad \begin{cases} \mathcal{A} = d_0^{(\alpha)}\mathbf{I} - \varepsilon\left(\mathbf{D}_x^2 + \mathbf{D}_y^2\right), \\ \mathcal{F}^{(n)} = d_0^{(\alpha)}U^{n-1} - \sum_{k=1}^{n-1}d_{n-k}^{(\alpha)}\delta U^k + f^n, \end{cases} \quad 1 \le n \le N. \tag{101}$$

- For L2-1_σ formula, one has

$$\mathcal{A}U^{n+1} = \mathcal{F}^{(n+\sigma)}, \quad 0 \le n \le N-1, \tag{102}$$

with

$$\begin{cases} \mathcal{A} = c_0^{(n)}\mathbf{I} - \varepsilon\left(\mathbf{D}_x^2 + \mathbf{D}_y^2\right), \\ \mathcal{F}^{(n+\sigma)} = c_0^{(n)}U^n - \sum_{k=0}^{n-1}c_{n-k}^{(n)}\delta U^k + \varepsilon(1-\sigma)\left(\mathbf{D}_x^2 + \mathbf{D}_y^2\right)U^n + \sigma f^{n+1} + (1-\sigma)f^n. \end{cases}$$

9.4. Analysis on stability and convergence

Since all the theorems presented in §8.2 also hold for the schemes derived in §9.3, we omit their repetition here.

9.5. Numerical illustrations

Example 9.1. In the final experiment, we consider the TFDE with the source term

$$f(x,y,t) = \left(\frac{\Gamma(p+1)}{\Gamma(p+1-\alpha)}t^{p-\alpha} - 2t^p\right)\exp(x+y),$$

and the corresponding analytical solution $u(x,y,t) = t^p\exp(x+y)$. We set $T = 1$ and $\varepsilon = 0.01$. The results are summarized in Tables 41–43, which correspond to two different scenarios.

In the first scenario, we solve Eq. (1) on the complex domain Ω_2 using Grünwald–Letnikov type approximations for $\alpha = 0.2, 0.5, 0.8$, and we set $p = 3$ in the exact solution. The numerical results validate the theoretical predictions established in §8.2, and the corresponding data are reported in Tables 41 and 42. Figure 9 displays the error distribution and contour plots generated by Scheme (98), corresponding to Table 42, for $\alpha = 0.5$ and $M = 40$.

In the second scenario, we solve the TFDE on the complex domain Ω_1 using L-type approximations for $\alpha = 0.3, 0.6, 0.9$, and set $p = 3 + \alpha$ in the exact solution. Again, the numerical results verify the theoretical predictions. Fig. 10 depicts the error distribution and contour plots obtained by Scheme (101) corresponding to Table 43 for $\alpha = 0.3$ and $M = 40$.

Table 41: Computational results in Example 9.1 on Ω_2.

		Scheme (95)		**Scheme (96)**		**Scheme (97)**	
α	M	$\mathcal{L}^2$	CO	$\mathcal{L}^2$	CO	$\mathcal{L}^2$	CO
0.2	10	5.6139×10^{-2}	–	4.8975×10^{-3}	–	3.0008×10^{-4}	–
	20	2.9803×10^{-2}	0.9135	1.3204×10^{-3}	1.8910	3.9362×10^{-5}	2.9304
	30	2.0264×10^{-2}	0.9514	6.0159×10^{-4}	1.9389	1.1848×10^{-5}	2.9611
	40	1.5347×10^{-2}	0.9661	3.4257×10^{-4}	1.9574	5.0376×10^{-6}	2.9730
0.5	10	1.5541×10^{-1}	–	1.4931×10^{-2}	–	8.9218×10^{-4}	–
	20	8.2284×10^{-2}	0.9174	4.0354×10^{-3}	1.8875	1.1597×10^{-4}	2.9436
	30	5.5903×10^{-2}	0.9534	1.8398×10^{-3}	1.9371	3.4796×10^{-5}	2.9690
	40	4.2321×10^{-2}	0.9675	1.0480×10^{-3}	1.9562	1.4770×10^{-5}	2.9786
0.8	10	2.7277×10^{-1}	–	2.8729×10^{-2}	–	1.7048×10^{-3}	–
	20	1.4397×10^{-1}	0.9219	7.7846×10^{-3}	1.8838	2.1877×10^{-4}	2.9621
	30	9.7718×10^{-2}	0.9558	3.5515×10^{-3}	1.9355	6.5345×10^{-5}	2.9801
	40	7.3940×10^{-2}	0.9692	2.0237×10^{-3}	1.9552	2.7675×10^{-5}	2.9865

Table 42: Computational findings in Example 9.1 for $p = 3$ using scheme (98).

	$\alpha = 0.2$		$\alpha = 0.5$		$\alpha = 0.8$	
M	$\mathcal{L}^2$	CO	$\mathcal{L}^2$	CO	$\mathcal{L}^2$	CO
10	1.5880×10^{-6}	–	1.5562×10^{-5}	–	6.3127×10^{-5}	–
20	9.3285×10^{-8}	4.0894	8.5205×10^{-7}	4.1909	3.1101×10^{-6}	4.3432
30	1.7661×10^{-8}	4.1047	1.5394×10^{-7}	4.2201	5.3417×10^{-7}	4.3448
40	5.4262×10^{-9}	4.1021	4.5133×10^{-8}	4.2649	1.4638×10^{-7}	4.4997
TCO		4.0000		4.0000		4.0000

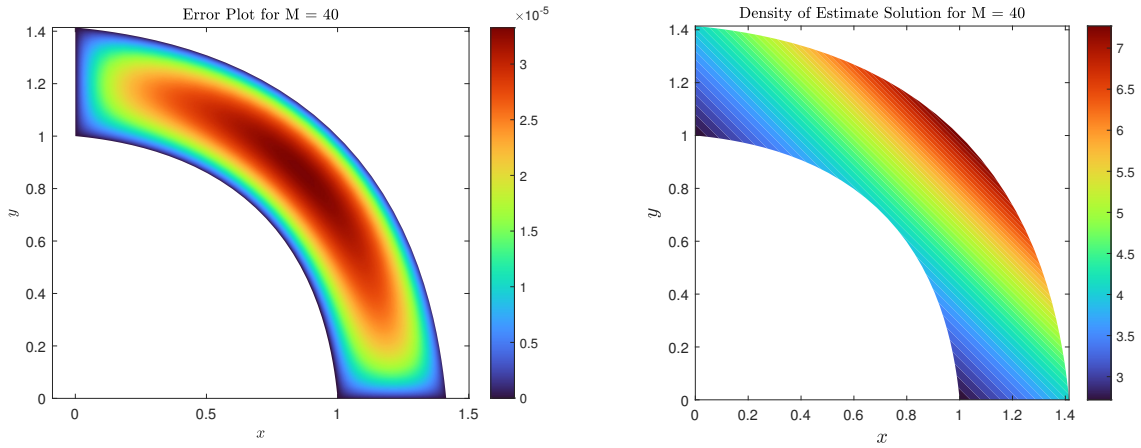

Figure 9: Graphs of error and contour plots, obtained by Scheme (98) associated with Table 42 for the values $\alpha = 0.5$ and $M = 40$.

10. Conclusions and discussions

In this paper, we present a survey of various numerical algorithms for the two-dimensional time-fractional diffusion equation. The primary focus is on L–type approximations and Grünwald–Letnikov-based formulas for the temporal fractional derivative, in combination with different spatial discretization techniques, including compact finite difference methods, the meshless MQ–RBF approach, finite element methods, spectral element methods, Chebyshev spectral methods, and the finite block method for irregular geometries.

For each spatial discretization technique, the corresponding numerical scheme is derived based on the chosen temporal approximation (either an L–type or a Grünwald–Letnikov-based formula). Theorems on stability and convergence are provided using the energy method, with the exception of the meshless method. In each section, numerical experiments are presented to validate the theoretical analysis.

Designing feasible and accurate numerical methods for FPDEs is a long-term challenge. Classical PDE methods

Table 43: Computational results in Example 9.1 on Ω_1.

Scheme	M	$\alpha = 0.3$		$\alpha = 0.6$		$\alpha = 0.9$	
		$\mathcal{L}^2$	CO	$\mathcal{L}^2$	CO	$\mathcal{L}^2$	CO
L1	10	8.2778×10^{-2}	–	3.5812×10^{-1}	–	1.1160×10^{0}	–
	20	2.9424×10^{-2}	1.4922	1.5050×10^{-1}	1.2507	5.5308×10^{-1}	1.0128
	30	1.5660×10^{-2}	1.5555	8.8645×10^{-2}	1.3054	3.6179×10^{-1}	1.0468
	40	9.9330×10^{-3}	1.5826	6.0485×10^{-2}	1.3287	2.6657×10^{-1}	1.0617
L1-2	10	7.8128×10^{-3}	–	4.4419×10^{-2}	–	1.7092×10^{-1}	–
	20	1.3487×10^{-3}	2.5342	9.4251×10^{-3}	2.2366	4.4974×10^{-2}	1.9262
	30	4.7253×10^{-4}	2.5867	3.7032×10^{-3}	2.3040	1.9970×10^{-2}	2.0023
	40	2.2309×10^{-4}	2.6089	1.8942×10^{-3}	2.3303	1.1131×10^{-2}	2.0316
L1-2-3	10	3.4746×10^{-4}	–	3.2009×10^{-3}	–	1.9551×10^{-2}	–
	20	2.8815×10^{-5}	3.5920	3.4706×10^{-4}	3.2052	2.6463×10^{-3}	2.8852
	30	6.5453×10^{-6}	3.6554	9.1227×10^{-5}	3.2953	7.8828×10^{-4}	2.9869
	40	2.2767×10^{-6}	3.6707	3.5053×10^{-5}	3.3249	3.3046×10^{-4}	3.0219
L2-1_σ	10	2.6020×10^{-2}	–	5.2743×10^{-2}	–	7.1024×10^{-2}	–
	20	7.1774×10^{-3}	1.8581	1.4558×10^{-2}	1.8571	1.9144×10^{-2}	1.8914
	30	3.3067×10^{-3}	1.9114	6.7291×10^{-3}	1.9033	8.7682×10^{-3}	1.9258
	40	1.8960×10^{-3}	1.9334	3.8701×10^{-3}	1.9228	5.0186×10^{-3}	1.9395

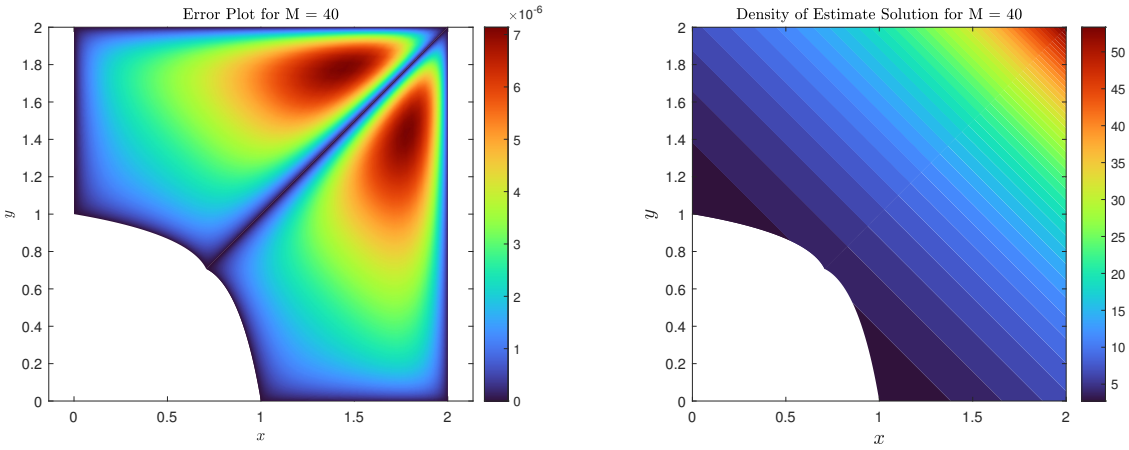

Figure 10: Graphs of error and contour plots, computed by Scheme (101) corresponding to Table 43 for the values $\alpha = 0.3$ and $M = 40$.

cannot be directly applied to FPDEs; instead, specialized computational approaches must be developed to faithfully capture the underlying physical and geometrical phenomena. It is our hope that this review offers new perspectives for the fractional calculus community and stimulates further advances in the development of robust numerical techniques for FPDEs.

Future research directions include extending this review to other classes of FPDEs, such as distributed-order equations, space-fractional PDEs, time–space fractional PDEs, and related generalizations.

References

[1] M. Abbaszadeh and H. Amjadian, *Second-order finite difference/spectral element formulation for solving the fractional advection-diffusion equation*, Communications on Applied Mathematics and Computation, 2 (2020), pp. 653–669.

[2] M. Abbaszadeh and M. Dehghan, *An improved meshless method for solving two-dimensional distributed order time-fractional diffusion-wave equation with error estimate*, Numerical Algorithms, 75 (2017), pp. 173–211.

[3] ——, *Direct meshless local Petrov–Galerkin (DMLPG) method for time-fractional fourth-order reaction–diffusion problem on complex domains*, Computers & Mathematics with Applications, 79 (2020), pp. 876–888.

[4] ——, *A meshless numerical investigation based on the RBF-QR approach for elasticity problems*, AUT Journal of Mathematics and Computing, 1 (2020), pp. 1–15.

[5] ——, *Meshless upwind local radial basis function-finite difference technique to simulate the time-fractional distributed-order advection–diffusion equation*, Engineering with Computers, 37 (2021), pp. 873–889.

[6] ——, *The proper orthogonal decomposition modal spectral element method for two-dimensional viscoelastic equation*, Thin-Walled Structures, 161 (2021), p. 107429.

[7] M. Abbaszadeh, M. Dehghan, A. Khodadadian, and T. Wick, *Legendre spectral element method (LSEM) to simulate the two-dimensional system of nonlinear stochastic advection–reaction–diffusion models*, Applicable Analysis, 101 (2022), pp. 2279–2294.

[8] M. Abbaszadeh, M. Dehghan, and Y. Zhou, *Alternating direction implicit-spectral element method (ADI-SEM) for solving multi-dimensional generalized modified anomalous sub-diffusion equation*, Computers & Mathematics with Applications, 78 (2019), pp. 1772–1792.

[9] M. Abbaszadeh, A. Ghoreyshi, and M. Dehghan, *A finite block method framework for nonlinear fractional integro-differential equations*, Mathematical Methods in the Applied Sciences, (2025), pp. 1–19.

[10] M. Abbaszadeh, A. Khodadadian, M. Dehghan, and T. Wick, *Analysis of a Legendre spectral element method (LSEM) for the two-dimensional system of a nonlinear stochastic advection-reaction-diffusion models*, arXiv preprint arXiv:1904.06263, (2019).

[11] M. Abbaszadeh, A. B. Salec, and A. S. Jebur, *Integrated radial basis function technique to simulate the nonlinear system of time fractional distributed-order diffusion equation with graded time-mesh discretization*, Engineering Analysis with Boundary Elements, 156 (2023), pp. 57–69.

[12] W. Abd-Elhameed, Y. Youssri, and A. Atta, *Adopted spectral tau approach for the time-fractional diffusion equation via seventh-kind Chebyshev polynomials*, Boundary Value Problems, 2024 (2024), p. 102.

[13] S. Adeeb, *Introduction to Solid Mechanics and Finite Element Analysis using Mathematica*, Kendall Hunt, Dubuque, Iowa, USA, 2011.

[14] N. Ahmadi, S. Wang, and G. Karniadakis, *Pharmacometrics modeling via physics-informed neural networks: Integrating time-variant absorption rates and fractional calculus for enhancing prediction accuracy*, arXiv preprint arXiv:2412.21076, (2024).

[15] A. Alikhanov, *A priori estimates for solutions of boundary value problems for fractional-order equations*, Differential Equations, 46 (2010), pp. 660–666.

[16] A. A. Alikhanov, *A new difference scheme for the time fractional diffusion equation*, Journal of Computational Physics, 280 (2015), pp. 424–438.

[17] A. A. Alikhanov and C. Huang, *A high-order L2 type difference scheme for the time-fractional diffusion equation*, Applied Mathematics and Computation, 411 (2021), p. 126545.

[18] J. Angulo, M. Ruiz-Medina, V. Anh, and W. Grecksch, *Fractional diffusion and fractional heat equation*, Advances in Applied Probability, 32 (2000), pp. 1077–1099.

[19] K. E. Atkinson, *An Introduction to Numerical Analysis*, John Wiley & Sons, New York, 2008.

[20] D. Baleanu, K. Diethelm, E. Scalas, and J. J. Trujillo, *Fractional Calculus: Models and Numerical Methods*, vol. 3, World Scientific, Toh Tuck Link, Singapore, 2012.

[21] D. Baleanu, S. S. Sajjadi, A. Jajarmi, and Ö. Defterli, *On a nonlinear dynamical system with both chaotic and nonchaotic behaviors: a new fractional analysis and control*, Advances in Difference Equations, 2021 (2021), p. 234.

[22] A. Bhrawy and M. Zaky, *Numerical algorithm for the variable-order Caputo fractional functional differential equation*, Nonlinear Dynamics, 85 (2016), pp. 1815–1823.

[23] A. H. Bhrawy and M. Zaky, *An improved collocation method for multi-dimensional space–time variable-order fractional Schrödinger equations*, Applied Numerical Mathematics, 111 (2017), pp. 197–218.

[24] A. H. Bhrawy and M. A. Zaky, *A method based on the Jacobi tau approximation for solving multi-term time–space fractional partial differential equations*, Journal of Computational Physics, 281 (2015), pp. 876–895.

[25] A. H. Bhrawy, M. A. Zaky, and D. Baleanu, *New numerical approximations for space-time fractional Burgers' equations via a Legendre spectral-collocation method*, Rom. Rep. Phys, 67 (2015), pp. 340–349.

[26] G. W. Bohannan, *Analog fractional order controller in temperature and motor control applications*, Journal of Vibration and Control, 14 (2008), pp. 1487–1498.

[27] H. Brezis, *Functional Analysis, Sobolev Spaces and Partial Differential Equations*, Springer Science & Business Media, New York, 2011.

[28] W. Bu, A. Xiao, and W. Zeng, *Finite difference/finite element methods for distributed-order time fractional diffusion equations*, Journal of Scientific Computing, 72 (2017), pp. 422–441.

[29] R. L. Burden and J. D. Faires, *Numerical Analysis*, Brooks Cole, Boston, Massachusetts, USA, 2010.

[30] K. Burrage, A. Cardone, R. D'Ambrosio, and B. Paternoster, *Numerical solution of time fractional diffusion systems*, Applied Numerical Mathematics, 116 (2017), pp. 82–94.

[31] C. Canuto, M. Y. Hussaini, A. Quarteroni, and T. A. Zang, *Spectral Methods in Fluid Dynamics*, Springer Science & Business Media, New York, 1988.

[32] C. Canuto, M. Y. Hussaini, A. Quarteroni, and T. A. Zang, *Spectral Methods: Fundamentals in Single Domains*, Springer, Berlin, Germany, 2006.

[33] J. Cao, C. Li, and Y. Chen, *High-order approximation to Caputo derivatives and Caputo-type advection-diffusion equations (II)*, Fractional Calculus and Applied Analysis, 18 (2015), pp. 735–761.

[34] M. C. Caputo and D. F. Torres, *Duality for the left and right fractional derivatives*, Signal Processing, 107 (2015), pp. 265–271.

[35] C. M. Chen, F. Liu, I. Turner, and V. Anh, *A Fourier method for the fractional diffusion equation describing sub-diffusion*, Journal of Computational Physics, 227 (2007), pp. 886–897.

[36] H. Chen, H. Qiao, W. Wei, and J. Li, *Time fractional diffusion equation based on Caputo fractional derivative for image denoising*, Optics & Laser Technology, 168 (2024), p. 109855.

[37] W. Chen, L. Ye, and H. Sun, *Fractional diffusion equations by the Kansa method*, Computers & Mathematics with Applications, 59 (2010), pp. 1614–1620.

[38] M. Cui, *Compact finite difference method for the fractional diffusion equation*, Journal of Computational Physics, 228 (2009), pp. 7792–7804.

[39] S. Das, *Analytical solution of a fractional diffusion equation by variational iteration method*, Computers & Mathematics with Applications, 57 (2009), pp. 483–487.

[40] M. Dehghan and M. Abbaszadeh, *The use of proper orthogonal decomposition (POD) meshless RBF-FD technique to simulate the shallow water equations*, Journal of Computational Physics, 351 (2017), pp. 478–510.

[41] ——, *An efficient technique based on finite difference/finite element method for solution of two-dimensional space/multi-time fractional Bloch–Torrey equations*, Applied Numerical Mathematics, 131 (2018), pp. 190–206.

[42] ——, *A finite difference/finite element technique with error estimate for space fractional tempered diffusion-wave equation*, Computers & Mathematics with Applications, 75 (2018), pp. 2903–2914.

[43] ——, *A Legendre spectral element method (SEM) based on the modified bases for solving neutral delay distributed-order fractional damped diffusion-wave equation*, Mathematical Methods in the Applied Sciences, 41 (2018), pp. 3476–3494.

[44] M. Dehghan, M. Abbaszadeh, and A. Mohebbi, *The numerical solution of nonlinear high dimensional generalized Benjamin–Bona–Mahony–Burgers equation via the meshless method of radial basis functions*, Computers & Mathematics with Applications, 68 (2014), pp. 212–237.

[45] ——, *An implicit RBF meshless approach for solving the time fractional nonlinear sine-Gordon and Klein–Gordon equations*, Engineering Analysis with Boundary Elements, 50 (2015), pp. 412–434.

[46] ——, *Analysis of a meshless method for the time fractional diffusion-wave equation*, Numerical Algorithms, 73 (2016), pp. 445–476.

[47] ——, *Legendre spectral element method for solving time fractional modified anomalous sub-diffusion equation*, Applied Mathematical Modelling, 40 (2016), pp. 3635–3654.

[48] M. Dehghan, N. Shafieeabyaneh, and M. Abbaszadeh, *Numerical and theoretical discussions for solving nonlinear generalized Benjamin–Bona–Mahony–Burgers equation based on the Legendre spectral element method*, Numerical Methods for Partial Differential Equations, 37 (2021), pp. 360–382.

[49] M. Delkhosh and K. Parand, *A new computational method based on fractional Lagrange functions to solve multi-term fractional differential equations*, Numerical Algorithms, (2021), pp. 1–38.

[50] W. Deng, *Finite element method for the space and time fractional Fokker–Planck equation*, SIAM Journal on Numerical Analysis, 47 (2009), pp. 204–226.

[51] L. Diening, P. Harjulehto, P. Hästö, and M. Ruzicka, *Lebesgue and Sobolev Spaces with Variable Exponents*, Springer, Heidelberg, Germany, 2011.

[52] H. Ding, *The development of higher-order numerical differential formulas of Caputo derivative and their applications (I)*, Computers & Mathematics with Applications, 84 (2021), pp. 203–223.

[53] ——, *The construction of an optimal fourth-order fractional-compact-type numerical differential formula of the Riesz derivative and its application*, Communications in Nonlinear Science and Numerical Simulation, 123 (2023), p. 107272.

[54] H. Ding and C. Li, *High-order compact difference schemes for the modified anomalous subdiffusion equation*, Numerical Methods for Partial Differential Equations, 32 (2016), pp. 213–242.

[55] ——, *High-order numerical algorithm and error analysis for the two-dimensional nonlinear spatial fractional complex Ginzburg–Landau equation*, Communications in Nonlinear Science and Numerical Simulation, 120 (2023), p. 107160.

[56] H. Ding and Q. Yi, *The construction of higher-order numerical approximation formula for Riesz derivative and its application to nonlinear fractional differential equations (I)*, Communications in Nonlinear Science and Numerical Simulation, 110 (2022), p. 106394.

[57] E. H. Doha, A. H. Bhrawy, and S. Ezz-Eldien, *Efficient Chebyshev spectral methods for solving multi-term fractional orders differential equations*, Applied Mathematical Modelling, 35 (2011), pp. 5662–5672.

[58] E. H. Doha, A. H. Bhrawy, and S. S. Ezz-Eldien, *A Chebyshev spectral method based on operational matrix for initial and boundary value problems of fractional order*, Computers & Mathematics with Applications, 62 (2011), pp. 2364–2373.

[59] M. Fardi, B. Azarnavid, and S. Mohammadi, *Numerical simulation of nonlinear fractional integro-differential equations on two-dimensional regular and irregular domains: RBF partition of unity*, Computers & Mathematics with Applications, 181 (2025), pp. 21–43.

[60] Y. Feng, L. Li, J. G. Liu, and T. Tang, *Some Grönwall inequalities for a class of discretizations of time fractional equations on nonuniform meshes*, SIAM Journal on Numerical Analysis, 62 (2024), pp. 2196–2221.

[61] L. L. Ferrás, N. J. Ford, M. L. Morgado, and M. Rebelo, *A numerical method for the solution of the time-fractional diffusion equation*, International Conference on Computational Science and Its Applications, (2014), pp. 117–131.

[62] G. H. Gao, A. A. Alikhanov, and Z. Z. Sun, *The temporal second order difference schemes based on the interpolation approximation for solving the time multi-term and distributed-order fractional sub-diffusion equations*, Journal of Scientific Computing, 73 (2017), pp. 93–121.

[63] G. H. Gao and Z. Z. Sun, *A compact finite difference scheme for the fractional sub-diffusion equations*, Journal of Computational Physics, 230 (2011), pp. 586–595.

[64] G. H. Gao, Z. Z. Sun, and H. W. Zhang, *A new fractional numerical differentiation formula to approximate the Caputo fractional derivative and its applications*, Journal of Computational Physics, 259 (2014), pp. 33–50.

[65] W. Gautschi, *Numerical Analysis*, Springer Science & Business Media, New York, NY, USA, 2011.

[66] A. Ghoreyshi, M. Abbaszadeh, M. A. Zaky, and M. Dehghan, *An accurate and robust numerical method for solving distributed-order space–time fractional PDEs*, Zeitschrift für angewandte Mathematik und Physik, 76 (2025), p. 242.

[67] ——, *Finite block method for nonlinear time-fractional partial integro-differential equations: Stability, convergence, and numerical analysis*, Applied Numerical Mathematics, 214 (2025), pp. 82–103.

[68] ——, *Two high-order numerical schemes based on the Lagrange polynomials for solving a distributed-order time-fractional partial integro-differential equation on non-rectangular domains*, Journal of Applied Mathematics and Computing, (2025), pp. 1–41.

[69] M. Giona, S. Cerbelli, and H. E. Roman, *Fractional diffusion equation and relaxation in complex viscoelastic materials*, Physica A: Statistical Mechanics and its Applications, 191 (1992), pp. 449–453.

[70] A. Golbabai, O. Nikan, and M. Molavi Arabshahi, *Numerical approximation of time fractional advection-dispersion model arising from solute transport in rivers*, TWMS Journal of Pure and Applied Mathematics, 10 (2019).

[71] D. Gottlieb and J. S. Hesthaven, *Spectral methods for hyperbolic problems*, Journal of Computational and Applied Mathematics, 128 (2001), pp. 83–131.

[72] S. Guo, L. Mei, C. Li, Z. Zhang, and Y. Li, *Semi-implicit Hermite–Galerkin spectral method for distributed-order fractional-in-space nonlinear reaction–diffusion equations in multidimensional unbounded domains*, Journal of Scientific Computing, 85 (2020), pp. 1–27.

[73] M. Haghi, M. Ilati, and M. Dehghan, *A fourth-order compact difference method for the nonlinear time-fractional fourth-order reaction–diffusion equation*, Engineering with Computers, 39 (2023), pp. 1329–1340.

[74] X. Hu and L. Zhang, *A compact finite difference scheme for the fourth-order fractional diffusion-wave system*, Computer Physics Communications, 182 (2011), pp. 1645–1650.

[75] C. C. Ji and Z. Z. Sun, *A high-order compact finite difference scheme for the fractional sub-diffusion equation*, Journal of Scientific Computing, 64 (2015), pp. 959–985.

[76] ——, *The high-order compact numerical algorithms for the two-dimensional fractional sub-diffusion equation*, Applied Mathematics and Computation, 269 (2015), pp. 775–791.

[77] S. Jiang, J. Zhang, Q. Zhang, and Z. Zhang, *Fast evaluation of the Caputo fractional derivative and its applications to fractional diffusion equations*, Communications in Computational Physics, 21 (2017), pp. 650–678.

[78] Y. Jiang and J. Ma, *High-order finite element methods for time-fractional partial differential equations*, Journal of Computational and Applied Mathematics, 235 (2011), pp. 3285–3290.

[79] B. Jin, R. Lazarov, J. Pasciak, and Z. Zhou, *Error analysis of semidiscrete finite element methods for inhomogeneous time-fractional diffusion*, IMA Journal of Numerical Analysis, 35 (2015), pp. 561–582.

[80] B. Jin, R. Lazarov, and Z. Zhou, *An analysis of the L1 scheme for the subdiffusion equation with nonsmooth data*, IMA Journal of Numerical Analysis, 36 (2016), pp. 197–221.

[81] V. John, *Finite Element Methods for Incompressible Flow Problems*, vol. 51, Springer, Cham, Switzerland, 2016.

[82] E. J. Kansa, *Multiquadrics—A scattered data approximation scheme with applications to computational fluid-dynamics—I surface approximations and partial derivative estimates*, Computers & Mathematics with Applications, 19 (1990), pp. 127–145.

[83] ——, *Multiquadrics—A scattered data approximation scheme with applications to computational fluid-dynamics—II solutions to parabolic, hyperbolic and elliptic partial differential equations*, Computers & Mathematics with Applications, 19 (1990), pp. 147–161.

[84] I. Karatay, N. Kale, and S. R. Bayramoglu, *A new difference scheme for time fractional heat equations based on the Crank-Nicholson method*, Fractional Calculus and Applied Analysis, 16 (2013), pp. 892–910.

[85] G. Karniadakis and S. J. Sherwin, *Spectral/hp Element Methods for Computational Fluid Dynamics*, Oxford University Press, 2005.

[86] E. Kharazmi, M. Zayernouri, and G. E. Karniadakis, *Petrov–Galerkin and spectral collocation methods for distributed order differential equations*, SIAM Journal on Scientific Computing, 39 (2017), pp. A1003–A1037.

[87] A. A. Kilbas, H. M. Srivastava, and J. J. Trujillo, *Theory and Applications of Fractional Differential Equations*, vol. 204, Elsevier, 2006.

[88] M. Lakestani, M. Dehghan, and S. Irandoust-Pakchin, *The construction of operational matrix of fractional derivatives using B-spline functions*, Communications in Nonlinear Science and Numerical Simulation, 17 (2012), pp. 1149–1162.

[89] S. Larsson, M. Racheva, and F. Saedpanah, *Discontinuous Galerkin method for an integro-differential equation modeling dynamic fractional order viscoelasticity*, Computer Methods in Applied Mechanics and Engineering, 283 (2015), pp. 196–209.

[90] M. Lei, M. Li, P. Wen, and C. Bailey, *Moving boundary analysis in heat conduction with multilayer composites by finite block method*, Engineering Analysis with Boundary Elements, 89 (2018), pp. 36–44.

[91] C. Li and A. Chen, *Numerical methods for fractional partial differential equations*, International Journal of Computer Mathematics, 95 (2018), pp. 1048–1099.

[92] C. Li, R. Wu, and H. Ding, *High-order approximation to Caputo derivatives and Caputo-type advection–diffusion equations (I)*, Communications in Applied and Industrial Mathematics, 6 (2014), pp. e–536.

[93] C. Li and F. Zeng, *Finite difference methods for fractional differential equations*, International Journal of Bifurcation and Chaos, 22 (2012), p. 1230014.

[94] ——, *Finite element methods for fractional differential equations*, Recent Advances in Applied Nonlinear Dynamics with Numerical Analysis, (2013), pp. 49–68.

[95] ——, *Numerical Methods for Fractional Calculus*, CRC Press, Boca Raton, FL, USA, 2015.

[96] H. Li, J. Cao, and C. Li, *High-order approximation to Caputo derivatives and Caputo-type advection–diffusion equations (III)*, Journal of Computational and Applied Mathematics, 299 (2016), pp. 159–175.

[97] M. Li, M. Lei, A. Munjiza, and P. Wen, *Frictional contact analysis of functionally graded materials with Lagrange finite block method*, International Journal for Numerical Methods in Engineering, 103 (2015), pp. 391–412.

[98] M. Li, L. Meng, P. Hinneh, and P. Wen, *Finite block method for interface cracks*, Engineering Fracture Mechanics, 156 (2016), pp. 25–40.

[99] M. Li, A. Monjiza, Y. Xu, and P. Wen, *Finite block Petrov–Galerkin method in transient heat conduction*, Engineering Analysis with Boundary Elements, 60 (2015), pp. 106–114.

[100] M. Li and P. Wen, *Finite block method for transient heat conduction analysis in functionally graded media*, International Journal for Numerical Methods in Engineering, 99 (2014), pp. 372–390.

[101] M. Li, X. Xiong, and Y. Wang, *A numerical evaluation and regularization of Caputo fractional derivatives*, Journal of Physics: Conference Series, 290 (2011), p. 012011.

[102] S. Li and H. Ding, *Numerical analysis of two-dimensional time-fractional Allen-Cahn equation on a new non-uniform mesh construction strategy*, Journal of Scientific Computing, 104 (2025), p. 81.

[103] ——, *A relaxed step-ratio constraint for time-fractional Cahn–Hilliard equations: Analysis and computation*, arXiv preprint arXiv:2508.17178, (2025).

[104] X. Li, S. Liu, W. Huang, and P. Wen, *Finite block method with automatic differentiation algorithm for Reissner plate nonlinear analysis*, Engineering Analysis with Boundary Elements, 179 (2025), p. 106354.

[105] X. Li and C. Xu, *Existence and uniqueness of the weak solution of the space-time fractional diffusion equation and a spectral method approximation*, Communications in Computational Physics, 8 (2010), p. 1016.

[106] Y. Li, F. Liu, I. W. Turner, and T. Li, *Time-fractional diffusion equation for signal smoothing*, Applied Mathematics and Computation, 326 (2018), pp. 108–116.

[107] H. L. Liao, D. Li, and J. Zhang, *Sharp error estimate of the nonuniform L1 formula for linear reaction-subdiffusion equations*, SIAM Journal on Numerical Analysis, 56 (2018), pp. 1112–1133.

[108] H. L. Liao, W. McLean, and J. Zhang, *A discrete Grönwall inequality with applications to numerical schemes for subdiffusion problems*, SIAM Journal on Numerical Analysis, 57 (2019), pp. 218–237.

[109] Y. Lin, X. Li, and C. Xu, *Finite difference/spectral approximations for the fractional Cable equation*, Mathematics of Computation, 80 (2011), pp. 1369–1396.

[110] Y. Lin and C. Xu, *Finite difference/spectral approximations for the time-fractional diffusion equation*, Journal of Computational Physics, 225 (2007), pp. 1533–1552.

[111] F. Liu, S. Shen, V. Anh, and I. Turner, *Analysis of a discrete non-Markovian random walk approximation for the time fractional diffusion equation*, The Proceedings of ANZIAM, 46 (2004), pp. C488–C504.

[112] G. R. Liu and Y. T. Gu, *An Introduction to Meshfree Methods and their Programming*, Springer, Dordrecht, The Netherlands, 2005.

[113] J. Liu, T. Wang, and T. Zhang, *A second-order finite difference scheme for the multi-dimensional nonlinear time-fractional Schrödinger equation*, Numerical Algorithms, 92 (2023), pp. 1153–1182.

[114] Q. X. Liu, Y. Gu, P. Zhuang, F. Liu, and Y. Nie, *An implicit RBF meshless approach for time fractional diffusion equations*, Computational Mechanics, 48 (2011), pp. 1–12.

[115] Y. Liu, Z. Fang, H. Li, and S. He, *A mixed finite element method for a time-fractional fourth-order partial differential equation*, Applied Mathematics and Computation, 243 (2014), pp. 703–717.

[116] Y. Liu, M. Zhang, H. Li, and J. Li, *High-order local discontinuous Galerkin method combined with WSGD-approximation for a fractional subdiffusion equation*, Computers & Mathematics with Applications, 73 (2017), pp. 1298–1314.

[117] C. Lv and C. Xu, *Error analysis of a high order method for time-fractional diffusion equations*, SIAM Journal on Scientific Computing, 38 (2016), pp. A2699–A2724.

[118] F. Mainardi, *The time fractional diffusion-wave equation*, Radiophysics and Quantum Electronics, 38 (1995), pp. 13–24.

[119] ——, *Fractional Calculus and Waves in Linear Viscoelasticity: An Introduction to Mathematical Models*, World Scientific, London, UK, 2022.

[120] M. M. Meerschaert and C. Tadjeran, *Finite difference approximations for fractional advection–dispersion flow equations*, Journal of Computational and Applied Mathematics, 172 (2004), pp. 65–77.

[121] ——, *Finite difference approximations for two-sided space-fractional partial differential equations*, Applied Numerical Mathematics, 56 (2006), pp. 80–90.

[122] R. Metzler and J. Klafter, *The random walk's guide to anomalous diffusion: a fractional dynamics approach*, Physics Reports, 339 (2000), pp. 1–77.

[123] K. S. Miller and B. Ross, *An Introduction to The Fractional Calculus and Fractional Differential Equations*, John Wiley & Sons, New York, 1993.

[124] A. Mohebbi, M. Abbaszadeh, and M. Dehghan, *A high-order and unconditionally stable scheme for the modified anomalous fractional sub-diffusion equation with a nonlinear source term*, Journal of Computational Physics, 240 (2013), pp. 36–48.

[125] ——, *The use of a meshless technique based on collocation and radial basis functions for solving the time fractional nonlinear Schrödinger equation arising in quantum mechanics*, Engineering Analysis with Boundary Elements, 37 (2013), pp. 475–485.

[126] ——, *The meshless method of radial basis functions for the numerical solution of time fractional telegraph equation*, International Journal of Numerical Methods for Heat & Fluid Flow, 24 (2014), pp. 1636–1659.

[127] R. Mokhtari and F. Mostajeran, *A high order formula to approximate the Caputo fractional derivative*, Communications on Applied Mathematics and Computation, 2 (2020), pp. 1–29.

[128] M. Molavi Arabshahi, J. Rashidinia, and S. Tanoomand, *An efficient spectral collocation method based on the generalized Laguerre polynomials to multi-term time fractional diffusion-wave equations*, AIP Advances, 14 (2024).

[129] ——, *Numerical solving of multi-term time fractional diffusion-wave equations using shifted Gegenbauer spectral collocation method*, Computational Methods for Differential Equations, 13 (2025), pp. 815–827.

[130] H. Nasir, B. Gunawardana, et al., *A second order finite difference approximation for the fractional diffusion equation*, International Journal of Applied Physics and Mathematics, 3 (2013), p. 237.

[131] R. R. Nigmatullin, *The realization of the generalized transfer equation in a medium with fractal geometry*, Physica Status Solidi (b), 133 (1986), pp. 425–430.

[132] O. Nikan, Z. Avazzadeh, and J. T. Machado, *An efficient local meshless approach for solving nonlinear time-fractional fourth-order diffusion model*, Journal of King Saud University-Science, 33 (2021), p. 101243.

[133] O. Nikan, S. M. Molavi-Arabshai, and H. Jafari, *Numerical simulation of the nonlinear fractional regularized long-wave model arising in ion acoustic plasma waves*, Discret. Contin. Dyn. Syst. S, 14 (2021), pp. 3685–3701.

[134] K. Oldham and J. Spanier, *The Fractional Calculus: Theory and Applications of Differentiation and Integration to Arbitrary Order*, Elsevier, San Diego, California, USA, 1974.

[135] G. Pang, L. Lu, and G. E. Karniadakis, *fPINNs: Fractional physics-informed neural networks*, SIAM Journal on Scientific Computing, 41 (2019), pp. A2603–A2626.

[136] A. T. Patera, *A spectral element method for fluid dynamics: laminar flow in a channel expansion*, Journal of Computational Physics, 54 (1984), pp. 468–488.

[137] P. Pedregal, *Functional Analysis, Sobolev Spaces, and Calculus of Variations*, Springer, Cham, Switzerland, 2024.

[138] I. Podlubny, *Fractional Differential Equations: An Introduction to Fractional Derivatives, Fractional Differential Equations, to Methods of their Solution and some of their Applications*, Elsevier, San Diego, California, USA, 1998.

[139] I. Podlubny, A. Chechkin, T. Skovranek, Y. Chen, and B. M. V. Jara, *Matrix approach to discrete fractional calculus II: Partial fractional differential equations*, Journal of Computational Physics, 228 (2009), pp. 3137–3153.

[140] A. Quarteroni, R. Sacco, and F. Saleri, *Numerical mathematics*, vol. 37, Springer Science & Business Media, New York, NY, USA, 2006.

[141] A. Quarteroni and A. Valli, *Numerical Approximation of Partial Differential Equations*, vol. 23, Springer Science & Business Media, Berlin, Germany, 2008.

[142] P. Rajput, N. Srivastava, and V. K. Singh, *A high order numerical method for the variable order time-fractional reaction-subdiffusion equation*, Chinese Journal of Physics, 85 (2023), pp. 431–444.

[143] M. Ramezani and R. Mokhtari, *A novel high-order finite-difference method for the time-fractional diffusion equation with smooth/nonsmooth solutions*, Bulletin of the Iranian Mathematical Society, 48 (2022), pp. 3987–4013.

[144] ——, *Numerical solution of distributed-order fractional diffusion equations using a high-order temporal scheme*, Communications on Applied Mathematics and Computation, (2025), pp. 1–15.

[145] M. Ramezani, R. Mokhtari, and G. Haase, *Some high order formulae for approximating Caputo fractional derivatives*, Applied Numerical Mathematics, 153 (2020), pp. 300–318.

[146] M. Ran and C. Zhang, *New compact difference scheme for solving the fourth-order time fractional sub-diffusion equation of the distributed order*, Applied Numerical Mathematics, 129 (2018), pp. 58–70.

[147] S. S. Ray and R. Bera, *Analytical solution of a fractional diffusion equation by Adomian decomposition method*, Applied Mathematics and Computation, 174 (2006), pp. 329–336.

[148] B. Ross, *The development of fractional calculus 1695–1900*, Historia Mathematica, 4 (1977), pp. 75–89.

[149] Y. A. Rossikhin and M. V. Shitikova, *Applications of fractional calculus to dynamic problems of linear and nonlinear hereditary mechanics of solids*, Applied Mechanics, (1997), pp. 15–67.

[150] A. Saadatmandi and M. Dehghan, *A new operational matrix for solving fractional-order differential equations*, Computers & Mathematics with Applications, 59 (2010), pp. 1326–1336.

[151] ——, *Numerical solution of hyperbolic telegraph equation using the Chebyshev tau method*, Numerical Methods for Partial Differential Equations: An International Journal, 26 (2010), pp. 239–252.

[152] ——, *A tau approach for solution of the space fractional diffusion equation*, Computers & Mathematics with Applications, 62 (2011), pp. 1135–1142.

[153] S. Sabermahani, Y. Ordokhani, and S. Yousefi, *Numerical approach based on fractional-order Lagrange polynomials for solving a class of fractional differential equations*, Computational and Applied Mathematics, 37 (2018), pp. 3846–3868.

[154] S. Sabermahani, Y. Ordokhani, and S. A. Yousefi, *Fractional-order general Lagrange scaling functions and their applications*, BIT Numerical Mathematics, 60 (2020), pp. 101–128.

[155] G. Sayyar, S. M. Hosseini, and F. Mostajeran, *A high-order scheme for time-space fractional diffusion equations with Caputo-Riesz derivatives*, Computers & Mathematics with Applications, 104 (2021), pp. 34–43.

[156] W. R. Schneider and W. Wyss, *Fractional diffusion and wave equations*, Journal of Mathematical Physics, 30 (1989), pp. 134–144.

[157] M. Shafiq, M. Abbas, K. M. Abualnaja, M. Huntul, A. Majeed, and T. Nazir, *An efficient technique based on cubic B-spline functions for solving time-fractional advection diffusion equation involving Atangana–Baleanu derivative*, Engineering with Computers, 38 (2022), pp. 901–917.

[158] J. Shen, *Efficient spectral-Galerkin method I. Direct solvers of second-and fourth-order equations using Legendre polynomials*, SIAM Journal on Scientific Computing, 15 (1994), pp. 1489–1505.

[159] J. Shen, T. Tang, and L. L. Wang, *Spectral Methods: Algorithms, Analysis and Applications*, vol. 41, Springer Science & Business Media, Berlin, 2011.

[160] S. Shen, F. Liu, V. Anh, and I. Turner, *Detailed analysis of a conservative difference approximation for the time fractional diffusion equation*, Journal of Applied Mathematics and Computing, 22 (2006), pp. 1–19.

[161] A. Shokri and M. Dehghan, *A Not-a-Knot meshless method using radial basis functions and predictor–corrector scheme to the numerical solution of improved Boussinesq equation*, Computer Physics Communications, 181 (2010), pp. 1990–2000.

[162] ——, *A meshless method using radial basis functions for the numerical solution of two—dimensional complex Ginzburg–Landau equation*, Computer Modeling in Engineering and Sciences, 84 (2012), p. 333.

[163] F. Song, C. Xu, and G. E. Karniadakis, *Computing fractional Laplacians on complex-geometry domains: Algorithms and simulations*, SIAM Journal on Scientific Computing, 39 (2017), pp. A1320–A1344.

[164] J. Stoer, R. Bulirsch, R. Bartels, W. Gautschi, and C. Witzgall, *Introduction to Numerical Analysis*, vol. 1993, Springer, 1980.

[165] M. Stynes, E. O'Riordan, and J. L. Gracia, *Error analysis of a finite difference method on graded meshes for a time-fractional diffusion equation*, SIAM Journal on Numerical Analysis, 55 (2017), pp. 1057–1079.

[166] Z. Z. Sun and G. H. Gao, *Fractional Differential Equations: Finite Difference Methods*, Walter de Gruyter GmbH & Co KG, 2020.

[167] Z. Z. Sun and X. Wu, *A fully discrete difference scheme for a diffusion-wave system*, Applied Numerical Mathematics, 56 (2006), pp. 193–209.

[168] N. Sweilam, M. Khader, and A. Mahdy, *Crank-Nicolson finite difference method for solving time-fractional diffusion equation*, Journal of Fractional Calculus and Applications, 2 (2012), pp. 1–9.

[169] N. H. Sweilam and M. Khader, *A chebyshev pseudo-spectral method for solving fractional-order integro-differential equations*, The ANZIAM Journal, 51 (2010), pp. 464–475.

[170] C. Tadjeran, M. M. Meerschaert, and H. P. Scheffler, *A second-order accurate numerical approximation for the fractional diffusion equation*, Journal of Computational Physics, 213 (2006), pp. 205–213.

[171] V. Thomée, *Galerkin Finite Element Methods for Parabolic Problems*, vol. 25, Springer Science & Business Media, Berlin, Germany, 2007.

[172] W. Tian, H. Zhou, and W. Deng, *A class of second order difference approximations for solving space fractional diffusion equations*, Mathematics of Computation, 84 (2015), pp. 1703–1727.

[173] L. N. Trefethen, *Spectral Methods in MATLAB*, SIAM, 2000.

[174] ——, *Approximation Theory and Approximation Practice, extended edition*, SIAM, Philadelphia, Pennsylvania, USA, 2019.

[175] J. Wang, F. X. Sun, Y. M. Cheng, and A. Huang, *Error estimates for the interpolating moving least-squares method*, Applied Mathematics and Computation, 245 (2014), pp. 321–342.

[176] Y. Wang, G. Wang, L. Bu, and L. Mei, *Two second-order and linear numerical schemes for the multi-dimensional nonlinear time-fractional Schrödinger equation*, Numerical Algorithms, 88 (2021), pp. 419–451.

[177] Z. Wang and S. Vong, *Compact difference schemes for the modified anomalous fractional sub-diffusion equation and the fractional diffusion-wave equation*, Journal of Computational Physics, 277 (2014), pp. 1–15.

[178] P. Wen, P. Cao, and T. Korakianitis, *Finite block method in elasticity*, Engineering Analysis with Boundary Elements, 46 (2014), pp. 116–125.

[179] W. Wyss, *The fractional diffusion equation*, Journal of Mathematical Physics, 27 (1986), pp. 2782–2785.

[180] S. Yan, F. Zhao, C. Li, and L. Zhao, *High order WSGL difference operators combined with Sinc-Galerkin method for time fractional Schrödinger equation*, International Journal of Computer Mathematics, 97 (2020), pp. 2259–2286.

[181] X. Yan, S. Liu, P. Wen, J. Sladek, and V. Sladek, *Homogeneous and functionally graded piezoelectric structure analysis with finite block method*, Composite Structures, 365 (2025), p. 119188.

[182] J. Yang, Z. Wang, O. Adetoro, P. Wen, and C. Bailey, *The thermal analysis of cutting/grinding processes by meshless finite block method*, Engineering Analysis with Boundary Elements, 100 (2019), pp. 68–79.

[183] X. Yang, H. Zhang, and D. Xu, *Orthogonal spline collocation method for the two-dimensional fractional sub-diffusion equation*, Journal of Computational Physics, 256 (2014), pp. 824–837.

[184] S. Yeganeh, R. Mokhtari, and J. S. Hesthaven, *A local discontinuous Galerkin method for two-dimensional time fractional diffusion equations*, Communications on Applied Mathematics and Computation, 2 (2020), pp. 689–709.

[185] Q. Yi, A. Chen, and H. Ding, *High order difference method for fractional convection equation*, Mathematics and Computers in Simulation, 234 (2025), pp. 286–298.

[186] M. Zayernouri and G. E. Karniadakis, *Exponentially accurate spectral and spectral element methods for fractional ODEs*, Journal of Computational Physics, 257 (2014), pp. 460–480.

[187] ——, *Fractional spectral collocation method*, SIAM Journal on Scientific Computing, 36 (2014), pp. A40–A62.

[188] ——, *Fractional spectral collocation methods for linear and nonlinear variable order FPDEs*, Journal of Computational Physics, 293 (2015), pp. 312–338.

[189] F. Zeng and C. Li, *A new Crank–Nicolson finite element method for the time-fractional subdiffusion equation*, Applied Numerical Mathematics, 121 (2017), pp. 82–95.

[190] F. Zeng, C. Li, F. Liu, and I. Turner, *The use of finite difference/element approaches for solving the time-fractional subdiffusion equation*, SIAM Journal on Scientific Computing, 35 (2013), pp. A2976–A3000.

[191] ——, *Numerical algorithms for time-fractional subdiffusion equation with second-order accuracy*, SIAM Journal on Scientific Computing, 37 (2015), pp. A55–A78.

[192] N. Zhang, W. Deng, and Y. Wu, *Finite difference/element method for a two-dimensional modified fractional diffusion equation*, Advances in Applied Mathematics and Mechanics, 4 (2012), pp. 496–518.

[193] X. Zhang, Y. Feng, Z. Luo, and J. Liu, *A spatial sixth-order numerical scheme for solving fractional partial differential equation*, Applied Mathematics Letters, 159 (2025), p. 109265.

[194] X. Zhang, P. Huang, X. Feng, and L. Wei, *Finite element method for two-dimensional time-fractional Tricomi-type equations*, Numerical Methods for Partial Differential Equations, 29 (2013), pp. 1081–1096.

[195] Y. Zhang and H. Ding, *An efficient high-order numerical algorithm for the time fractional Fokker–Planck equations*, International Journal of Computer Mathematics, 98 (2021), pp. 357–366.

[196] Y. N. Zhang and Z. Z. Sun, *Alternating direction implicit schemes for the two-dimensional fractional sub-diffusion equation*, Journal of Computational Physics, 230 (2011), pp. 8713–8728.

[197] Y. N. Zhang, Z. Z. Sun, and H. L. Liao, *Finite difference methods for the time fractional diffusion equation on non-uniform meshes*, Journal of Computational Physics, 265 (2014), pp. 195–210.

[198] Y. N. Zhang, Z. Z. Sun, and H. W. Wu, *Error estimates of Crank–Nicolson-type difference schemes for the subdiffusion equation*, SIAM Journal on Numerical Analysis, 49 (2011), pp. 2302–2322.

[199] X. Zhao and Z. Z. Sun, *A box-type scheme for fractional sub-diffusion equation with neumann boundary conditions*, Journal of Computational Physics, 230 (2011), pp. 6061–6074.

[200] H. Zheng, J. Xiong, Y. Yuan, and P. Wen, *Mixed-mode dynamic stress intensity factors by variation technique with finite block method*, Engineering Analysis with Boundary Elements, 106 (2019), pp. 27–33.

[201] H. Zhong and H. Ding, *Caputo-tempered subdiffusion problems: Blended nonuniform L1 and compact difference formulations*, Mathematical Methods in the Applied Sciences, (2025), pp. 1–20.

[202] Y. Zhou, W. Huang, J. Yang, and P. Wen, *Galerkin finite block method with Lagrange multipliers method for cracked solids in functionally graded materials*, Engineering Analysis with Boundary Elements, 163 (2024), pp. 606–615.

[203] H. Zhu and C. Xu, *A highly efficient numerical method for the time-fractional diffusion equation on unbounded domains*, Journal of Scientific Computing, 99 (2024), p. 47.

[204] P. Zhuang and F. Liu, *Implicit difference approximation for the time fractional diffusion equation*, Journal of Applied Mathematics and Computing, 22 (2006), pp. 87–99.

[205] ——, *Finite difference approximation for two-dimensional time fractional diffusion equation*, Journal of Algorithms & Computational Technology, 1 (2007), pp. 1–16.

Please cite this article using:

Amin Ghoreyshi, Mostafa Abbaszadeh, Mehdi Dehghan, Numerical methods for the time-fractional diffusion equation: A review, AUT J. Math. Comput., 7(2) (2026) 213-269
https://doi.org/10.22060/AJMC.2026.24592.1441